Critical Behavior of Asphalt Mixtures Undergoing Glass Transition and Physical Hardening

By:

Hassan Ali Tabatabaee

A dissertation submitted in partial fulfillment of

the requirements for the degree of

Doctor of Philosophy

(Civil & Environmental Engineering)

University of Wisconsin – Madison

2012

Date of Final Oral Examination: 08/21/2012

The dissertation is approved by the following members of the Final Oral Committee:
Hussain U. Bahia, Professor, Civil and Environmental Engineering
Steven M. Cramer, Professor, Civil and Environmental Engineering
Tuncer B. Edil, Professor, Civil and Environmental Engineering
Dante Fratta, Associate Professor, Civil and Environmental Engineering
Roderic S. Lakes, Professor, Engineering Physics

Acknowledgements

Many people have helped me on the path toward completing the present study, without which none of this would have been possible. I would like to express my deep appreciation for the knowledgeable guidance and support of my advisor, Professor Hussain Bahia, as well as the valuable feedback and contribution from my esteemed committee members, Professor Steven Cramer, Professor Tuncer Edil, Professor Dante Fratta, and Professor Roderic Lakes. I must acknowledge Dr. Raul Velasquez, whose invaluable input and contribution, both as a friend and as a mentor, was instrumental to the development of this work.

I sincerely acknowledge the effort and dedication of my parents, always motivating me to reach for the stars and providing the opportunities for me to do so. I undoubtedly owe this accomplishment to the constant support and inspiration of my wife, Mozhdeh, whose boundless patience and dedication drove me forward even at the hardest of times. Finally I'd like to state my sincere appreciation to all my friends at the Modified Asphalt Research Center (MARC) who have made this experience much more pleasant and enjoyable with their warm presence and friendship.

Hassan A. Tabatabaee

8/22/2012

Abstract

Asphalt binders have been shown to undergo significant time dependent stiffening when stored at low temperatures. This phenomenon, often referred to as physical hardening, has a significant impact on the laboratory performance of asphalt binders. However, the importance of isothermal conditioning for asphalt mixtures and its effect on thermal cracking performance has been a subject of significant debate.

In this dissertation a theoretical approach accounting for the glass transition and physical hardening in the thermal stress buildup in asphalt mixtures was derived using relaxation modulus master curves, the William-Landel-Ferry equation, Boltzmann superposition principle, and a model describing the isothermal contraction of asphalt as a continuous function of conditioning time and temperature. Using the model predictions it is shown that thermal stress relaxation and stress build-up induced by physical hardening can continuously affect thermal stress throughout the cooling process. Cooling rate also affected the amount of delayed stress buildup occurring after the temperature had stabilized at isothermal conditions, as a result of the physical hardening.

A relatively simple testing device developed by researchers at UW-Madison was used for verification and support of the thermal stress model [1, 2]. Mixture testing performed at different cooling rates and isothermal conditions supported the theoretical predictions. The device simultaneously tests two asphalt mixture beams; one unrestrained, and the other with restrained ends. The unrestrained beam is used to measure the one dimensional change of length with temperature, and consequently the glass transition temperature (T_g) and coefficients of expansion/contraction above and below the Tg (α_l and α_g). The restrained beam is used to capture

the induced thermal stress buildup due to prevented contraction in the sample. This device is being referred to as the Asphalt Thermal Cracking Analyzer (ATCA).

In the proposed model, the input thermal strain includes two components (cooling shrinkage and isothermal shrinkage). Each component is divided into step increments for which the relaxation response can be easily computed and added in time. Preliminary validation results indicate that this model can capture experimental data very well, and can also explain previously reported deviations between predicted and measured thermal stress, especially when mixture samples are subjected to isothermal conditioning. The rate of isothermal stress buildup in this model gradually decreases as the modulus further relaxes with time, ultimately resulting in a gradual stress relaxation.

An experimentally calibrated multi-phase micromechanical model for asphalt mixture undergoing thermal shrinkage and glass transition was also developed in a finite element platform. The results where compared to experimental data measured using the ATCA device, which allowed measuring strain and stress build up during cooling.

The results of this study indicate that physical hardening of binders has important effects on the thermal stress and thermal strain accumulation in mixtures during cooling cycles. Failure to consider this time dependent behavior, which varies among binders, could lead to failure in predicting performance. The existing modulus and strain used in predicting thermal cracking of asphalt pavements need revisions to integrate a function for the time dependent changes.

Table of Contents

List of Figures

List of Tables

1. Overview and Objective

1.1. Background and Problem Statement

The change in asphalt binder isothermal behavior near or below the glass transition temperature has been noted by many researchers in recent years [3, 4, 5, 6, 7, 8, 9]; the increase in brittleness as well as the time-dependent hardening in this temperature range can have a detrimental effect on actual binder performance during its service life. Researchers have also reported that the midpoint of the binder's glass transition, typically referred to as the "glass transition temperature," is in the vicinity of the pavement critical cracking temperature [10]. Furthermore, it has been shown that this time-dependent hardening (also called Physical Hardening) can affect the position of the glass transition temperature of binders [7]. Change in relaxation properties has been noted in binder and many polymers during physical hardening in a number of studies [10, 6, 7]. Despite the mounting evidence, most pavement low temperature stress calculation and analysis methods used today do not account for glass transition behavior in asphalt binder, and none have the ability to include the effects of physical hardening caused by time dependent contraction in their analysis. Current specifications and models are based on single event failure, not accounting for glass transition and the effect of extended isothermal conditions. There is a critical need for showing how glass transition behavior and the physical hardening phenomenon in asphalt binders can affect mixtures behavior under various climatic conditions, and also a need for a suitable model that allows better prediction of these effects.

1.2. Objectives

This dissertation is focused on achieving the following objectives:

1. Modification of current thermal stress buildup and relaxation models to account for glass transition and physical hardening in asphalt pavement.
2. Using experimentally derived data and thermal stress measurements of mixtures using the ATCA test, binder fracture using the Single edged Notched Beam (SENB) test, binder dilatometric glass transition measurements, and the Bending Beam Rheometer (BBR) to verify model and define critical experimental model inputs.
3. Development of suitable limiting criteria for prevention of asphalt pavement thermal cracking.

1.3. Hypothesis

Asphalt pavement thermal cracking cannot be accurately predicted without consideration of the effect of glass transition and physical hardening of asphalt binders.

1.4. Research Methodology and Scope

A comprehensive literature review was conducted to assess the current state of knowledge on low temperature thermal stress prediction in binders and viscoelastic material. This stage focused on developing methodology for measuring and quantifying the effect of isothermal contraction and physical hardening, as well as defining the asphalt mixture thermo-volumetric properties (i.e. glass transition zone and coefficients of expansion/contraction).

Laboratory experiments were carried out and the results were used in the development of the aforementioned theory and model.

A mechanism and model accounting for the effect of glass transition and conditioning time in thermal stress buildup and relaxation was developed using information gathered through conduction of experiments in the previous steps and experimentally verified. The importance and relevance of the studied properties were investigated by comparison to field performance of pavement sections.

2. Literature Review

2.1. Low Temperature Performance Testing of Asphalt Mixtures

Low temperature cracking is a major distress in many regions with cold climates. It is believed that the excessive brittleness due to the increase in stiffness and decrease in the ability to relax stress leads to the buildup of thermally induced stress and ultimately cracking of mixtures in pavements.

Thermal cracking is widely recognized as a critical failure mode for asphalt pavements. Due to its importance a reliable test method capable of capturing asphalt material response to environmental loading as function of both time and temperature is needed. The current low temperature specifications in the US and other countries rely heavily on measuring asphalt mixture properties obtained under mechanical loading in the Indirect Tensile (IDT) creep and strength tests. However, these tests have limited capabilities in terms of simulating thermal cracking. These limited capabilities have been recognized and to address them a test method such as the Thermal Stress Restrained Specimen Test (TSRST) has been used. Furthermore, in conventional thermal cracking tests, linear viscoelastic concepts are used to infer mechanical response to thermal loading while making assumptions about coefficients of contraction and ignoring glass transition change.

Visco-elastic materials such as asphalt mixtures can relax stress by viscous flow. Asphalt pavements are restrained from significant movement, thus thermally induced contraction can lead to significant stress build-up in the pavement. Due to the time dependent behavior of visco-elastic materials, the higher the capability of the material to relax stress, the lower the thermal stress buildup will be at a given temperature, and consequently the pavement can withstand

lower temperatures before fracture [11, 10]. Thus, stress relaxation has been considered an important factor in the thermal cracking resistance of asphalt pavements [12]. Researchers also consider factors such as the rate of cooling, coefficients of expansion/contraction, glass transition temperature, shape of master curve at low temperatures and the tensile strength to affect the critical cracking temperature [10]. Measuring all these factors in a controlled laboratory environment has been exceedingly difficult; therefore theoretical calculations of thermal stress have often utilized simplifying assumptions in place of many of the aforementioned factors.

Monismith et al. [13] developed a theoretical calculation method for the thermally induced stress in asphalt pavements. This method is currently used for the estimation of critical cracking temperature by researchers and designers in many design procedures and software. However, this method does not take into account the glass transition behavior and physical hardening observed in asphalt binders, utilizing a constant coefficient of thermal expansion/contraction.

The TSRST standardized system was developed under SHRP A-400 contract by Jung and Vinson [11]. In this test, as the temperature drops the specimen is restrained from contracting thus inducing tensile stresses. The results from TSRST are the cracking temperature and cracking strength due to a single low temperature event. This test method has been extensively used in the past to investigate thermal cracking performance. Research performed by Monismith et al. [13], Arand [14], Vinson et al. [15], Romero et al. [16], Sebaaly et al. [17], Chehab et al. [18], Sauzéat et al. [19], and Velasquez et al. [20], among others showed that TSRST can be used to evaluate the susceptibility of asphalt mixtures to low temperature cracking.

A recently developed method for estimating low temperature performance of asphalt mixtures tests small prismatic asphalt mixture beams in creep under a three point bending load configuration. The results of this test are used to determine the creep compliance of the mixture at different temperatures and loading times, and may consequently be used to develop master curves and calculate thermal stress in the asphalt mixtures [21].

2.2. Physical Hardening of Amorphous Material

Glasses usually exist in a non-equilibrium state, and relaxation toward equilibrium is commonly referred to as physical aging. This term was first coined by Struik [22, 23, 24] to distinguish glassy state relaxation from other time-dependent processes such as recrystallization and chemical degradation. In the inorganic glass literature, it is traditionally referred to as structural relaxation, annealing, or stabilization [23, 24]. Physical hardening is usually explained by the free volume theory proposed by Struik [25] and Ferry [26]. Struik described physical hardening in polymers as a type of thermo-reversible relaxation process, taking place in the glass transition region of amorphous materials [25].

A number of researchers have noted the close correspondence between enthalpy relaxation and volume relaxation during isothermal aging, thus relating the physical aging phenomenon to the relaxation of excess enthalpy in the non-equilibrium state during glassy transition toward the equilibrium enthalpy state [27, 28, 29, 24, 30, 31, 32].

Although the equilibrium enthalpy state has commonly been estimated through the extension of the liquid enthalpy equilibrium state to sub-Tg levels, a number of studies have suggested that enthalpy relaxes toward a glassy equilibrium enthalpy state, resulting in a lower ultimate enthalpy relaxation during aging [33, 24]. An ideal glassy state has been described as

existing below the “Kauzmann Temperature” of an amorphous material, which in term will happen below the apparent glass transition temperature. The Kauzmann temperature and ideal glass phase concept was suggested as a solution to the apparent paradox pointed out by Kauzmann [34]. The Kauzmann paradox states that if one is to cool a glass forming liquid at a sufficiently low rate as to prevent deviation from equilibrium (or extend the liquid volume/enthalpy/specific heat/entropy equilibrium line below the glass transition) not very far below the Tg a temperature can be reached at which theoretically the extended property will be equal to that of the completely crystalized phase. Extending lower than this temperature will lead to volume/enthalpy/specific heat/entropy lower than that of crystalline phase of the material, which thermodynamically impossible. A resolution to this paradox would be the existence of an ultimate ideal glassy phase change temperature below the apparent glass transition, below which “A non-vitreous stable liquid cannot exist, and it is operationally meaningless to extrapolate the entropy, energy, and specific volume curves below that temperature” [34]. It has been shown that for some material the Kauzmann temperature and the end of the glass transition region may be one and the same [35], as shown in Figure 2.

A similar concept was used by Adam and Gibbs [36] to define the temperature “T_2” below the glass transition temperature, at which there is only one possible molecular configuration in the material, thus the “configurational entropy” is zero. Adams and Gibbs defined a “cooperative rearranging region” to explain the temperature dependence of the volume relaxation phenomena in glass-forming liquids. The cooperatively rearranging region was defined as the smallest region as a subset of a material’s molecular structure that can undergo a transition to a new configuration without requiring simultaneous configurational change on and outside its boundary. The size of this cooperative region was shown to be determined by the

configuration restrictions associated with amorphous packing that was described by the configurational entropy of the melt, which in turn is temperature dependent.

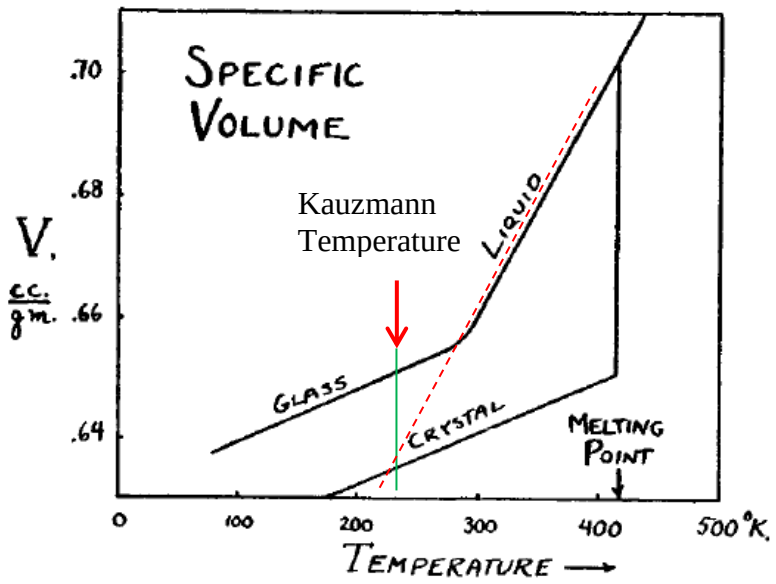

Figure 1 The concept of the "Kauzmann Temperature" for glass forming material [34]

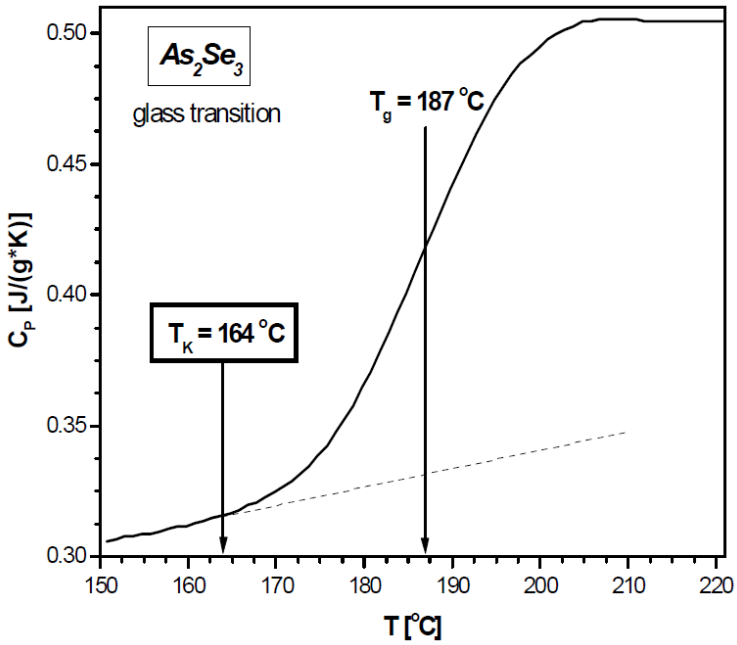

Figure 2 The Kauzmann temperature relative to the DSC measurement of the glass transition range and temperature of As_2Se_2 [35]

Struik defined the region of significant physical aging for a number of amorphous materials. He defined the lower bound of this range as the temperature below sufficiently below the Tg at which segmental molecular motion and aging disappears, while defining the Tg as the upper limit. Following the discussion in previous paragraphs, it is expected that physical aging and the corresponding volume relaxation to take place within the glass transition region, bounded at the upper end by the temperatures at which deviation from equilibrium occurs and at the lower end by the ideal glassy state temperature, as defined by the "Kauzmann temperature", T_K, [34, 35] or the Adam-Gibbs "T_2" [36, 24]. Figure 3 [37] shows that boundaries in isothermal volume relaxation temperatures are experimentally observable.

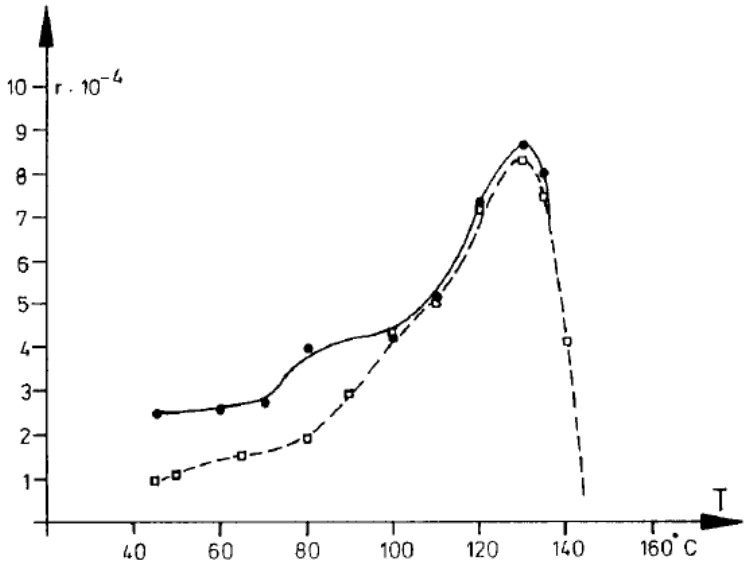

Figure 3 Isothermal volume relaxation rate for isotropic (solid line) and drawn (dashed line) polycarbonate, plotted against aging temeprature [37]

Struik studied the physical aging for 35 plastics and other organic glasses, as well as a variety of mechanical properties. He found that physical aging effects appeared to be very important, often dominating the mechanical behavior in the practical temperature range. He

concluded that nearly all aspects of aging can be explained from the free-volume concept. Furthermore, the aging behavior and the small-strain mechanical properties were found to be very similar for all studied polymers as well as many nonpolymeric materials [22]. Struik studied the creep of PVC and PMMA at a number of temperatures below the Tg and experimentally concluded that mechanical stresses may enhance aging, but such effects occur only at large strain levels [38]. Recently an optical photobleaching technique was utilized to directly measure the segmental mobility in PMMA glasses during tensile creep deformation to investigate the interaction between physical aging, mobility, and mechanical deformation. Results indicated that the effects of aging and stress on mobility act as two independent processes; thus no erasure of aging occurs as a result of increased mobility induced by stressing the material [39]. Struik concluded that the time frame during which physical aging occurs increases exponentially as temperature drops below the Tg, approximately by a factor of 10 per 3°C; such that at no more than 20°C below Tg, aging time frame approaches 100 years. Struik noted that comprehensive proof of this conclusion was not experimentally possible [22]. In later studies Struik observed physical aging in semi-crystalline polymers and some filled rubbers above their Tg, which he explained by attributed the aging to the portion of amorphous material which may be in a glassy phase at this temperature range [40].

For semi-crystalline material it has been observed that crystalline regions constrain the amorphous regions in partially crystalline polymers which has a marked effect on the glass transition and the mobility of the chain segments in the non-crystalline regions, such that the observed Tg is raised well above that of the completely amorphous sample [41]. Similar results have been shown for PET, for which both the extent and rate of physical aging decreased with increasing percent crystallinity [42]. Free volume formation below the glass transition has also

been noted for glass forming metals, especially bulk glass forming alloys [43]. Metallic glass is obtained if the liquid metal alloy is cooled fast enough to avoid nucleation and growth of crystalline structures [43].

2.2.1. Mechanical Properties of Physical Aging Material

It has been noted that material properties, such as yield stress, tensile and flexural modulus, increase progressively with physical aging, while the fracture toughness, impact strength and compliance decrease [41, 44]. It has been shown that other than the decrease of free volume during physical aging, the narrowing trend of free volume size distribution during aging contributes to the modification of mechanical properties in physically aged material [37]. Free volume distribution has been measured for amorphous material during aging using small-angle X-ray scattering and spin-probe mobility techniques [37].

Tensile experimentation on PET showed that although physical aging increased the yield stress, it also increased the rate at which stress decreased after yielding, effectively decreasing the post-peak resistance of the material [44]. Study of physically aged epoxy resins [45] showed a decrease in fracture toughness and the occurrence of stick-slip failure behavior in aged epoxies. This was explained by stating that the aging increased the yield point of the material, thus suppressing the crack-blunting mechanisms (toughening) associated with unaged epoxies. In another study an increased degree of physical aging was found to produce shorter lifetimes in materials that failed in a predominantly brittle manner [46]. The main cause of this weakening was attributed to the reduced craze strength due to the reduction in toughness caused by aging. The authors concluded that neglecting the effects of physical aging could lead to measurements that significantly overestimate the failure strength of polymeric materials.

Researchers have shown that time-temperature superposition cannot be used for long term creep when significant physical aging occurs, due to the simultaneous effect of aging during creep time frame, resulting in significant over estimation of creep [47, 48]. The same reasoning was extended to the Boltzmann's superposition principle, stating that this principle is invalid in the range of physical aging. Figure 4 shows the comparison between the time-temperature superposition master curves and the actual data for two different aging times (1 h and 1 day) before the start of the creep test, with samples being aged at the same temperature as the test [47]. Within the aging range, temperature and aging effects on the creep behavior have been shown to be comparable in magnitude [48]. In fact, it has been claimed that without physical aging many glassy polymers could not be used to make load bearing structures [48].

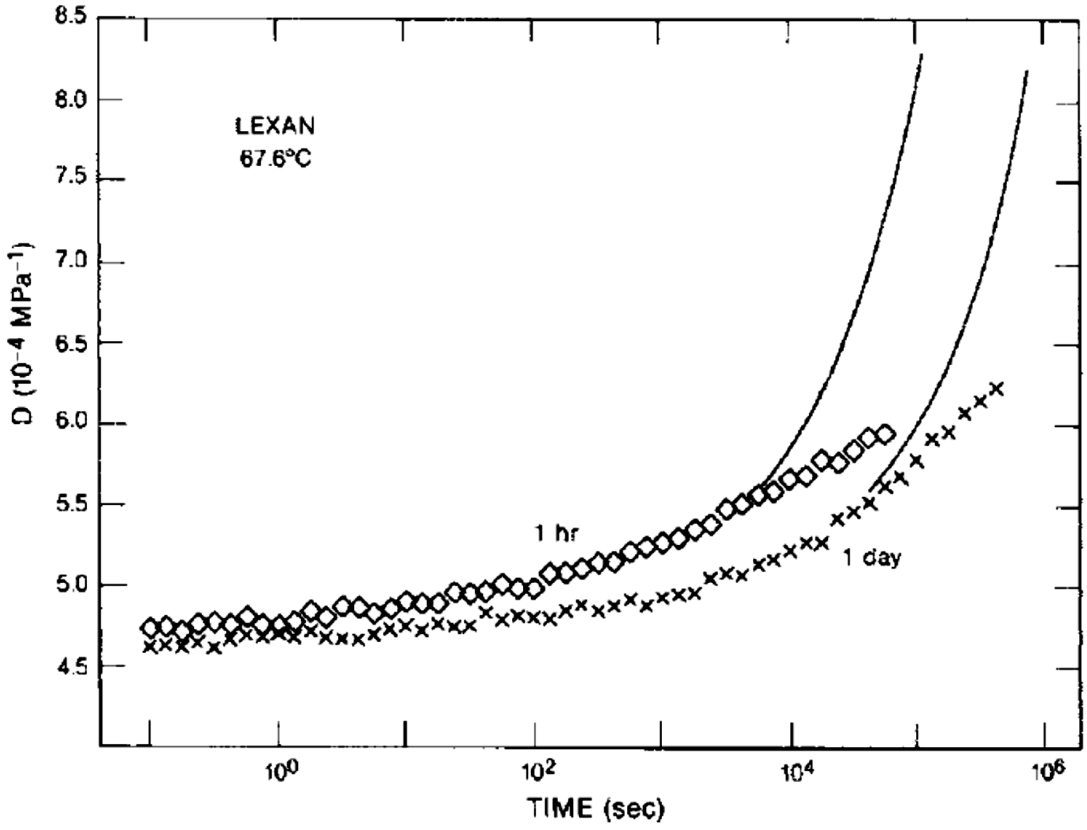

Figure 4 Comparison between the time-temperature superposition master curves and the actual data for two different aging times (1h, 1 day) before the start of the test [47].

The evolution of the dynamic mechanical properties of poly(vinyl acetate) in the Tg region during physical aging at 32.5°C and 35.0°C, following a temperature down-jump from 40°C was measured by Delin et al. [49], and compared with the isothermal volume relaxation behavior through dilatometric measurements. The approach of dynamic mechanical properties towards equilibrium was observed to be slower than that for volume relaxation at the same temperatures. The authors postulated that the evolution of dynamic mechanical properties in the Tg region can be retarded by rejuvenation resulting from low strain, and that this rejuvenation is more noticeable the higher the strain amplitude and the damping.

Guagadno et al. [28] studied the effect of physical aging for the case of Syndiotactic polypropylene (sPP), a semi-crystalline polymer, and noted that the 7% increase of crystallinity from 19 to 26% after a month of aging was not sufficient to explain the more than 200% increase observed in the elastic modulus during aging (Figure 5), measured using a Polymer Laboratories Dynamic Mechanical Thermal Analyzer.

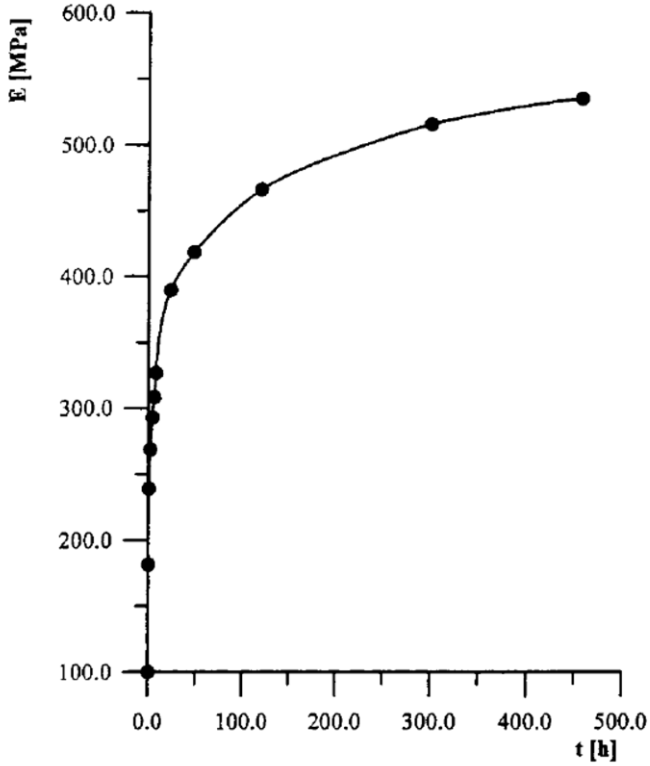

Figure 5 Increase in elastic modulus of Syndiotactic polypropylene during physical aging [28]

2.2.2. Volume Relaxation Studies for Amorphous Materials

Measuring free volume is absolute units has proven difficult, but its variation has been measured by various techniques including dilatometry [29, 50], resistivity, position annihilation [43], viscosity/stiffness measurements [51], positron lifetime technique [30], as well as the fluorescence response of mobility- or free volume-sensitive molecule, julolidene-malono-nitrile (JMN) [52, 53].

Results for positron lifetime technique on poly (vinyl acetate) (PVAc) indicated that the procedure can be a reliable method for monitoring not only free-volume changes but also changes in the distribution of free-volume elements in polymers. Physical aging in melt-quenched polypropylene was studied and found to be accompanied by no change in crystallinity

and in the crystalline density. The increase in the density of the material associated with aging was therefore attributed to a shrinking of the non-crystalline regions due to isothermal collapse of molecular free volume [54]. In metallic glasses, change of free volume has been measured through x-ray dilatation curves achieved from analysis of the diffraction spectra from transmission of a high-intensity high-energy monochromatic beam to the material while heating material through its glass transition region [43]. Such studies have shown that depending on cooling rate down to Tg, different amounts of free volume will be quenched into the glass forming metallic alloy [43].

Volume relaxation during isothermal aging of amorphous materials has been recognized and measurements have been performed for many years [27, 31, 29]. One such study was performed on polystyrene using dilatometric testing at constant cooling rates from equilibrium at above Tg to the aging temperature [29]. During the aging process the volume of the sample is monitored using the mercury-in-glass (MIG) dilatometry method. Before starting the cooling to the aging temperature of 92°C, the sample was annealed at 115°C for 15 min. Time zero for collecting of relaxation data was set at the moment the aging temperature was reached. Tg was obtained at different cooling rates ranging from 1.0 to 0.0037 °C/min. It was observed that changing the cooling rate by more than 2 orders of magnitude shifted the Tg by about 5°C, as shown in Figure 6. In another study decreasing the cooling rate of polyvinyl acetate by one order of magnitude resulted in an approximately 2°C decrease in the measured Tg, as seen in Figure 7 [49]. Tg changes of only a few degrees when changing cooling rates a number of orders of magnitude has also been reported elsewhere in the literature [24].

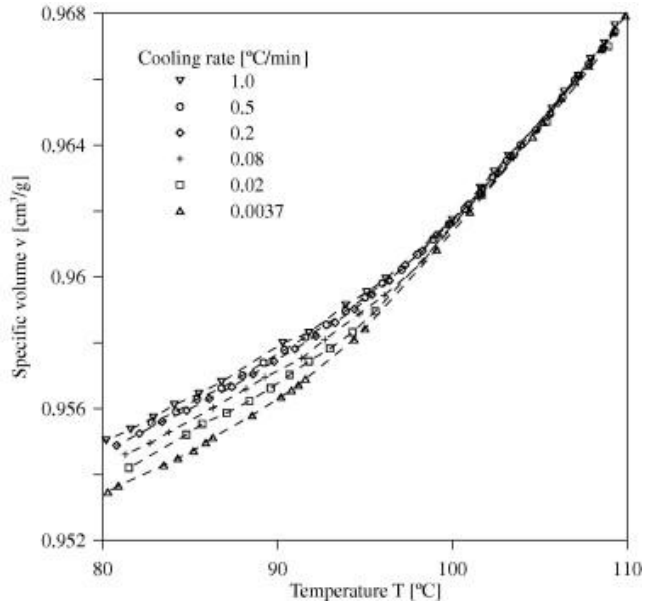

Figure 6 Glass transition measurements for polystyrene at different cooling rates [29]

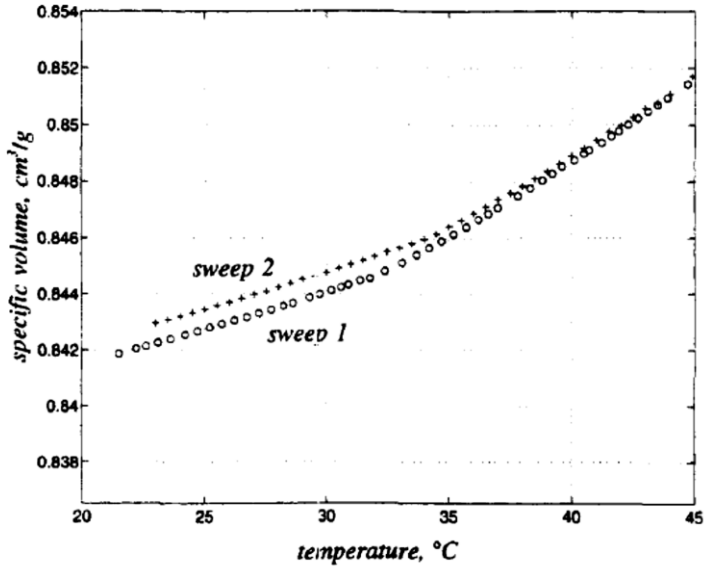

Figure 7 Measurement of glass transition for PVAc at two rates, sweep 1 and 0.075°C/min, and sweep 2 at 0.75°C/min [49].

Once isothermal conditions were established the isothermal volume change was measured as physical aging progressed. This volume change was referred to as "excess volume" in this study. Figure 8 shows the change of excess volume with cooling rates and aging temperature. It is observed that the faster the cooling rate, the larger the amount of isothermal

volume change. Furthermore, for the 3 temperatures tested, the lower aging temperatures showed higher isothermal volume change. This is also in agreement with results from aging of a-PMMA by other researchers [50], as seen in Figure 9. The non-linear trend of volume change plotted against the log of time shows that the rate of isothermal volume relaxation is not logarithmic against time.

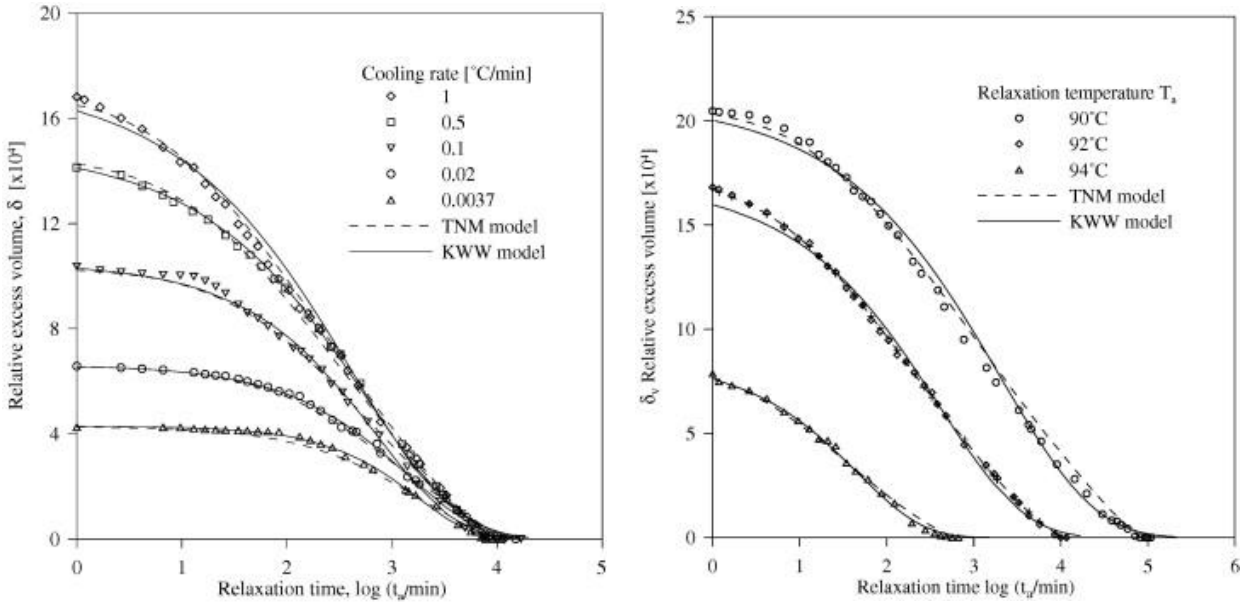

(a) **(b)**

Figure 8 Isothermal volume relaxation of polystyrene with aging time, (a) after varying cooling rate, and (b) at different aging temperatures [29]

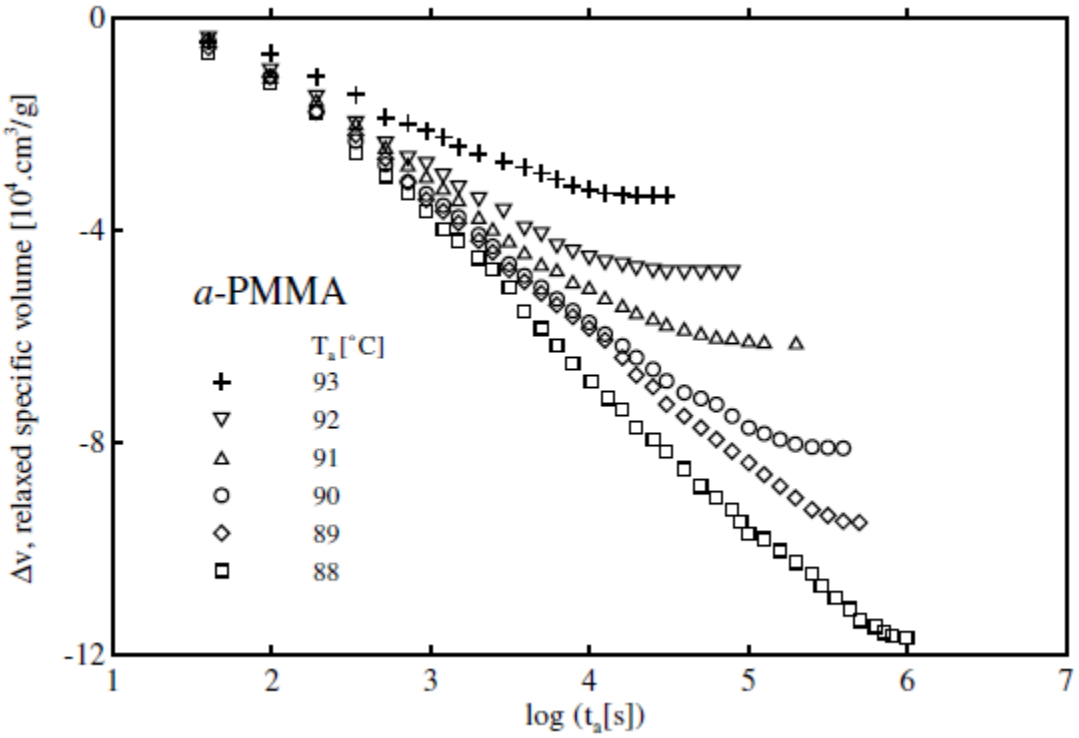

Figure 9 Isothermal specific volume change for a-PMMA at different aging temperature [50]

Adachi and Kotaka [27] showed that the molecular weight distribution does not significantly affect the rate of volume relaxation, with no particular change of behavior observed between broad and narrow distributions. A slight decrease in volume relaxation was noted with increasing molecular weight. They indicated the agreement of these observations with the usually small effect of molecular weight distribution on mechanical properties in the glass transition region. The authors also observed a "memory effect" when increasing aging temperature at a stepwise fashion, such that volume originally increased, before subsequently decreasing toward the equilibrium volume. Later researchers have also noted an asymmetry between aging when cooled or heated to the aging temperature [31, 50] (Figure 11).

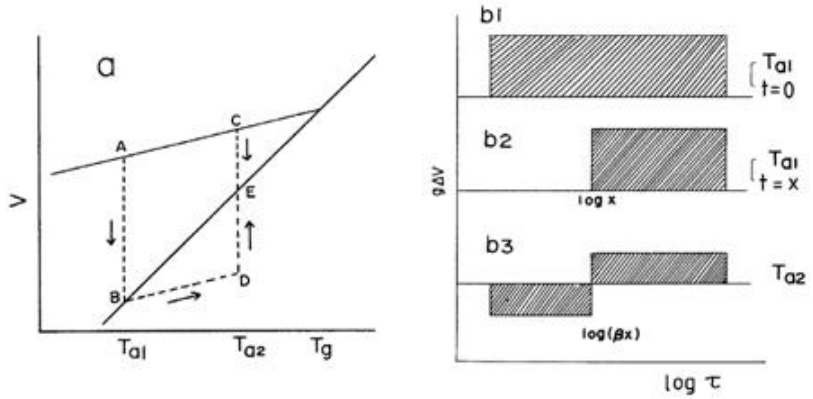

(a) Temperature dependence of specific volume.
(b1) Spectrum of $g\Delta V$ at T_{a1} immediately following the first temperature jump.
(b2) The spectrum after annealing for x seconds at T_{a1}.
(b3) The spectrum immediately following the second temperature jump from T_{a1} to T_{a2}. The parameter β is the factor for correction of the temperature dependence of the relaxation time.

Figure 10 Volume relaxation during stepwise increase of aging temperature [27]

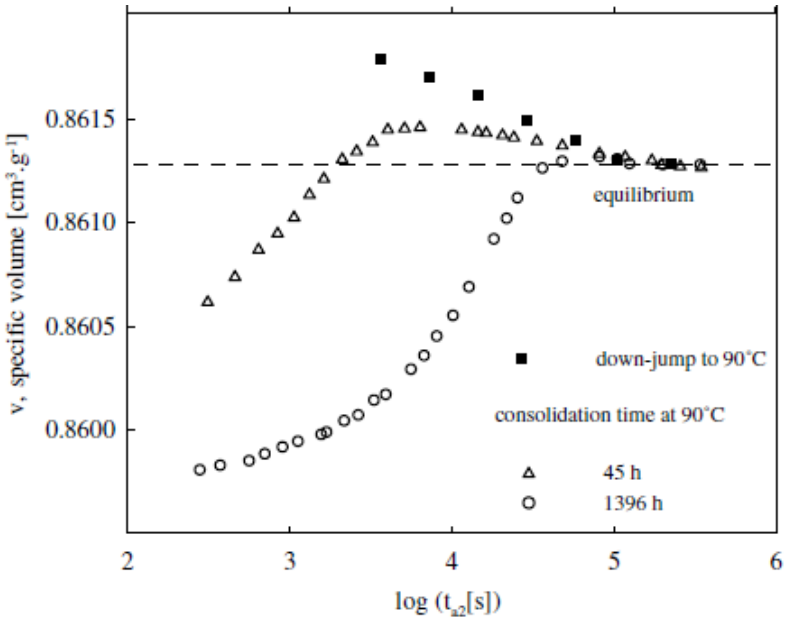

Figure 11 Asymmetry in volume relaxation between jump-up and jump-down to aging temperature for a-PMMA [50]

2.3. Physical Hardening of Asphalt

The time dependent hardening of asphalt binders has been recognized and studied in asphalt binders since the 1930s. Traxler studied the phenomenon at intermediate temperatures, calling it age- or time-hardening [55, 56]. Time dependent hardening was observed near the glass transition temperature of asphalt binders during the Strategic Highway Research Program (SHRP) contract A002-A and was referred to as "physical hardening" by the researchers [3, 9]. It was shown that this phenomenon causes an increase in the asphalt binder stiffness when stored at a constant low temperature. The SHRP researchers attributed this phenomenon to the rate of collapse of inter-molecular "free volume" in the binder, as described by Struik for amorphous materials [3, 9, 25, 57, 58, 59]. Traxler described this phenomenon as reversible progressive hardening of asphalt over time that "varies markedly by the type and source" of the binder [55, 56]. He believed the phenomenon to be thixotropic by nature due to the reversibility of hardening upon application of shearing stress [56]. Brown et al. [60] further studied the time dependent hardening of asphalt at ambient temperatures, referring to the phenomenon as "steric hardening". He attributed this hardening to the formation of internal structures in the asphaltene fraction of the binder [60]. Some researchers have also associated physical hardening with the crystalline domain and wax fraction of the asphalt binder [5, 6, 8].

Bahia and Anderson found that the approach used to account for the effect of changing temperature in viscoelastic materials (i.e., time-temperature superposition principle) can be applied to the stiffening effect of physical hardening with conditioning time by using a shift factor on the time scale [9].

The study of physical hardening during the SHRP program resulted in a requirement in the M320 specification [61] of testing in the Bending Beam Rheometer (BBR) after 1 and 24 hours. Although this requirement was not implemented [62], recent work by Hesp and Subramani [63] has shown that better correlations with field performance are observed if physical hardening is taken into account. The importance of accounting for physical hardening was also discussed by Basu et al. [64], in which the Superpave assumption of the general applicability of a 10°C time-temperature superposition shift factor was found to be very inaccurate for unconditioned binders, but accuracy was observed to greatly improve after 72 hrs of isothermal conditioning. One of the main reasons physical hardening has been neglected is the absence of a reliable and simple procedure to estimate the changes in properties (e.g., creep stiffness and m-value) of binders caused by this phenomenon from relatively short and simple laboratory tests.

Romero et al. [16] investigated the effect of different mineral fillers and different volumetric properties on the physical hardening of asphalt mixture using the Thermal Stress Restrained Specimen Test (TSRST). The authors concluded that fracture rather than strength properties are affected by physical hardening. They also concluded that it cannot be inferred that a mixture will show the effects of physical hardening solely based on the binder exhibiting changes during testing after low-temperature isothermal storage. It must be noted that the researchers conditioned the specimens in unrestrained conditions, thus the stress buildup due to isothermal contraction was not considered in the conclusions.

Researchers such as Shenoy [65] have claimed that stress relaxation in the binder phase in mixtures can cancel out any effect of physical hardening in mixtures, thus believing the phenomenon to be of no practical importance. Recent studies by others such as Falchetto et al.,

[66] and Evans and Hesp [67] have concluded otherwise. Falchetto and his co-workers measured the increase in stiffness in both binder and mixture BBR beams, showing that the semi-empirical Hirsch model can be used to predict the hardening of the mixture beams based on the binder beam hardening [68]. Evans and Hesp [67] showed that binders that had higher BBR grade loss after 72 hrs of conditioning retained more residual stress after relaxation. These researchers believe that inconclusive results pertaining to the importance of physical hardening in mixture performance, is due to shortcomings and difficulties associated with the current Thermal Stress Restrained Specimen Test (TSRST) method used for low temperature performance assessment in asphalt mixtures.

2.4. Mechanism of Physical Hardening

Although many researchers agree upon the effects of physical hardening, there is some disagreement about the exact mechanism responsible for this phenomenon as well as the temperature range in which physical hardening occurs [3, 9, 57, 58, 59, 25, 69, 70]. Some researchers have reported on the dependence of the hardening rate on the chemical composition of the asphalt binder (e.g., length of molecular chains and wax content) [71, 72, 4]. Although some researchers believe that the time dependent hardening observed in ambient room temperatures and near the binder's glass transition temperature are the same phenomenon, namely "steric hardening" [69], the difference in attributed mechanisms to these two temperature ranges has led other researchers to differentiate between the two phenomena [70, 58, 57].

Studies by Doolittle [73], Doolittle and Doolittle [74], and Williams et al. [75] showed that the internal mobility of amorphous materials is better related to the free volume rather than temperature. Based on this concept, Struik [25] described the occurrence of physical hardening

to be the consequence of isothermal reduction of free volume at temperatures close to the glass transition temperature. He showed that physical hardening causes an increase in stiffness and a reduction of the stress relaxation capacity in amorphous materials [25].

Struik described the total volume of the material as being constituted by a fraction of occupied volume, which is the volume of molecules and their vibrational motion, and a fraction of free volume due to packing irregularities. As the amorphous material is cooled, the molecular mobility and the molecular free volume decrease simultaneously. Since molecules attract to each other and free volume consists of voids within the molecules, the existence of free volume represents an increase in internal energy with respect to the zero-free volume state. The existence of free volume is accompanied by an increase in entropy. Thus, the increase in internal energy due to free volume must be balanced with $T \cdot \Delta S$, where T is temperature and ΔS is the change in entropy. The rate of this process is determined by the molecular mobility which itself is a function of the free volume [25]. The aforementioned mechanism proposed by Struik implies that the rate of physical hardening is closely related to the material temperature.

The free volume cannot decrease indefinitely as temperature decreases, and at a certain temperature, mobility becomes very small and consequently the decrease in free volume becomes insignificant at the imposed rate of temperature differential. This temperature is referred to as the glass transition temperature, T_g. The small values of molecular mobility at temperatures below T_g indicates that the volume continues to decrease very slowly over time [25].

Anderson and Marasteanu [5] showed that physical hardening in asphalt binders occurs both above and below the glass transition temperature, in contrast to amorphous polymers, for

which physical hardening occurs only below T_g [25, 76]. The data presented in their study supported the hypothesis that physical hardening is caused in addition to free volume collapse by the formation of crystalline fractions, as proposed by Claudy, Planche and other researchers [3, 72, 4, 5]. The authors showed that asphalt binders with higher wax content show stronger physical hardening effects both above and below their T_g.

Glass transition temperature is commonly considered as the temperature at which the two asymptotes to the linear regions on the volume-temperature curve intersect (Figure 12). However, the glassy transition begins well before this point (i.e., where the material starts to deviate from thermodynamic equilibrium), thus according to the free volume concept physical hardening will occur as the material enters this transition region. In the glass transition region the asphalt binder is in a meta-stable state (i.e., not in thermodynamic equilibrium) in which first order properties, such as entropy, remain continuous but second order properties, such as coefficients of thermal expansion/contraction and heat capacity, are discontinuous [9, 57, 58, 59, 5, 76].

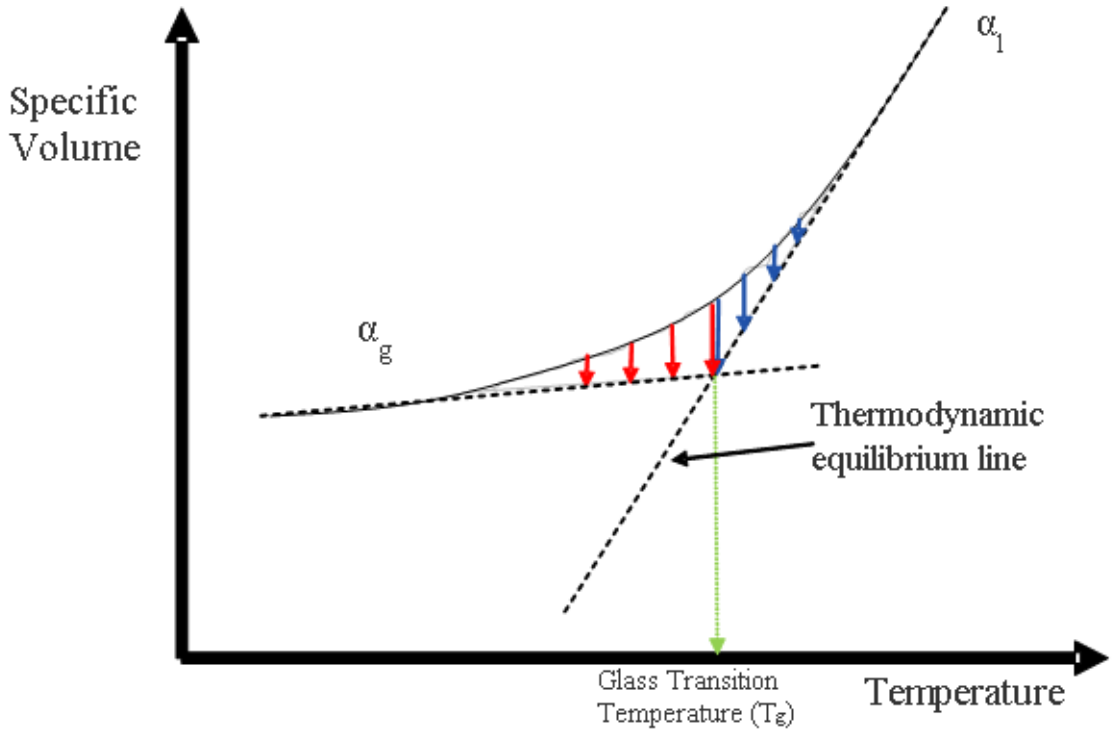

Figure 12 Schematic of proposed material behavior in glass transition region.

Some researchers have observed multiple glass transitions in asphalt binders, attributed to the multi-phase nature of asphalt. In these studies it is postulated that the T_g of asphalt is the result of the overlap of several smaller transitions due to different asphalt fractions [77, 78]. In this study, dilatometric measurements of the glass transition temperature in the range of 30 to -50°C clearly showed one major glass transition in the binder. Other smaller transitions existing in the temperature range may be too small to be detected by this method. In the present study, it is hypothesized that this major glass transition, whether resulting from multiple fraction transitions or only one, is mainly responsible for the measurable physical hardening observed in asphalt binders at low service temperatures.

2.5. Thermal Cracking and Failure Properties of Asphalt Pavements

Asphalt thermal cracking studies have traditionally focused on limiting strength values as the temperature decreases in the pavement, thus predicting crack occurrence temperature based on the comparison between the predicted thermal tensile stress curve and the ultimate tensile strength on a temperature axis [79, 80, 81]. The basic principal is shown in Figure 13. Stress calculation methodologies used have included elastic, pseudo-elastic, and viscoelastic analysis on a beam or slab.

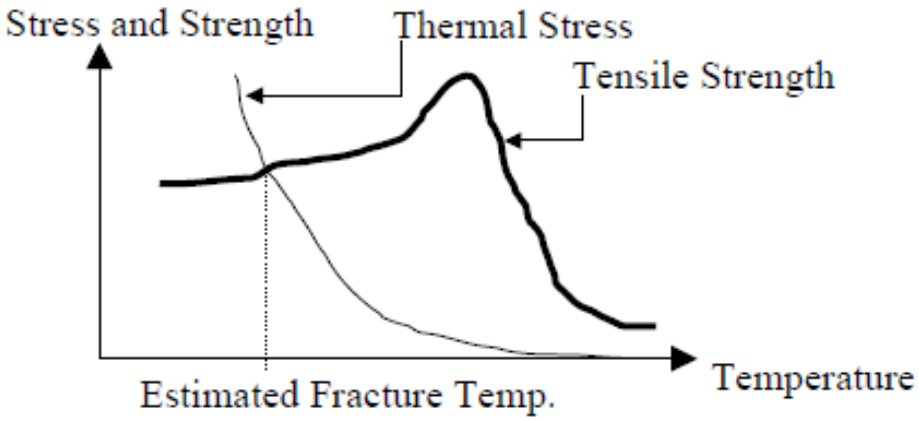

Figure 13 Estimation of low temperature cracking temperature [79]

Alternatively, some researchers have used crack tip stress calculations for a pre-cracked pavement and subsequent comparison with estimated pavement fracture toughness through Linear Elastic Fracture Mechanics (LEFM), to predict cracking temperature and crack propagation in the pavement. In this method the pavement layer is discretized into a number of sub-layers or beams, for which the stress is calculated similar to the approach discussed above, based on temperature in each sub-layer, resulting in a stress gradient estimation for the whole layer [82]. This approach was used in the development of the SHRP thermal cracking model, the

TC-Model used in the Mechanistic Empirical Design Guide (MEPDG). Arguments against this approach include the initiation of pavement thermal cracks from an un-cracked condition; and that the precedence of the actual cracks with micro-cracking, thus there is no well-defined crack tip and furthermore a significant process zone exists, contrary to the assumptions used in LEFM [83].

2.5.1. Failure Properties in Viscoelastic Materials

The study of stress and strain response in viscoelastic materials in not a new topic, and has been investigated at length for many decades. Theoretical solution and constitutive equations have been developed for almost any loading geometry and time-temperature condition, taking into account temperature and rate dependency, and more recently non-linear viscoelasticity. In contrast to the current state of relative theoretical robustness in constitutive relationships of viscoelastic materials, the study and prediction of failure in viscoelastic materials is still as much dependent on empiricism as to sound mechanistic concepts. To some extent this is due to the reliance of such mechanisms on inter-molecular interactions that are difficult to quantify and even more difficult to expand to mechanical behavior of material [84, 85].

A failure prediction method that has received less attention in recent years is the use of "Failure Envelopes," developed based on the ultimate failure stress and strain of viscoelastic materials in various conditions. This section summarizes some of the important research carried out in developing failure criteria and failure envelopes, as well as how such concepts have been employed in the study of asphalt concrete.

Researchers have shown that for linear viscoelastic material time temperature superposition is not only applicable to measurements of viscosity and stiffness, but to various

other physical properties, provided they involve the same molecular motions governing the viscoelastic stiffness properties [84, 85]. This is illustrated in Figure 14 and Figure 15 in which the shift factors used to construct the creep compliance master curve for a viscoelastic polymer are shown to also be applicable to the failure stress and failure strain [84]. This property has also been shown for other elastomeric polymers such as Styrene Butadiene Rubber (SBR) [84, 85].

Such observations have led some researchers to the idea that for viscoelastic materials a "failure strength envelope" could be plotted as a function of ultimate strain [86]. A failure envelope is developed by plotting failure stress against strain at reduced strain rates [86, 84]. Furthermore, the applicability of time temperature superposition to failure stress and strain in viscoelastic material implies that the viscoelastic response of the amorphous chains dominates failure properties [84].

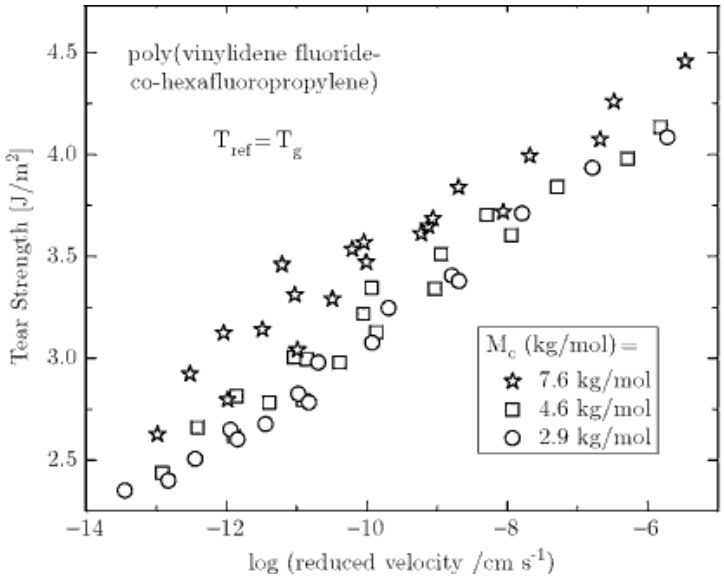

Figure 14 Fracture energy of an elastomeric polymer plotted against time temperature-shifted cross-head speed (original measurements over 2 decades of rate, shifted to cover 7 decades) [84].

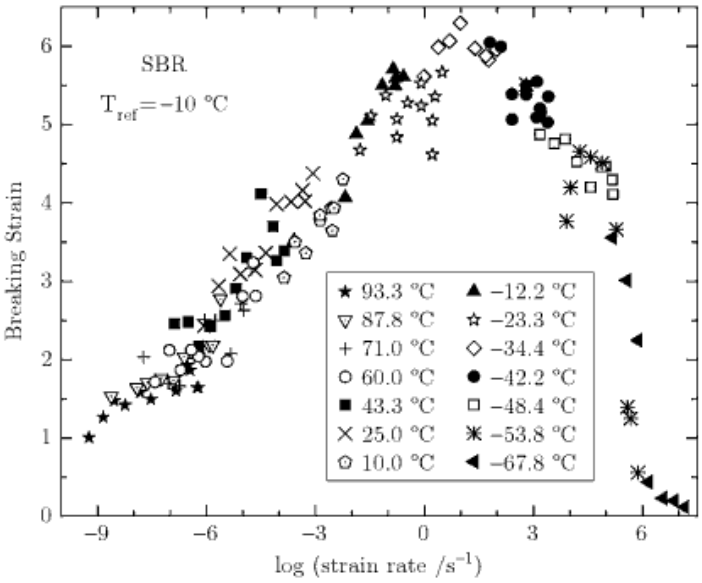

Figure 15 Strain at Failure for SBR plotted against reduced strain rate [84]

One of the first researchers to study the failure behavior of viscoelastic materials in terms of a failure envelope was Smith [86]. Smith created a failure envelope by plotting σ_f 263/T against 100ε_f in a log-log scale, in which σ_f and ε_f are stress and strain at failure and T is degrees Kelvin (Figure 16). He showed that for SBR, the failure envelope defined at one strain rate but multiple temperatures may be matched to that obtained by testing at various strain rates but a single temperature.

Many researchers studying viscoelastic fracture have shown that there is a close dependency between failure stress and strain rate, such that the stress decreases monotonically as the strain rate is decreased. On the other hand, researchers have observed the existence of a "definite maximum strain at failure" for viscoelastic material tested to failure at different strain rates [84, 85, 86, 87]. The strain at failure increases as the strain rate decreases down to a certain strain rate, after which any decrease in strain rate will cause the strain at failure decrease [85].

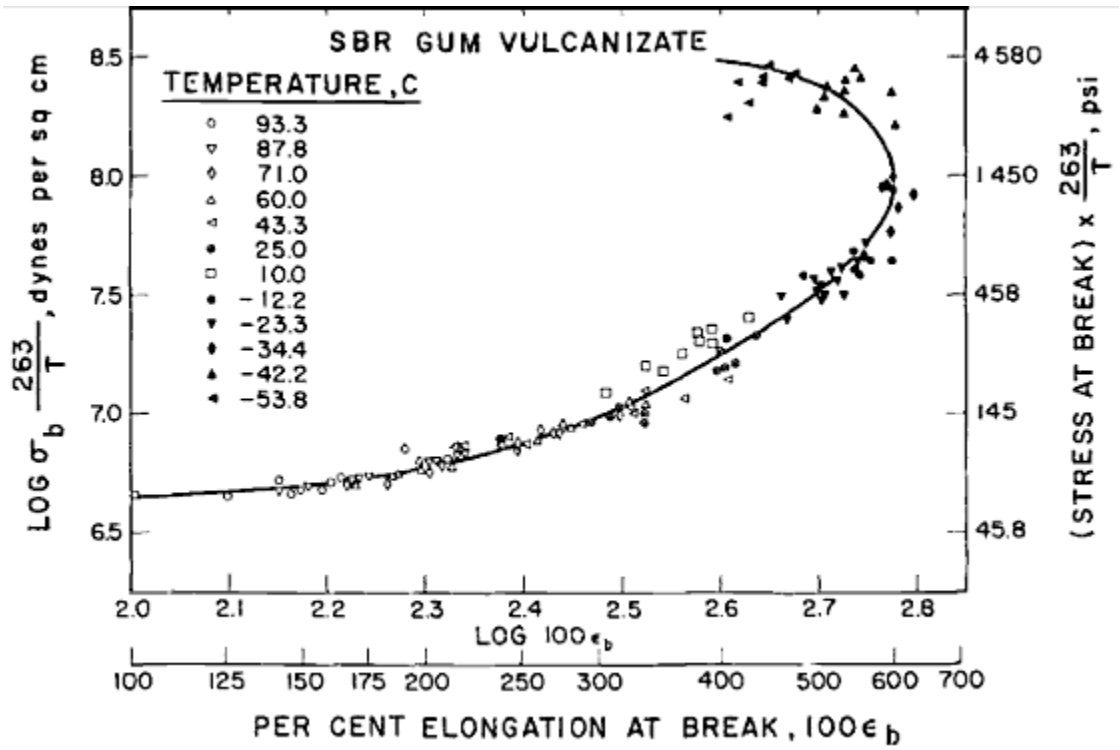

Figure 16 Failure envelope created by plotting failure stress at reduced strain rates against failure strain [86]

Based on experimental observations and using knowledge of the dependency of failure to behavior in the molecular level of materials, Zak [85] developed the following simple uniaxial failure envelope for viscoelastic materials.

$$\sigma_f = A10^{-k\frac{\epsilon_f}{\sigma_f \lambda_f}} \qquad [1]$$

In which A and k are regression constants, σ_f and ε_f are stress and strain at failure, and λ_f is the material extension at the point of failure. The relationship was shown to fit well with elastomeric polymers such as SBR. The key feature of this theory is its ability to predict a maximum failure strain that is not exceeded no matter the imposed strain rate.

Another early researcher focused on failure envelopes of viscoelastic materials was Dong [87]. Dong developed a simple envelope function for 2 dimensional axial stress problems as

shown in [2], which he further developed to account for multi-axial stress problems in three dimensions.

2.5.2. Failure Envelopes in Asphalt Mixtures

Studies in the asphalt community on development and implementation of failure envelopes for asphalt mixtures have been performed since the early 60s. Most early studies focused on the use of the “Smith Failure Envelope” [86], showing that such an envelope in many instances works sufficiently well for asphalt mixtures [88, 13]. A study by Bynum and Traxler [88] showed that the smith criterion for failure could be fitted to failure data in both tension and compression for asphalt mixtures tested at various temperatures (Figure 17). They also noticed that increasing the mixing and compaction temperatures above normal ranges increased failure stress but decreased ultimate failure strain in the tested asphalt mixtures. Due to a change of over 2 orders of magnitude in failure stress compared to a change of a factor of 3 in the ultimate failure strain as temperature was varied, the authored concluded that failure stress is not a suitable criterion for asphalt mixture failure, while normalized failure strain could be adopted as proper failure criterion.

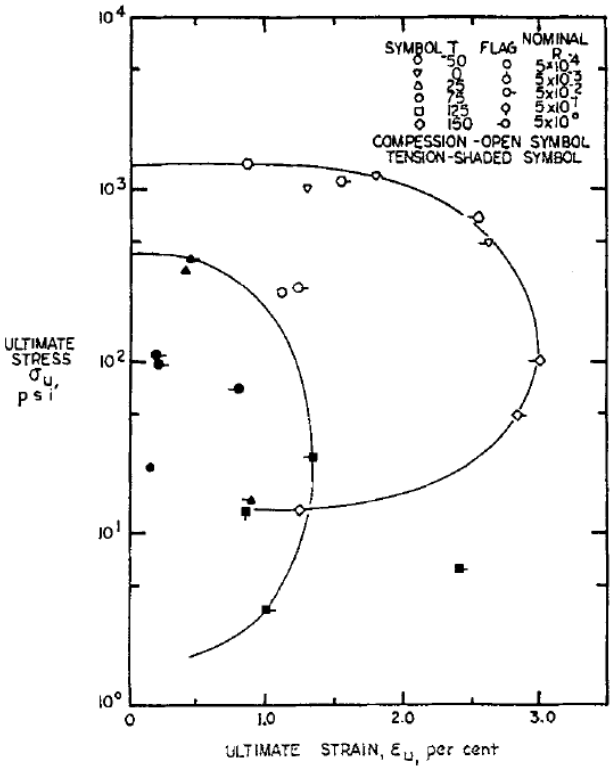

Figure 17 Asphalt concrete failure results in tension and compression fitted using the Smith failure criterion (4)

Monismith et al. also showed that asphalt concrete failure stress at different temperatures, strain rates and test conditions behaved in a fashion similar to that described by Smith [86, 13]. Figure 18 shows a failure envelope developed for asphalt pavement tested at different temperatures and conditions. The higher stress levels correspond to lower test temperatures and higher strain rates. It can also be seen that failure for samples tested under constant strain can be plotted on the same failure envelope as those tested at the same temperature but under constant stress.

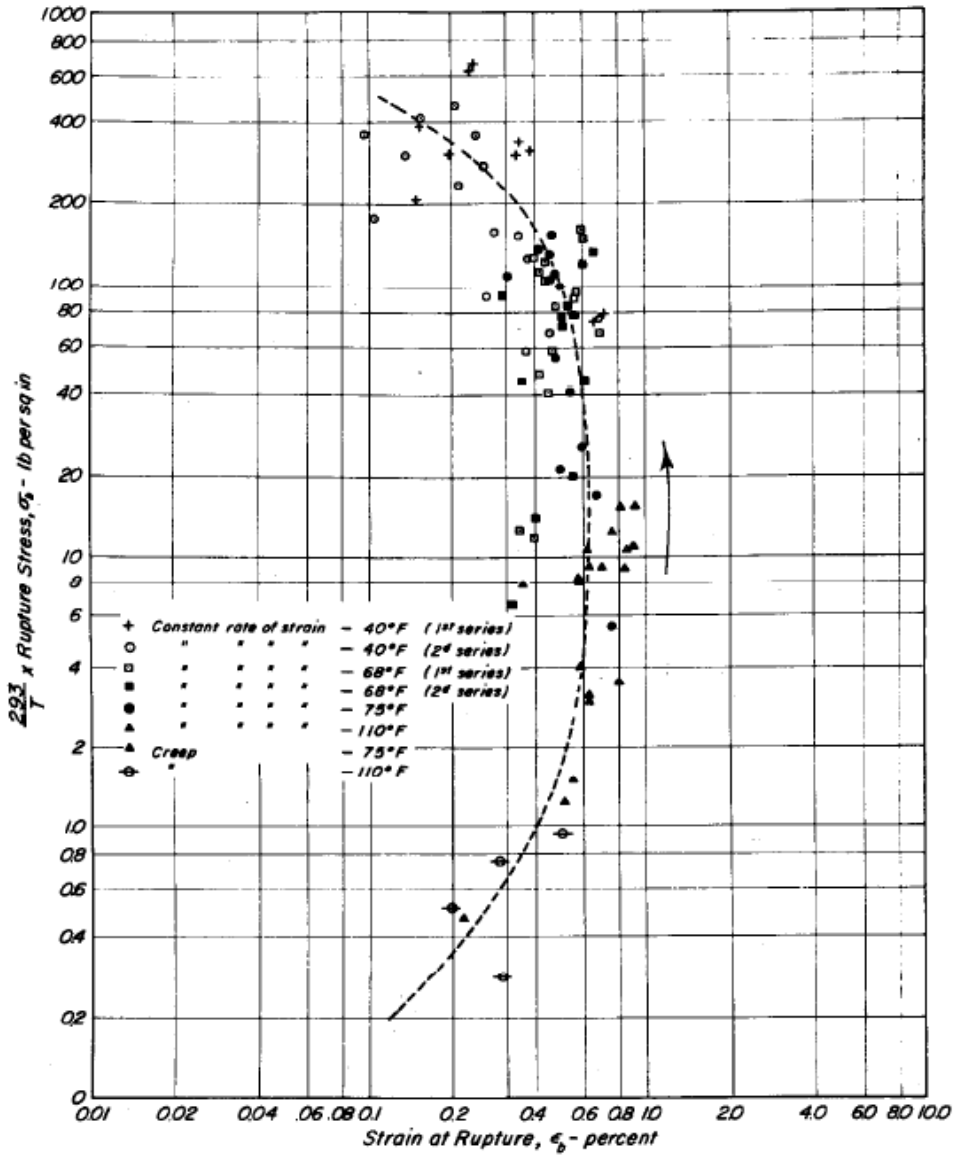

Figure 18 Failure results for asphalt samples tested under constant strain rate or stress at different temperatures [13]

A potential area of interest when considering failure envelopes is the application to prediction of thermal cracking. Although some researchers have previously used such methods for comparison of thermal stress buildup and predicted point of fracture based on failure envelopes [89] (Figure 19), such analysis raises a few challenges. The foremost question is how to handle the constantly varying temperature and consequently the varying modulus for in thermal cracking.

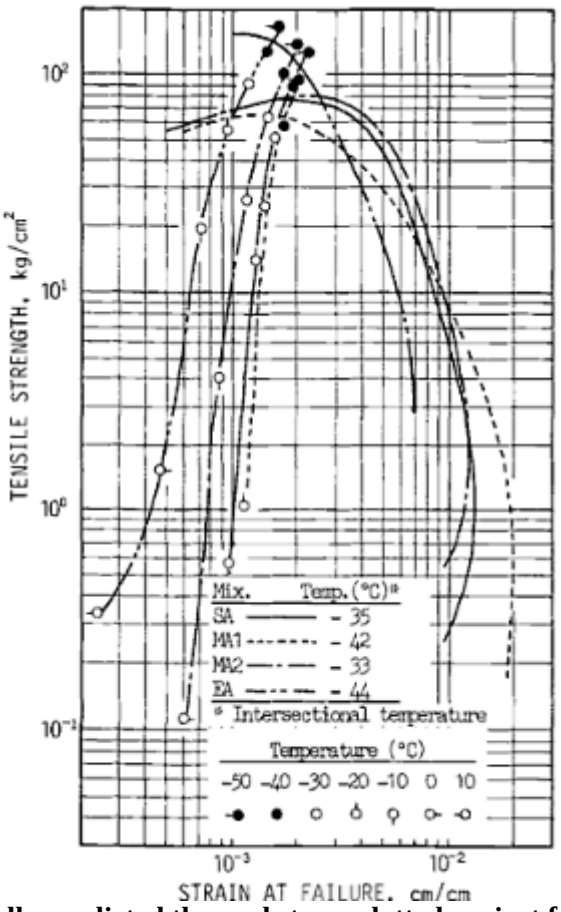

Figure 19 Theoretically predicted thermal stress plotted against failure envelopes [89]

Although a failure envelope as discussed before should be applicable for any range of strain rates and temperatures, thus rendering it a valid criterion for thermal stress problems, challenge is in defining the position of the thermal failure with regards to the envelope. One may investigate the usage of time-temperature shifting to reduce the test temperature and the strain rate to a reference temperature and constant rate. The accuracy of such an approach would need to be evaluated experimentally.

3. Methods and Materials

3.1. Materials

The results used in this thesis were collected for various projects. To verify that physical hardening affect mixture performance asphalt mixtures were collected from a large field project in Minnesota. Table 1 includes the description of the loose asphalt mixtures that were collected from field pavement sections in Minnesota, USA and compacted using the Superpave Gyratory compactor targeting typical design parameters. The asphalt binders and aggregates used for production of these mixes represent typical materials placed in pavements in the mid-west. As indicated in Table 1, asphalt binders placed in these sections were modified with commonly used chemical and polymer additives.

Table 1 Description of Asphalt Mixtures Tested.

Asphalt Mixture	Location	Description
PG58-34 PPA	MnROAD 33	Modified with Polyphosphoric Acid (PPA)
PG58-34 SBS+Acid	MnROAD 34	Modified with Styrene-Butadiene Styrene (SBS) and PPA
PG58-34 SBS	MnROAD 35	Modified with SBS
PG58-34 Elvaloy +Acid	MnROAD 77	Modified with PPA and Elvaloy
PG58-28	MnROAD 20	Neat
PG58-34	MnROAD 22	Unknown modification
Wisconsin	Wisconsin	Binder used in construction of SMA pavement
PG 58-28 (VAL)	MN CR 112	Valero binder
PG 58-28 (CIT)	MN CR 112	CITGO binder

To develop a model for physical hardening of binders, a set of published results were used as well as new data were generated. Results published for the eight core SHRP binders at thin film oven (TFO) aged condition, and results measured for seven binders obtained from MnROAD test sections and aged using the rotating thin film oven (RTFO), were used in the development and validation of the prediction model. In addition to the aforementioned binders, an additional 40 binders from a study conducted by Lu and Isacsson [69] were used to develop

the concepts behind the model. The binders studied cover a wide range of neat and modified binders, including binders modified with different types and combinations of Styrene Butadiene Styrene (SBS), Elvaloy® and Polyphosphoric Acid (PPA).

3.2. Binder Test Methods

Binders were tested using a dilatometric glass transition (Tg) measurement method, the Superpave Bending Beam Rheometer (BBR) and Single Edge Notch Beam (SENB) fracture test method. The Tg measurements were used to determine the glass transition range using a given cooling rate. The BBR tests include tests run during an extended conditioning period at different temperatures near the glass transition ranges for the various binders. Similar test were ran using the SENB. The purpose of these tests is to determine the change in creep stiffness and relaxation (as measured by the BBR creep stiffness and m-value) as well as the effect of continued conditioning on fracture properties as measured by the SENB. It is hypothesized that at temperatures approaching the glass transition, physical hardening may have a counter effect on relaxation of the binders, thus affecting the expected performance. The extent of this change and its potential importance is assessed using these tests. The results are also used in the theoretical explanation of the mixture stress buildup and relaxation as measured by the ATCA.

3.2.1. Measurement of Physical Hardening Using the Bending Beam Rheometer

The measurements of physical hardening were obtained by using the Bending Beam Rheometer (BBR), following AASHTO T 313 [71], and measuring the change in creep stiffness (i.e., S(t)) and the m-value (i.e., m(t)) of asphalt binder beams with isothermal age at different temperatures. The m-value is the slope of the curve of the creep stiffness (S(t)) and loading time, plotted on a log-log scale. The Superpave specification sets criterion limits for the values of the

creep stiffness and m-value at 60 seconds of BBR creep loading, designated S(60) and m(60), respectively. The asphalt binder beams from the MnROAD cells were tested after isothermal conditioning at -12, -18 and -24°C; the SHRP binders were tested at -10, -15, -25, and -35°C; and the binders studied by Lu and Isacsson [69] were tested at -15, -25, and -35°C. BBR creep stiffness, S(t), was measured at different intervals during conditioning, ranging from 1 to 96 hrs. Table 2 shows the binder BBR tests conducted for this study.

Table 2 BBR tests on binders

Binder Type	Temperature (°C)	Conditioning Times	Reported Parameters
Neat 1 (PG XX-22)	-12, -18, -24	1, 6, 24, 48, 72 hrs	S(t), m-value
Neat 3 (PG XX-28)	-12, -18, -24	1, 6, 24, 48, 72 hrs	S(t), m-value
Modified (PG XX-34)	-12, -18, -24	1, 6, 24, 48, 72 hrs	S(t), m-value
SBS Modified	-12, -18, -24	1, 6, 24, 48, 72 hrs	S(t), m-value
Elvaloy Modified	-12, -18, -24	1, 6, 24, 48, 72 hrs	S(t), m-value
PPA Modified	-12, -18, -24	1, 6, 24, 48, 72 hrs	S(t), m-value
Warm Mix Additive	-12, -18, -24	1, 6, 24, 48, 72 hrs	S(t), m-value
Neat 2 (PG-22)	-12, -18, -24	1, 2, 4, 6, 24, 48 hrs	S(t), m-value
Neat 2 + Granite filler	-12, -18, -24	1, 2, 4, 6, 24, 48 hrs	S(t), m-value
Neat 2 + Dolomite filler	-12, -18, -24	1, 2, 4, 6, 24, 48 hrs	S(t), m-value
Neat 2 + Limestone filler	-12, -18, -24	1, 2, 4, 6, 24, 48 hrs	S(t), m-value
VAL MN CR 112	Binder Tg	1, 2, 24, 46 hrs	S(t), m-value
MTN MN CR 112	Binder Tg	1, 2, 24, 46 hrs	S(t), m-value
CAN MN CR 112	Binder Tg	1, 2, 24, 46 hrs	S(t), m-value
CIT MN CR 112	Binder Tg	1, 2, 24, 46 hrs	S(t), m-value

3.2.2. Glass Transition (T_g) Test Procedure

A dilatometric system was used to measure the glass transition temperature of the asphalt binders. Currently no formal standard for this device is available and therefore the test was performed following a modified version of the procedure developed by Bahia and Anderson [57]. The concept behind the procedure is based on precise measurements of volume change in time for an asphalt binder specimen, as temperature is decreased at a constant rate. The binder sample is prepared by pouring 10 g of hot asphalt into a circular silicone rubber mold with a

diameter of 40 mm and a height of 8.0 mm. The dilatometric cell is connected to a vertical capillary tube (inner diameter is 1 mm) with its top end open. The volume change in the sample is calculated by estimating the change in the height of the ethyl alcohol column inside the capillary tube. In this study, the system was further modified by using a very precise pressure transducer to measure the changes in alcohol column height. Table 3 shows the binder tests conducted for this study.

Table 3 Binder glass transition tests

Binder Type	Temperature range (°C)	Cooling Rate	Reported Parameters
Neat1 (PG XX-22)	30 to -50	1°C/min	Tg, α_l, α_g
Neat2 (PG XX-22)	30 to -50	1°C/min	Tg, α_l, α_g
Neat3 (PG XX-28)	30 to -50	1°C/min	Tg, α_l, α_g
Modified (PG XX-34)	30 to -50	1°C/min	Tg, α_l, α_g
SBS Modified	30 to -50	1°C/min	Tg, α_l, α_g
Elvaloy Modified	30 to -50	1°C/min	Tg, α_l, α_g
PPA Modified	30 to -50	1°C/min	Tg, α_l, α_g
Neat 2 + Granite filler	30 to -50	1°C/min	Tg, α_l, α_g
Neat 2 + Dolomite filler	30 to -50	1°C/min	Tg, α_l, α_g
Neat 2 + Limestone filler	30 to -50	1°C/min	Tg, α_l, α_g
VAL MN CR 112	30 to -50	1°C/min	Tg, α_l, α_g
MTN MN CR 112	30 to -50	1°C/min	Tg, α_l, α_g
CAN MN CR 112	30 to -50	1°C/min	Tg, α_l, α_g
CIT MN CR 112	30 to -50	1°C/min	Tg, α_l, α_g

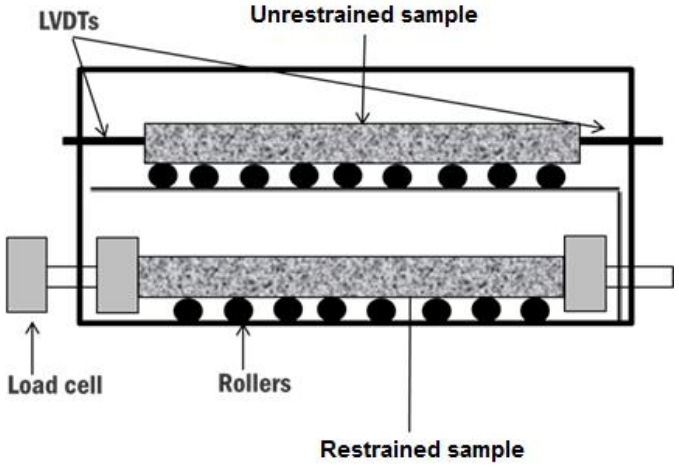

Figure 20 Illustration of the Asphalt Thermal Cracking Analyzer (ATCA)

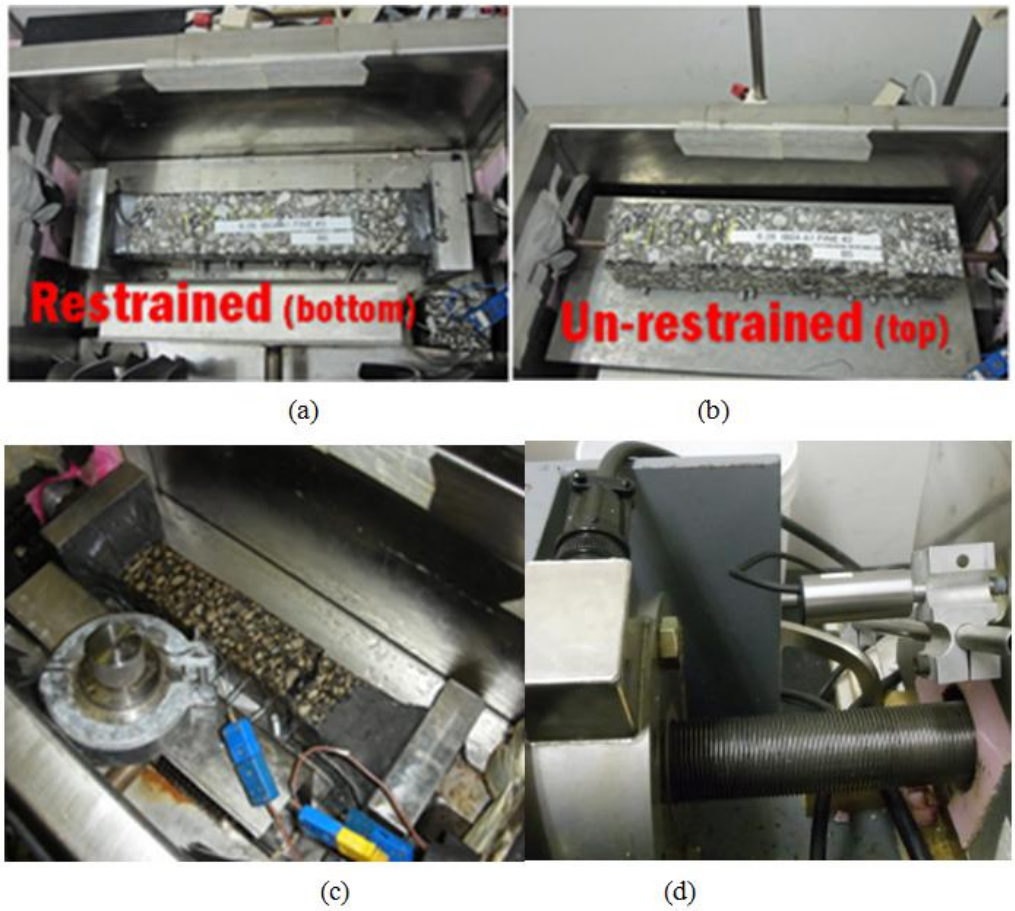

Figure 21 (a) Restrained beam setup, (b) unrestrained beam setup, (c) restrained beam after failure, and (d) load cell and LVDT's.

In this study the preparation of the beam samples was modified to use the Superpave Gyratory Compactor (SGC). The unrestrained and restrained samples are produced from one SGC sample. Using a masonry saw, four prismatic beams of 5 by 5-cm in cross section and 15 cm long are cut from 17 cm gyratory samples. Two of these beams are sawed in half to produce four 7.5 cm blocks. By gluing a 7.5 cm block to each end of the two 15 cm blocks, two 30 cm beams are produced (Figure 22). As both beams are produced from the same sample and both are exposed to the same thermal history, the stress build-up, glass transition temperature, α_l and α_g

can be used to get a comprehensive picture of the low temperature performance of the asphalt mixture.

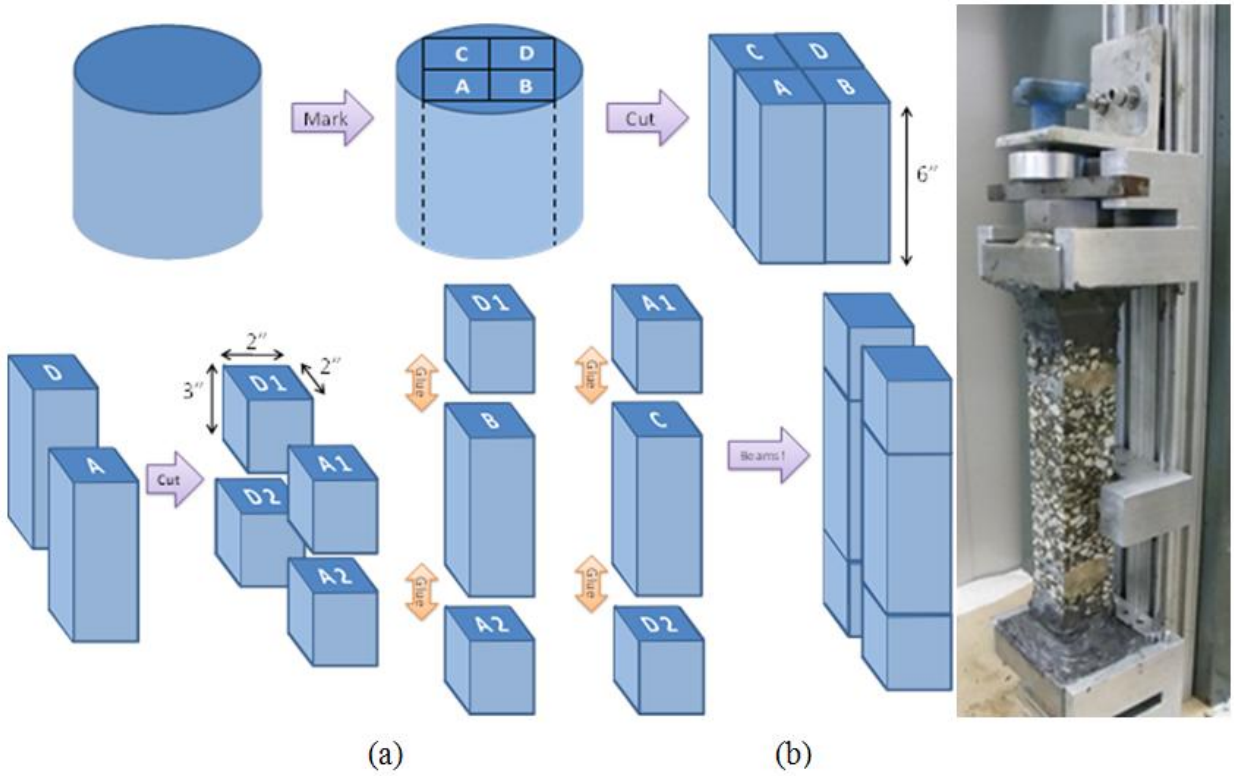

Figure 22 (a) Cutting of SGC sample for ACTA testing. (b) Sample gluing setup

Tests are conducted on both asphalt mixture and binders. The newly developed Asphalt Thermal Cracking Analyzer (ATCA) will be used to measure the Glass Transition properties, coefficients of thermal expansion/contraction, Thermal stress buildup and mixture critical cracking temperature and strength. A series of pilot tests were performed to determine the ideal cooling rate and relaxation temperature for the samples. Table 4, Table 5, and Table 6 show the tests proposed for asphalt mixtures in the present study.

Table 4 ATCA mixture glass transition tests

Mixture Binder Type	Temperature range (°C)	Cooling Rate	Reported Parameters
Neat 1 (PG XX-22)	30 to -70	1°C/min	Tg, α_l, α_g
Neat 2 (PG XX-22)	30 to -70	0.1, 1°C/min	Tg, α_l, α_g
Neat 3 (PG XX-28)	30 to -70	1°C/min	Tg, α_l, α_g
Modified (PG XX-34)	30 to -70	1°C/min	Tg, α_l, α_g
SBS Modified	30 to -70	1°C/min	Tg, α_l, α_g
Elvaloy Modified	30 to -70	1°C/min	Tg, α_l, α_g
PPA Modified	30 to -70	1°C/min	Tg, α_l, α_g
Neat 2 Plastomer modified	30 to -70	0.1, 1°C/min	Tg, α_l, α_g
VAL MN CR 112	30 to -70	1°C/min	Tg, α_l, α_g
CIT MN CR 112	30 to -70	1°C/min	Tg, α_l, α_g

Table 5 ATCA thermal stress and relaxation tests

Mixture Binder Type	Isothermal Conditioning Temperature (°C)	Cooling Rate	Reported Parameters
Neat1 (PG XX-22)	-20	1°C/min	Stress, Strain
Modified (PG XX-34)	-20	1°C/min	Stress, Strain
SBS Modified	-20	1°C/min	Stress, Strain
Elvaloy Modified	-20	1°C/min	Stress, Strain
PPA Modified	-20	1°C/min	Stress, Strain
Warm Mix Additive	-20	1°C/min	Stress, Strain
VAL MN CR 112	-20	1°C/min	Stress, Strain
CIT MN CR 112	-20	1°C/min	Stress, Strain

Table 6 ATCA mixture failure tests

Mixture Binder Type	Temperature range (°C)	Cooling Rate	Reported Parameters
Neat 1 (PG XX-22)	30 to -70	1°C/min	Failure Stress, Strain
Neat 2 (PG XX-22)	30 to -70	0.1, 1°C/min	Failure Stress, Strain
Neat 3 (PG XX-28)	30 to -70	1°C/min	Failure Stress, Strain
Modified (PG XX-34)	30 to -70	1°C/min	Failure Stress, Strain
SBS Modified	30 to -70	1°C/min	Failure Stress, Strain
Elvaloy Modified	30 to -70	1°C/min	Failure Stress, Strain
Neat 2 Plastomer modified	30 to -70	0.1, 1°C/min	Failure Stress, Strain

4. Importance of Physical Hardening in Performance of Asphalt Mixtures

4.1. Overview

Asphalt is known to undergo significant time-dependent stiffening when stored at low temperatures. This phenomenon, often referred to as physical hardening, has been shown to have significant impact on the laboratory performance of asphalt binders. However, the importance of isothermal conditioning for asphalt and its effect on thermal cracking performance has been a subject of debate.

This chapter summarizes testing conducted to investigate the effects of cooling rate and isothermal conditioning on thermal stress buildup and relaxation of different asphalt materials obtained from field pavement sections in MnROAD, Minnesota, USA [90].

Tests performed using the ATCA at different cooling rates and various relaxation periods showed that at high cooling rates, isothermal contraction significantly affects the rate of thermal stress buildup. Furthermore, contrary to the expectation of full stress relaxation for visco-elastic materials, the thermal stress in restrained samples held at isothermal conditions for extended periods of time did not completely relax, converging to a constant residual stress. Fracture of specimens held isothermally occurred at a temperature higher than fracture temperature measured when specimen is monotonically cooled down. These results indicate that physical hardening may be responsible for unexpected thermal cracking observed in the field. The findings show the need to measure the glass transition of the asphalt binder, their behavior under isothermal conditioning, and the use of realistic cooling rates for better prediction of thermal cracking.

4.2. Physical Hardening in Asphalt Mixtures

Using the ATCA, cooling and relaxation experiments were carried out at different rates, isothermal temperatures and isothermal relaxation times. For all experiments thermal stress was observed to build up as the temperature decreases in the restrained beam. Temperature reduction was stopped at a predefined temperature to start the isothermal stage. Although the temperature measured at the core of the mixture sample was kept constant, the sample stress continued to build up even after the core temperature had stabilized. Isothermal contraction was also observed simultaneously in the unrestrained beam. As the isothermal conditions continued, the stress gradually started to relax. This trend, which was observed for all mixture samples tested, is shown in Figure 23 in which two identical mixture samples were cooled to -20°C and then held isothermally for 5 and 10 hrs. It is observed that after the initial isothermal stress buildup, the rate of build-up gradually decreases, followed by a relaxation of stress until stabilizing at a constant value over time.

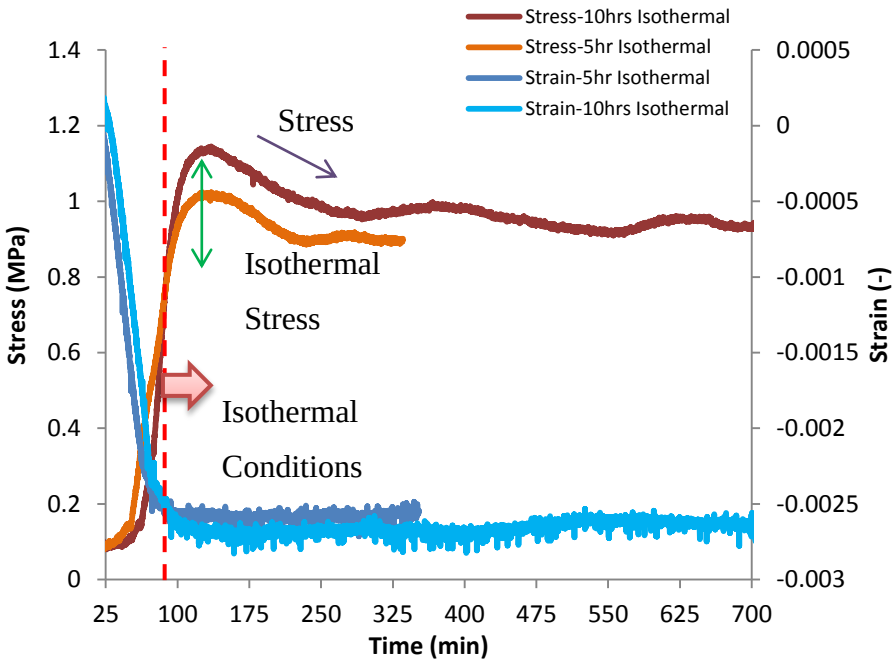

Figure 23 Isothermal stress behavior in asphalt mixture after 5 and 10 hrs of isothermal conditions.

To further evaluate the effects of time, cooling rates were varied while measuring stress and strain. Results of such experiment is shown in Figure 24, in which it can be noted that the amount of isothermal stress (Figure 24b) and strain (Figure 24a) buildup are dependent on the rate of cooling. When a rate of 0.1°C/min (6°C/hr) was used as much as 10% of the ultimate stress continued to build up after achieving a stable core temperature (Figure 24b). On the other hand at an extremely fast cooling rate of 1°C/min, most of the stress was built-up during the isothermal stage of the test, and the specimen ultimately reached the same stress levels as with the slower rate, as indicated in Figure 24b. Tests performed at an intermediate rate of 0.5°C/min resulted in isothermal stress buildup in between the two extreme cooling rates.

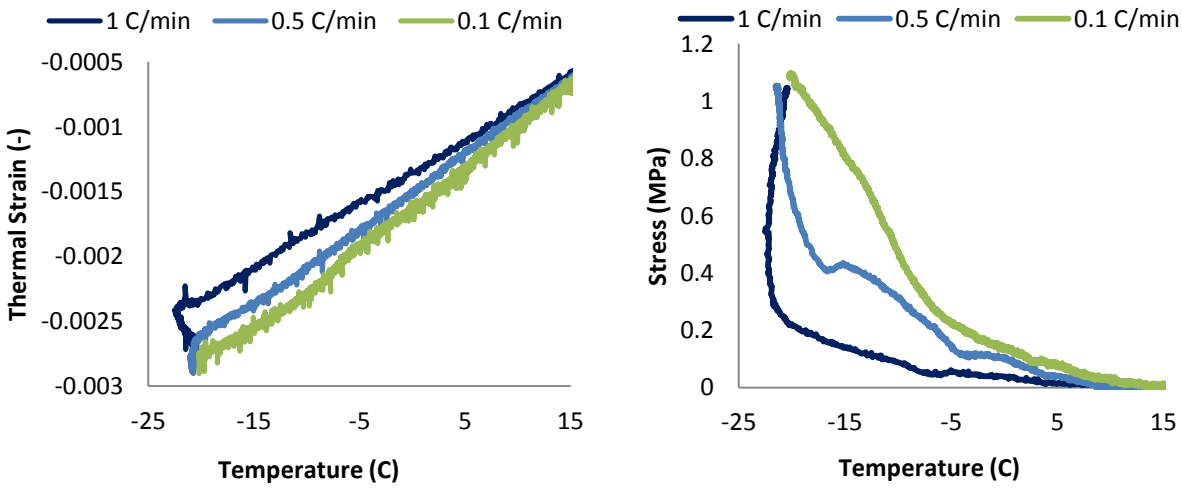

(a) **(b)**

Figure 24 Comparison of thermal stress and strain during cooling and isothermal conditions at 0.1, 0.5 and 1°C/min cooling rates.

Researchers in earlier studies have used many cooling rates to test and model field conditions. Bouldin et al. [10] used 3°C/hr to match studied field sections, while suggesting that resulting cracking temperature may be "bumped" up or down for faster and slower rates, respectively. Modeling by Bahia et al. [8] for rates lower than 10°C/hr showed that reducing cooling rate corresponded to a shift in thermal stress buildup toward lower temperatures. SHRP researchers reported that although typical field cooling rates seldom exceed 2.7°C/hr, most TSRST tests are done at rates of 10°C/hr or higher to reduce testing time [11]. Tests conducted during the SHRP study showed a decrease in fracture temperature as the cooling rate varied between 1 to 5°C/hr, while the effect on tensile strength varied for different samples. They noted that previous researchers reported little or no effect on fracture temperature and tensile strength for different cooling rates higher than 5°C/hr. They concluded that although these cooling rates do not necessarily match typical field conditions, they are sufficient to assess relative performance of specimens.

In this study, it is hypothesized that the observed isothermal behavior is due to the time-dependent nature of thermal contraction as temperature approaches the glass transition region. The complete explanation of the mechanism of glass transition and physical hardening is beyond scope of this paper and can be found in Bahia and Anderson [57], Tabatabaee et al. [91] and Bahia and Velasquez [92].

If cooling rate is sufficiently slow, the specimen has ample time to fully contract; but as the cooling rate increases, although core of samples can reach conditioning temperature, the amount of delayed contraction increases. The delayed contraction takes place over time after sample core reaches isothermal contraction, hence causing the specimen to buildup thermal stress while at a constant temperature. After sufficient time has passed, all samples achieve full

contraction, thus ultimately building up the same amount of thermal stress. An example of this behavior is shown in Figure 24(a) and (b).

An important consequence of the observed behavior is that thermal stress will build up at slower rate during cooling if the rate is high enough to not allow for complete contraction during the cooling period, as shown in Figure 25. Although at first glance this seems counter intuitive, it must be pointed out that for sufficiently slow cooling rates in which full contraction is taking place during cooling, the trend will be opposite, as the slower cooling rates will allow for more thermal stress relaxation and consequently a lower rate of stress build up during cooling. It is important to note that relaxation and time-dependent strain happen continuously and simultaneously during thermal loading. Depending on the relative rate of these two competing phenomenon at any given time, temperature, and cooling rate, one or the other will be dominant. Thus, an increase in thermal stress will result when time-dependent strain is accumulating at a rate higher than the decreasing effect of modulus relaxation, and vice versa.

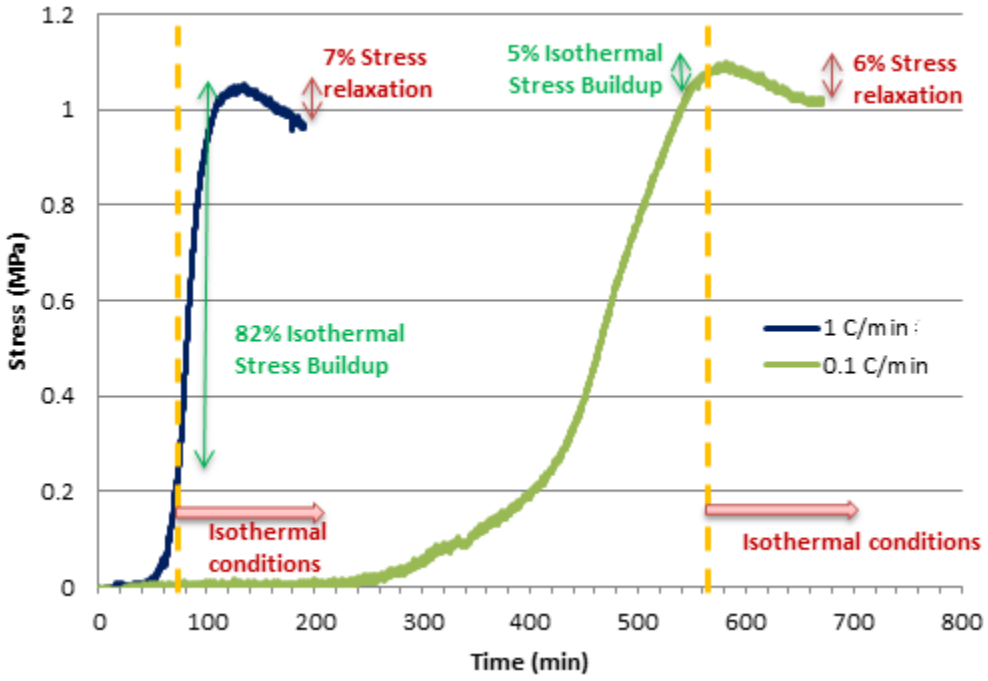

Figure 25 Comparison of thermal stress during cooling and isothermal conditions at 0.1 and 1°C/min cooling rates.

Figure 26 highlights a noteworthy observation during sample thermal stress buildup with and without isothermal conditioning. It can be seen that the trend of stress buildup when the temperature was decreased at a constant rate down to the point of cracking varies significantly from the sample which is cooled at the same rate but held isothermally at a certain temperature. The asphalt mixture beam held isothermally built up stress over time at a constant temperature to stress levels achieved at temperatures about 12°C lower when the sample was continually cooled (see Figure 26). This important observation points out the possibility of pavements cracking at temperatures well above what is expected, if held isothermally at low temperatures for a period of time.

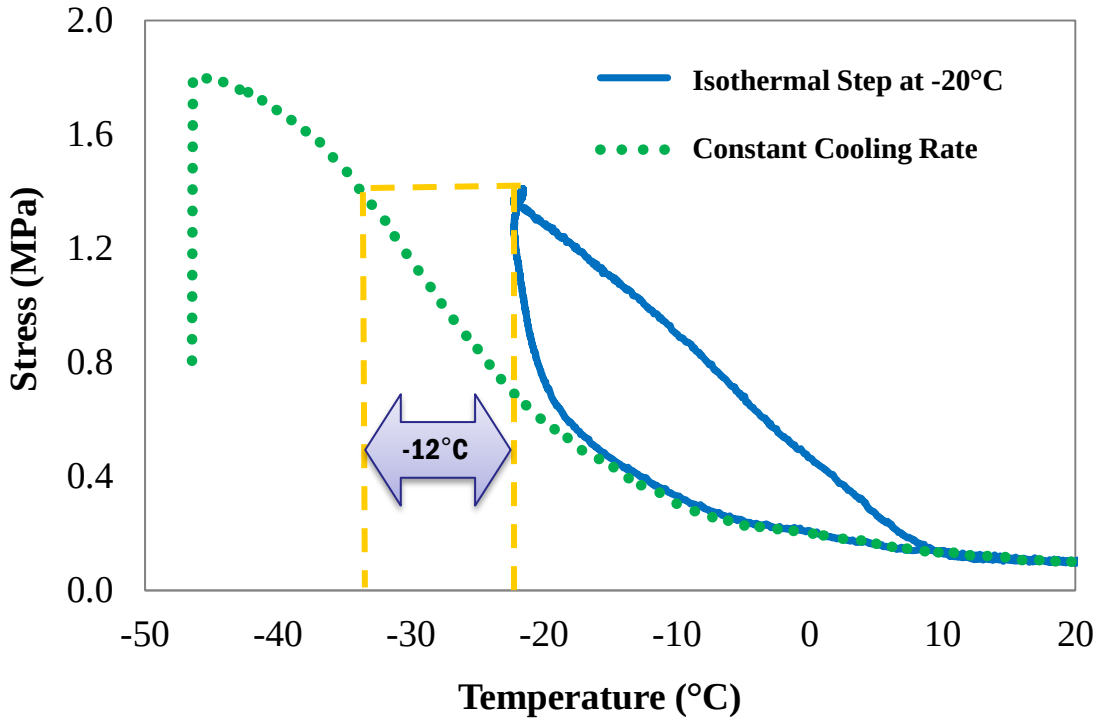

Figure 26 Typical stress build up in restrained beam using the ATCA, with and without the isothermal conditioning step.

Another important observation made during isothermal conditioning of various asphalt mixtures is shown in Figure 27 and Figure 28. It is observed that during isothermal conditions, mixture samples can reach a critical value of thermal stress that result in sample fracture. The importance of this observation becomes more apparent when considering that under continuous constant cooling these samples would not have built up this level of stress until temperatures well below the current fracture temperature. This may easily explain discrepancy between predicted low temperature cracking temperatures and observed under- performance in the field, underscoring the importance of considering the potential of isothermal contraction and time-dependent strain in asphalt material when selecting appropriate material for specific climatic conditions.

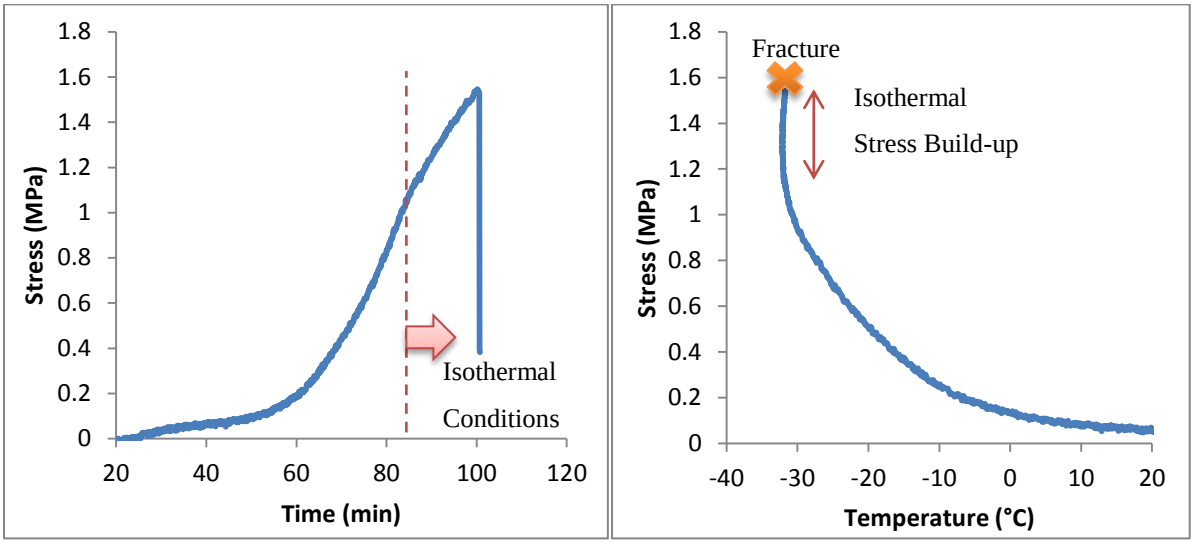

Figure 27 ATCA restrained beam fracture during isothermal conditions (MN County Road 112-Valero).

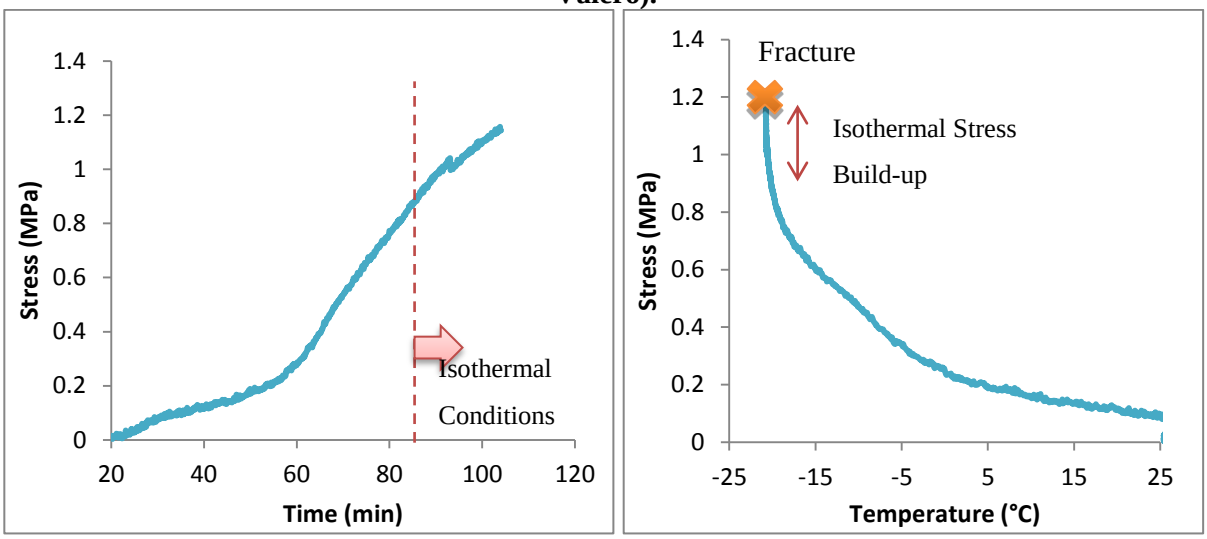

Figure 28 ATCA restrained beam fracture under isothermal conditions (MN County Road 112-CITGO).

The relationship between isothermal physical hardening of asphalt binders with that observed in asphalt mixtures was also investigated by comparing the performance of field sections constructed in a county road in Minnesota. Mixtures using binders of identical Superpave performance grades (PG 58-28) were used in the construction of the test sections. After being exposed to identical climatic conditions, one of the sections was observed to have cracked two times more than the others. Although various performance tests failed to

differentiate the asphalt binders significantly, physical hardening tests using both the Bending Beam Rheometer for the binders and the ATCA for the asphalt mixtures showed that one of the binders has considerably higher susceptibility to isothermal contraction than the other. This binder corresponds to the worse field performance, as indicated in Figure 29.

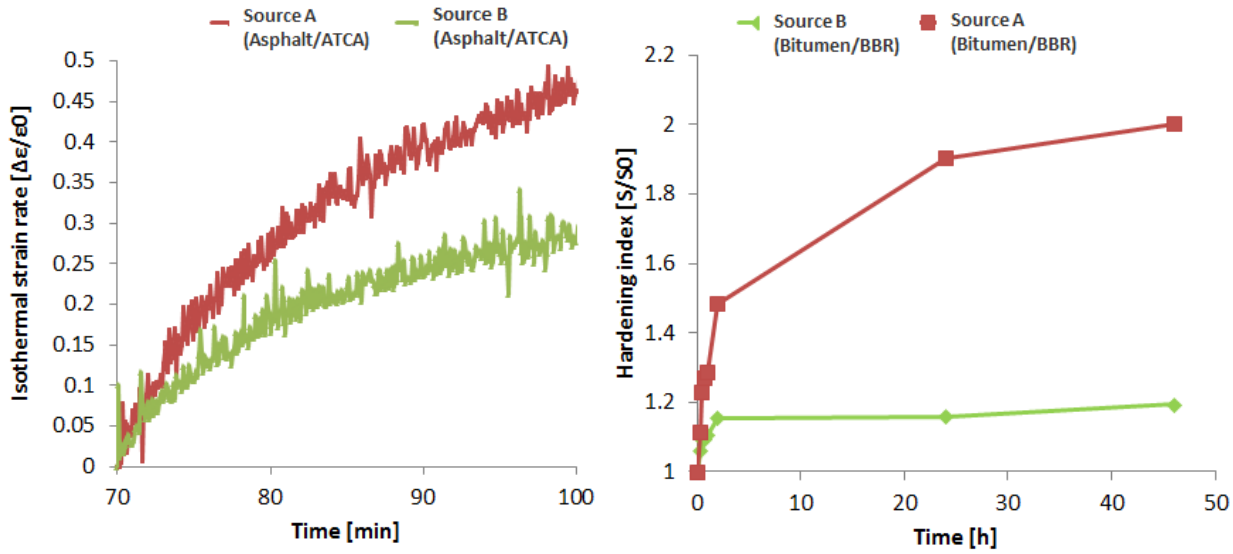

(a) **(b)**

Figure 29 Comparison of physical hardening susceptibility of two binders of identical Superpave performance grades through (a) testing the mixture in the ATCA, and (b) testing the binder in the BBR (S is BBR creep stiffness, S_0 is initial stiffness measurement).

5. Modeling Physical Hardening in Asphalt Materials

5.1. Overview

Although many researchers have recognized and measured physical hardening of asphalt binders, the factors that affect the rate of this phenomenon are not well defined, and there is no simple model for predicting its effects on binder rheology. The purpose of this chapter is to explain the factors affecting physical hardening in an asphalt binder, as the amorphous viscoelastic component of an asphalt pavement, and to propose a model in which the physical hardening of asphalt binders can be quantified and extended to different conditioning times and temperatures without lengthy tests.

Results from the experimental data produced as part of this study were combined with experimental data from previous studies to enable a broad analysis and derivation of conceptual conclusions regarding the nature of physical hardening in asphalt binders. Following the free volume concept, it is shown that physical hardening can be modeled as a function of isothermal time by a modified mechanical creep model. The model is used to predict physical hardening as a function of glass transition, conditioning time, and temperature. The findings and conclusions of this chapter serve as the basis for overall thermal cracking analysis framework that is further developed in the consequent chapters.

5.2. Quantification of Physical Hardening

Pavement material researchers have commonly used parameters based on the BBR creep stiffness, S(t), to assess the amount of physical hardening in asphalt binders. The most common parameter is the hardening index (i.e., S_i/S_0), defined as the ratio of the BBR creep stiffness after a specific conditioning time (t_i) to the initial creep stiffness, often measured after 1 hour of conditioning at the test temperature (t_o). In this study, the hardening index was modified to

reflect relative changes in stiffness, which will be called "hardening rate" ($\Delta S/S_0$). The change in stiffness (ΔS) is calculated as the difference in S(60) at time t_i to the initial S(60), which was measured after one hour of conditioning.

Material behavior trends were analyzed for the 55 binders included in the study, as a function of isothermal conditioning time and temperature. Although it is generally assumed that at lower isothermal condition temperatures the rate of physical hardening increases, the experimental data showed otherwise for many binders. For all SHRP binders, the hardening rate at -35°C was in fact less than the rate at -25°C. Lu and Isacsson [69] tested a wide array of modified and unmodified binders and observed that for three of the five tested base binders the maximum hardening index (i.e., S_i/S_0), was achieved at the lowest experimental temperature (i.e., -35°C), while for the other two base binders and their corresponding modified binders, the maximum index was observed at higher temperatures [69].

Thus from the total of 55 binders considered, 21 binders showed a decrease in hardening rate when the temperature decreased beyond a binder-specific temperature. The existence of a "peak" in the hardening rate as the temperature is decreased, and the subsequent decreasing rate of hardening observed in the experimental data, suggests that a limiting lower temperature may be reached at which physical hardening no longer takes place within experimental time. This was schematically shown in Figure 12 on page 31 of this document. Based on the free volume concept it may be inferred that when conditioning temperature is lower than this limiting temperature, the material volume no longer tends toward the original equilibrium line over time, instead it tends toward a state with a higher energy level than the theoretical thermodynamic equilibrium state. In other words it is hypothesized that the ultimate volume after physical

hardening ceases to take place is represented by the extension of the linear region on the specific volume-temperature curve that occurs below the glass transition region (Figure 12).

Based on this hypothesis in this dissertation it is suggested that the occurrence of measureable physical hardening within experimental time frames is limited to the glass transition region. Furthermore, the peak physical hardening rate would happen at the temperature specified by the intersection of the two asymptotic lines of the specific volume-temperature curve (Figure 12). At this point the molecular free volume level has the highest deviation from the two linear "non-transition" states. This temperature is commonly referred to as the "glass transition temperature". Thus any accurate prediction model for physical hardening should include the position of the target conditioning temperature relative to the glass transition region of the binder.

5.3. Model Development

5.3.1. Development of Model to Predict Physical Hardening

The proposed hardening model is based on concepts of rheological response of viscoelastic materials. In rheology, creep is defined as the progressive deformation under a constant stress. Creep in a linear material is a function of time only [93, 26]. One may describe creep as the gradual redistribution of the molecules or change in morphology, resulting in a decrease in the creep stiffness. Physical hardening can similarly be described as a time dependent change in the morphology due to deviation from thermodynamic equilibrium, causing increase in stiffness. The Burger's model is often used to model the creep behavior in asphalt:

$$\gamma(t) = \frac{\tau}{G_0} + \frac{\tau}{G_1}\left(1 - e^{-t\frac{G_1}{\eta_1}}\right) + \frac{\tau}{\eta_0}t \quad (1)$$

Where, $\gamma(t)$ is the strain as a function of loading time, t, τ is the applied stress, and G_0, G_1, η_0 and η_1 are the elastic and viscous material constants. Burger's model consists of a Maxwell and Kelvin models in series. At lower temperatures the effect of physical hardening can be described by the Kelvin model:

$$\gamma(t) = \frac{\tau}{G_1}\left(1 - e^{-t\frac{G_1}{\eta_1}}\right) \quad (2)$$

The basic property that changes during physical hardening is segmental or molecular mobility due to reduction of free volume; which is also claimed to be directly related to deformation under creep loading [25]. The amount of free volume controls molecular mobility, which in turn controls the rate of volume change which is responsible for the rate of hardening. Thus, the controlling factor in the hardening rate would be the volume difference relative to the equilibrium state, as previously shown in Figure 12. This difference increases as temperature approaches the glass transition temperature, after which it starts to decrease. This concept explains the mechanism behind the observed trend in hardening rate as temperature decreases.

A modified creep model can be adjusted to explain physical hardening behavior. In such a model, strain or relative change in deflection (i.e., $\Delta l/l_0$), can be replaced by relative change in volume, $\Delta V/V_0$, which according to the free volume concept can be taken to be directly proportional to relative change in stiffness, or hardening rate (i.e., $\Delta S/S_0$). Hardening rate can be measured in the laboratory using the BBR and thus used as input in the model in place of $\Delta V/V_0$.

Creep is usually driven by the stress of an applied load. In the physical hardening case, the "creep" can be considered to be induced by the excess internal energy due to the deviation of the material from thermodynamic equilibrium within the glass transition region, thus a "stress" parameter based on the relative position of the conditioning temperature from the glass transition

temperature, and the length of the glass transition region is used for the model. In this case the loading time corresponds to the conditioning time (t_c).

As described previously, the rate of physical hardening (i.e, $\Delta S/S_0$), peaks at a certain temperature, and decreases toward zero as the temperature approaches the beginning and the end of the glass transition region, as shown in Figure 30. This trend is taken into account to formulate the "stress" term for the hardening model. In this study, the following empirical equation was shown to fit the observed behavior of physical hardening very well:

$$\tau_T = e^{\frac{-9(T-T_g)^2}{2(x)^2}} \quad (3)$$

Where τ_T is the "stress" term as a function of the conditioning temperature, T. T_0 is the temperature at which physical hardening peaks, found to be equivalent to the glass transition temperature, thus hereby replaced by T_g,, and 2x is the length of the glass transition region.

From the experimental data it is recognized that the variation of τ_T around temperature T_g is not completely symmetrical, but is in fact slightly skewed toward the higher temperatures (resulting in a larger transition region below T_g), but for simplicity a symmetric formulation is used in (3). Figure 30 schematically explains the symmetry, as well as defining the parameter "2x". Using (2) and (3), the model can be rewritten as:

$$\gamma \approx \frac{\Delta V}{V_0} \approx \frac{\Delta S}{S_0} = \frac{e^{\frac{-9(T-T_g)^2}{(2x)^2}}}{G}\left(1 - e^{-t_c\frac{G}{\eta}}\right) \quad [4]$$

In which:

- $\frac{\Delta S}{S_0}$ is the hardening rate,

- $\frac{\Delta V}{V_0}$ is free volume relaxation rate,
- T_g is the glass transition temperature and peak temperature for hardening rate (°C),
- T is the conditioning temperature (°C),
- t_c is the conditioning time (hrs),
- $2x$ is the length of the temperature range of the glass transition region (°C), and
- G and η are model constants, derived by fitting the model

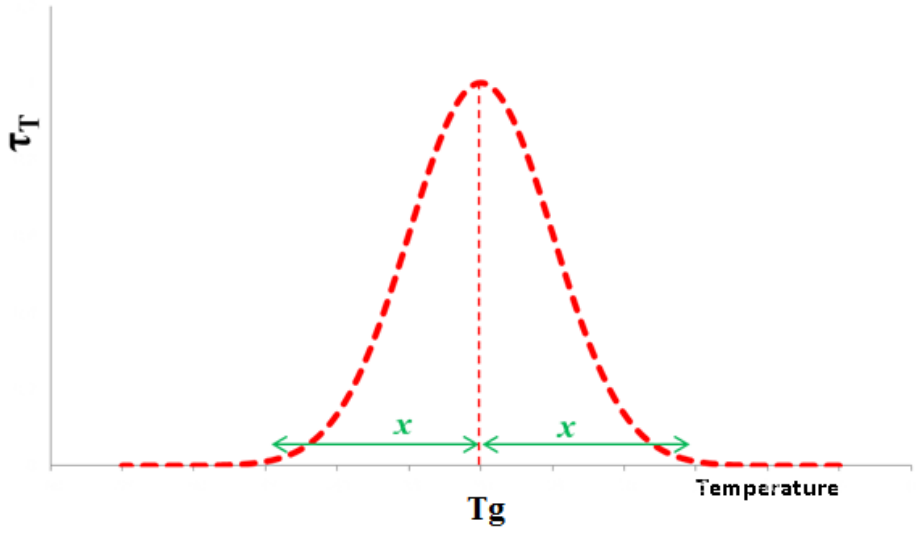

Figure 30 Empirical function used to account for glass transition temperature in prediction model. (2x is the length of the glass transition region)

A three-dimensional representation of the physical hardening as a function of conditioning time and temperature is shown in Figure 31.

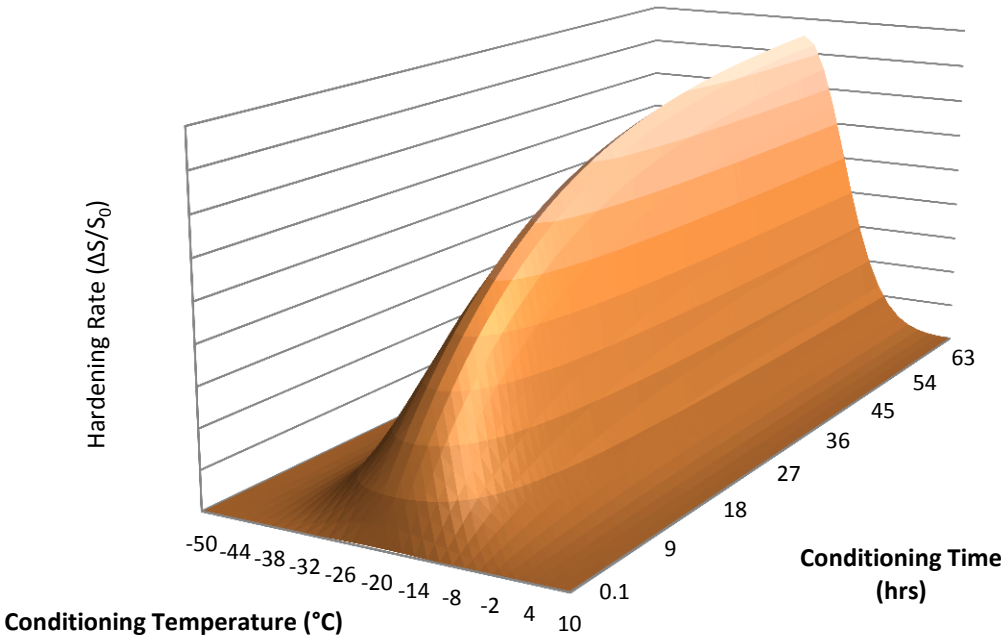

Figure 31 3-D representation of the physical hardening model for a glass transition temperature of -20°C

This model was fitted to the experimental data using the least squared errors, using T_g (the glass transition temperature) measured using the dilatometric method reported by Bahia and Anderson [57] and allowing the model to fit the length of the glass transition region to the data. As shown in Figure 32 through Figure 34, the results closely predict the experimental data. Furthermore, the model predicted a decrease in hardening rate as the temperature passed the glass transition temperature, as was evident in the experimental data from the samples conditioned at -35°C. A goodness of fit of 92% observed between measured and predicted hardening rates for the 8-core SHRP binders indicates the validity of assuming the glass transition temperature to be the peak temperature for the rate of physical hardening (Figure 33).

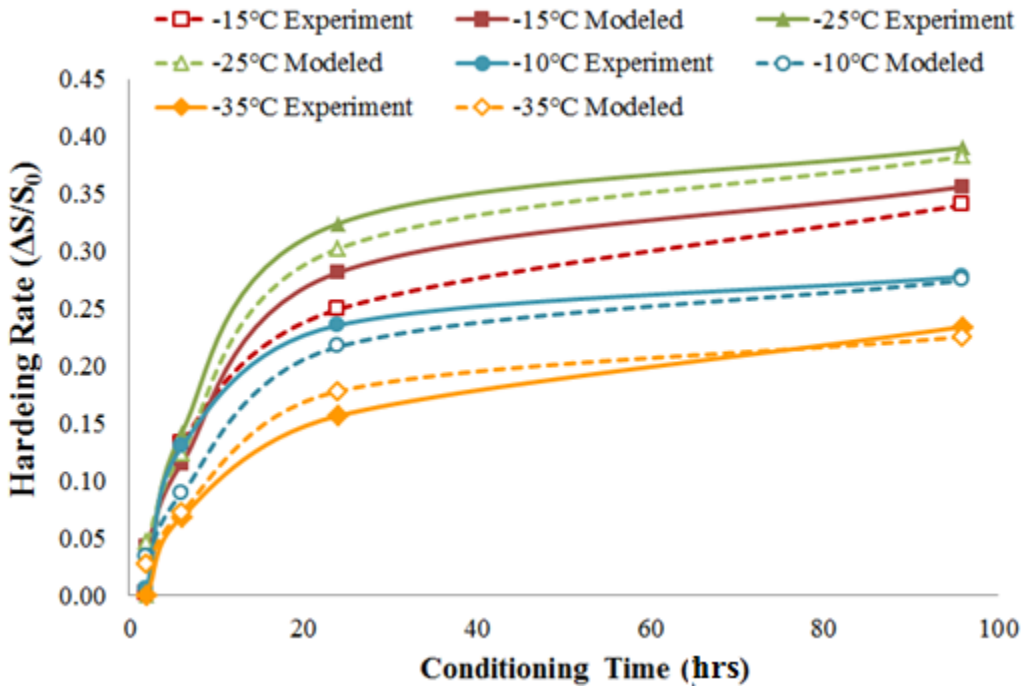

Figure 32 Comparison of model described by (4) with experimental data. (Hardening rate= ΔS/S0)

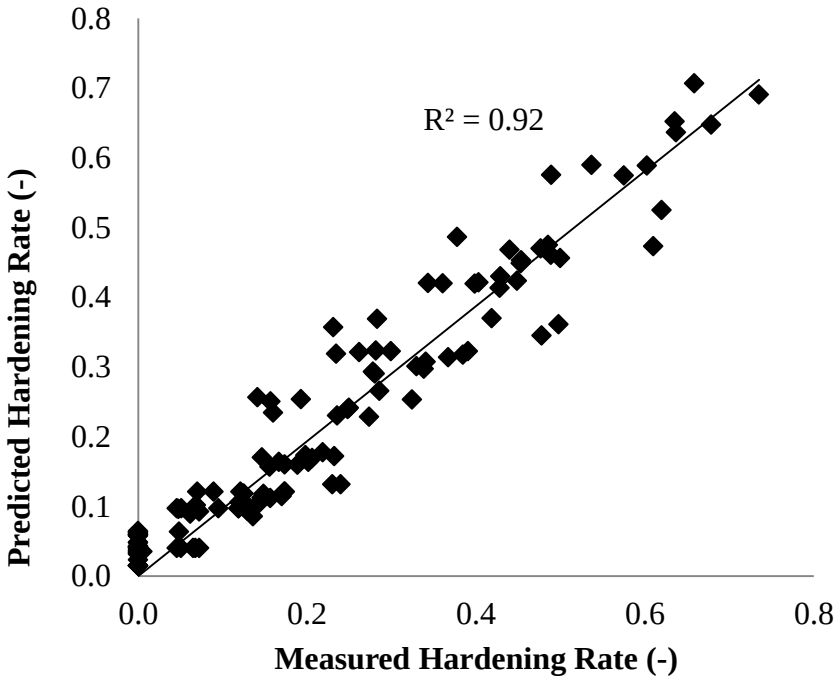

Figure 33 Goodness of fit between the predictions using Equation (4) using T_g for T_0 and the experimental data. (Hardening rate= ΔS/S0)

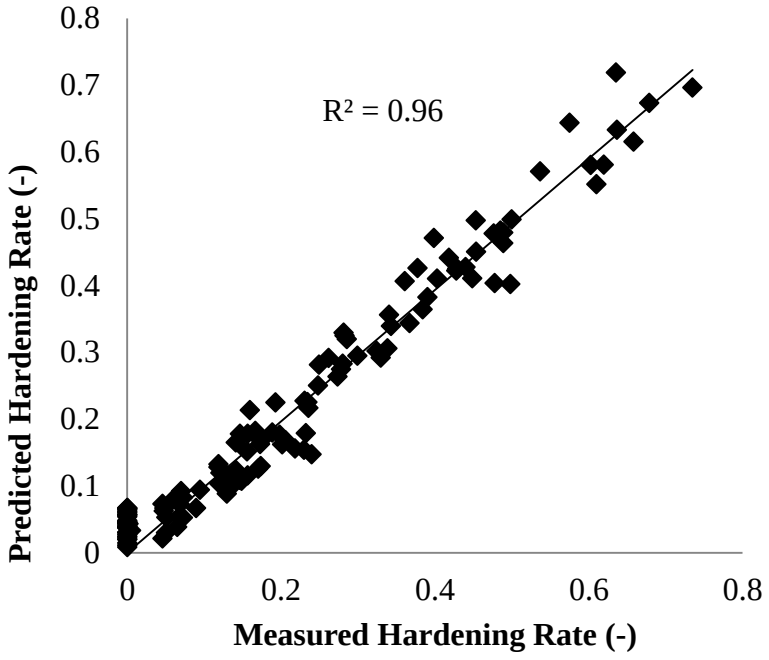

Figure 34 Goodness of fit between model described by (4) with fitted T0 and experimental data. (Hardening rate= ΔS/S0)

In a second set of runs instead of using the glass transition temperature as the peak temperature, the model was allowed to find the peak temperature based on the best fit to the experimental data. The resulting fitted peak temperatures were only within a few degrees of the measured glass transition temperatures. This indicates that if BBR data from a few testing temperatures is available; the model can be used to estimate the T_g from the experimental hardening rate data. Figure 34 shows the goodness of fit of the model for fitted values. Figure 35 shows the experimental and modeled trend of hardening rate after 24 hrs of conditioning against the difference between the conditioning temperature and the fitted T0. It can be seen that the hypothesized bell shaped trend shown in Figure 30 resembles the experimental data in Figure 35. A similar trend can also be observed in data reported by Planche et al. [4].

It must be noted that for every binder, G and η are unique material parameters which are independent of temperature and conditioning time. Thus, by fitting the model to data from a single temperature, one may use the resulting G and η to predict the physical hardening at any other temperature or conditioning time.

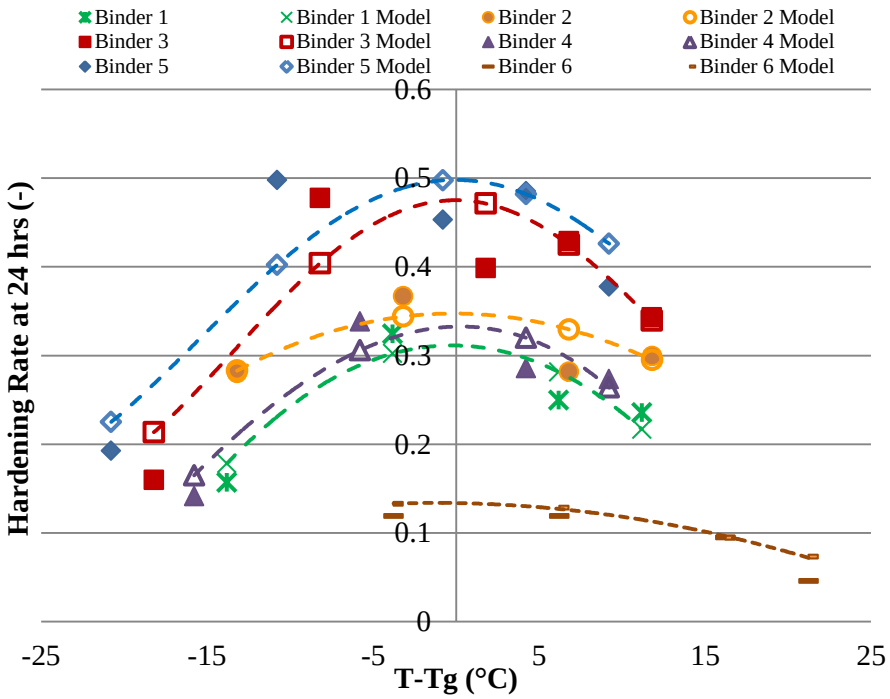

Figure 35 Predicted and experimental hardening rates after 24 hrs plotted against difference of conditioning temperature to estimated Tg (T-Tg). (Hardening rate= ΔS/S0)

One of the main objectives of developing this model is the ability to predict behavior from fewer tests or easily available data. For the proposed model, two possible prediction methods are considered. The first and simplest method would be to use three hardening rate data points from a BBR test carried out at a single temperature after relatively short conditioning times, along with the glass transition temperature to fit the model and use the resulting G and η

to predict the effect of much longer conditioning times or other conditioning temperatures. Although this is an improvement compared to the much longer conditioning times as well as other temperatures. It must be noted that as with any non-linear model, the closer the input data points are to each other (or in this case, the shorter the conditioning times used), the lower the accuracy of the extrapolation of the model to much longer conditioning times.

The second method is to find regression functions that can be used to relate BBR creep stiffness, S(60), or m-value at 1 hour conditioning, to predict the model parameters *G* and η. A promising relationship was observed between S(60) and conditioning temperature from the SHRP binders and the model parameters. As shown in Figure 36, a power law was fitted to the curve for all binders and the *A* and *B* parameters were determined as described in (5).

$$S(60) = A|T|^B \quad (5)$$

Where *A* and *B* are statistically fitted constants and *T* is the measurement temperature in °C.

The *A* and *B* parameters were plotted against *G* and η. No apparent relationship existed with the *A* parameter. However, an interesting correlation was established using *B* from the SHRP binders. The relationships can be seen in Figure 37.

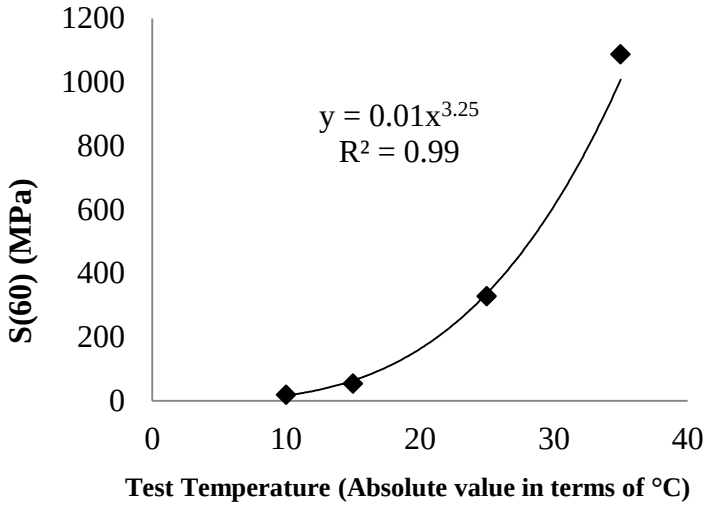

Figure 36 S(60) after 1 hr conditioning for one of the SHRP binders plotted against test temperature.

The correlations showed that parameter *G* and parameter *B* are very similar. This equality is very important and more investigation into this relationship should be considered. Using the relationships shown in Figure 37, (4) can be rewritten as:

$$\frac{\Delta S}{S_0} = \frac{1.4 * e^{\frac{-9(T-Tg)^2}{2(x)^2}}}{B}\left(1-e^{\frac{-t_c B}{19.41\ln(B)+14.54}}\right) \quad (6)$$

in which:

- $\frac{\Delta S}{S_0}$ is the hardening rate
- T_0 is the peak temperature for hardening rate, assumed to be the T_g (°C)
- T is conditioning temperature (°C)
- t_c is the conditioning time (hrs)
- $2x$ is the length of the temperature range of the glass transition region (°C)
- B is derived from (5)

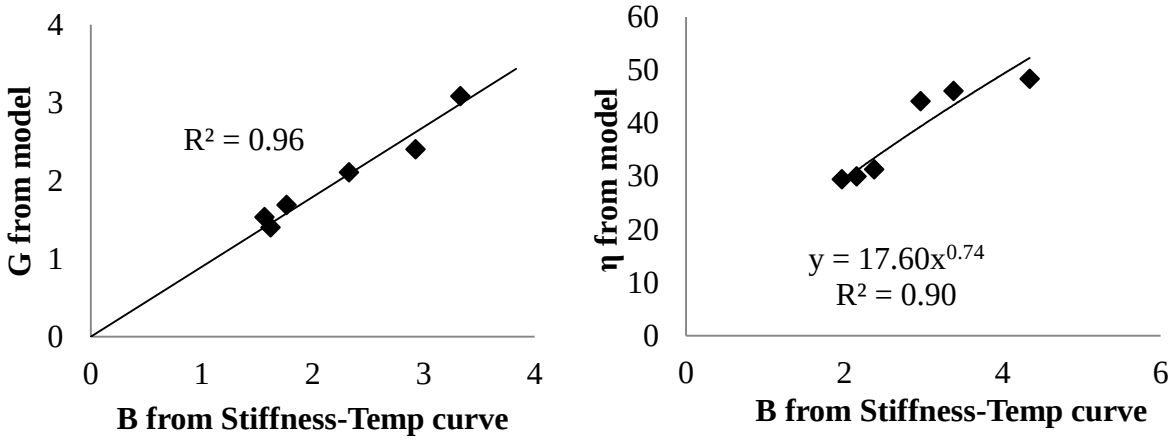

(a) **(b)**

Figure 37 Correlation between G and B (a), and η and B (b) for the SHRP binders.

Equations such as (6) can be used to predict the hardening rate for other binders at any temperature and conditioning time, using only S(60) at 1 hr from BBR grading tests and the T_g. A comparison between this predicted model and the measured data is presented in Figure 38 for the tested binders. The applicability of using the proposed physical hardening model for different binders will increase as data from more binders are used to refine the observed relationship between the parameters. Although requiring measuring T_g may be inconvenient, this study has clearly shown that the glass transition behavior of a binder is one of the controlling factors in the physical hardening phenomenon and no model can accurately describe it without taking the glass transition into account.

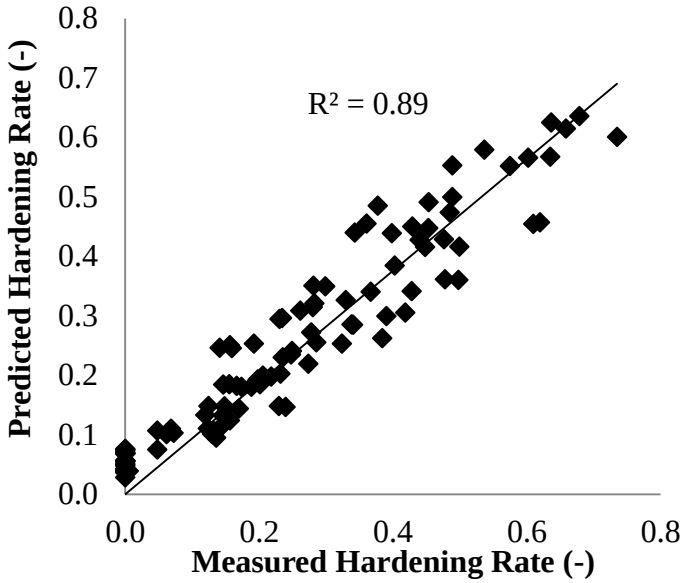

Figure 38 Goodness of fit between model described by (6) using T_g for T_0 and experimental data.

5.3.2.

5.3.3. Extension of Model for Prediction of m-value

It has been observed by researchers that physical hardening not only affects the binder stiffness, but also changes the binder relaxation properties, commonly quantified by the BBR m-value [3, 71]. Knowing the changes in both S(60) and m(60) over the course of isothermal conditioning is critical if an assessment of Superpave performance grade change with physical hardening is desired.

Bahia and Anderson [59] found that the approach used to account for the effect of changing temperature in viscoelastic materials (i.e., time-temperature superposition principle) could be applied to the stiffening effect of physical hardening with conditioning time by using a shift factor on the time scale [57, 58, 59, 94]. They reported that creep curves obtained at the same temperature but at different conditioning times can be superimposed into a "hardening" master curve [9].

Thus for physical hardening of asphalt binders, similar to temperature shifting, stiffness at isothermal conditioning time (t_c) and loading time ξ, can be shifted to a reference conditioning time ($t_{c\text{-}ref}$) and a reduced loading time ξ_r. This concept is expressed in (7) and shown in Figure 39.

$$S(\xi)_{t_c} = S(\xi_r)_{t_{c-ref}} \quad (7)$$

Extending this reasoning, one may conclude that the m-value after isothermal conditioning time t_c, and loading time ξ, or "m(ξ)$_{tc}$", can be shifted to match the m-value at a reduced loading time ξ_r at the reference conditioning time $t_{c\text{-}ref}$. This is expressed as Equation (8):

$$m(\xi)_{t_c} = m(\xi_r)_{t_{c-ref}} \quad (8)$$

Using this method, m(60) at any conditioning time can be predicted using the model described in the previous section to first predict S(60)$_{tc}$, then shifting the creep stiffness to the reference condition to find ξ_r based on (7) and the hardening master curve at the reference conditioning time (Figure 40). Finally (8) is used to find the m-value for the target conditioning time.

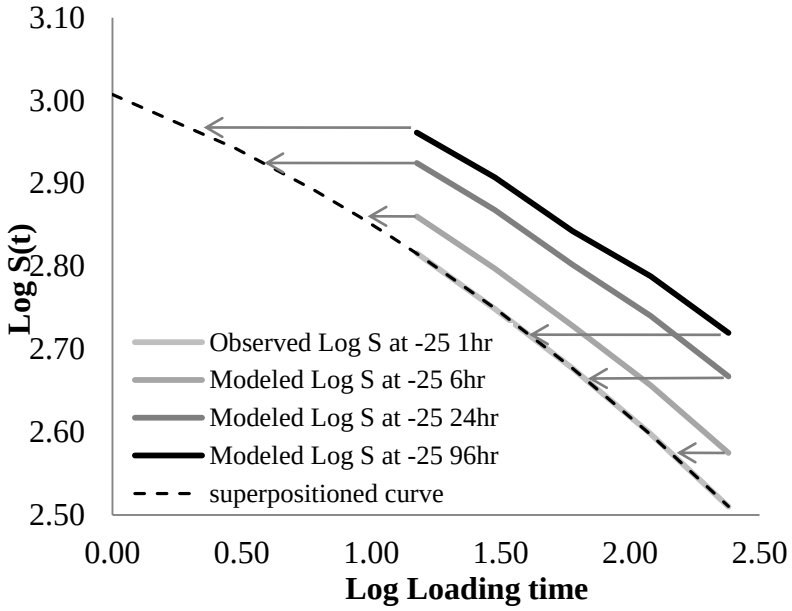

Figure 39 Shifting of creep stiffness curves at different conditioning time, to the reference conditioning time (tc=1 hr)

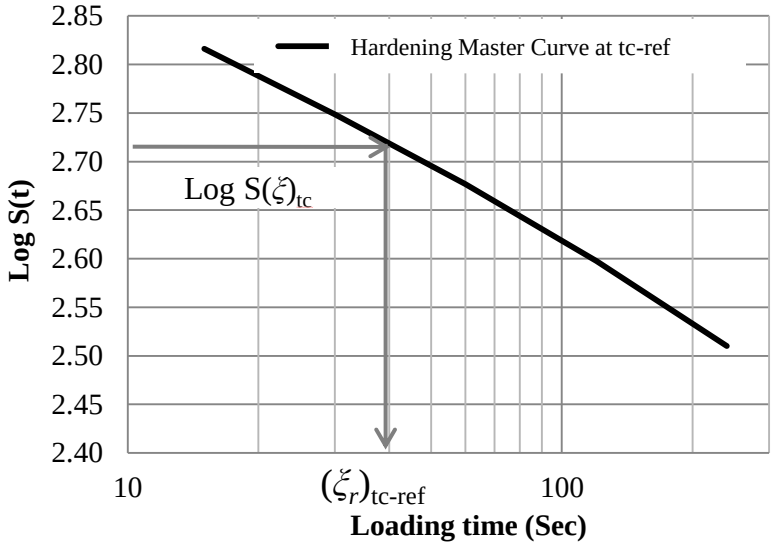

Figure 40 Hardening master curve at the reference conditioning time.

This method was used to predict the m-value using the model predictions for a number of the studied binders at four temperatures ranging from -10 to -35°C and conditioning times up to 96 hrs. The results were plotted against the actual m-values measured using the BBR at the target conditioning time and temperatures, in Figure 41.

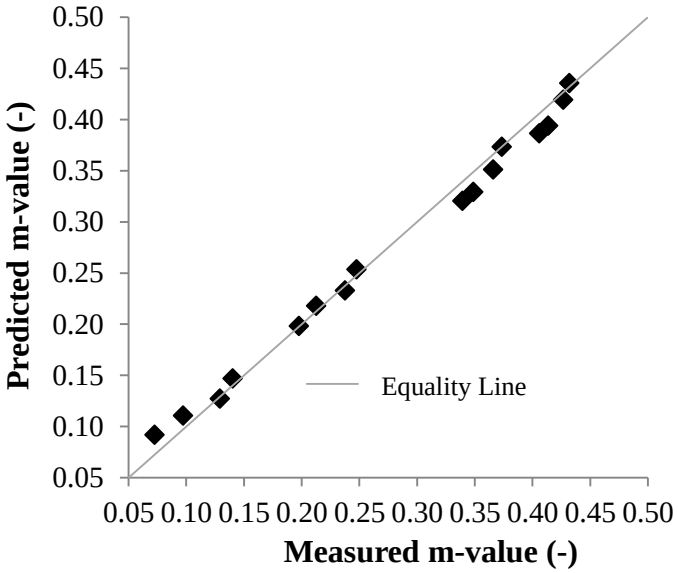

Figure 41 Goodness of fit between predicted m-values described by (9) and experimental data.

It can be seen that the predictions and measured results agree very well. Thus the model can be used to predict both the S(60) and the m(60) after isothermal conditioning. This can be very useful for specifications requiring performance grading after isothermal conditioning, without the need for carrying out lengthy physical hardening tests.

5.4. Extending Asphalt Binder Physical Hardening to Mastics and Mixtures

5.4.1. Physical Hardening of Asphalt Mastics

Previous sections discussed the development of a model for prediction of physical hardening in asphalt binders. Asphalt binders perform as the continuous phase of a composite material. Often asphalt mixtures are considered in a multi-scale fashion, the finest of which would be the binder scale, followed by the "mastic" scale which is a composite of aggregate filler particles (particles smaller than 0.075 mm) in a binder matrix and finally the asphalt mixture scale in which asphalt mastic forms the continuous phase in a composite with larger aggregates.

In order to relate binder physical hardening to that of asphalt mixtures it was determined that mastic behavior at isothermal conditions must be first investigated. To achieve this a neat binder was modified with 40% by volume of three types of filler mineralogy, namely granite, limestone, and dolomite. These mastics were conditioned at -12, -18, and -24°C for 48 hours and the evolution of stiffness was monitored using BBR measurements after 1, 2, 4, 24, and 48 hours of conditioning.

The binder phase, as the only fraction undergoing hardening, only accounts for 60% of the mastic, while the remaining 40% of volume is taken by non-hardening mineral filler particles. Thus any hardening in the mastic will only be the result of the hardening of the binder phase as modified by the interaction with the mineral filler. For this reason, in order to define a hardening rate one must isolate binder hardening from the measured total mastic hardening. The simplest method for doing so would be following the procedure shown in equations (9) to (12):

$$S_{mi} = \varphi_f S_f + \varphi_b S_{bi} \quad (9a)$$

$$S_{mc} = \varphi_f S_f + \varphi_b S_{bc} \quad (9b)$$

$$\Delta S_m = \varphi_f \Delta S_f + \varphi_b \Delta S_b \quad (10)$$

$$\Delta S_{b_f} = \frac{\Delta S_m}{\varphi_b} \quad (11)$$

$$HI_b = \frac{\Delta S_{b_f}}{S_{b0_f}} \cong \frac{\frac{\Delta S_m}{\varphi_b}}{S_{b0}} \quad (12)$$

The resultant hardening index would be that of the binder phase of the mastic, and any difference from that of the pure binder hardening would be due to the association of the binder and filler. Results are shown in Figure 42.

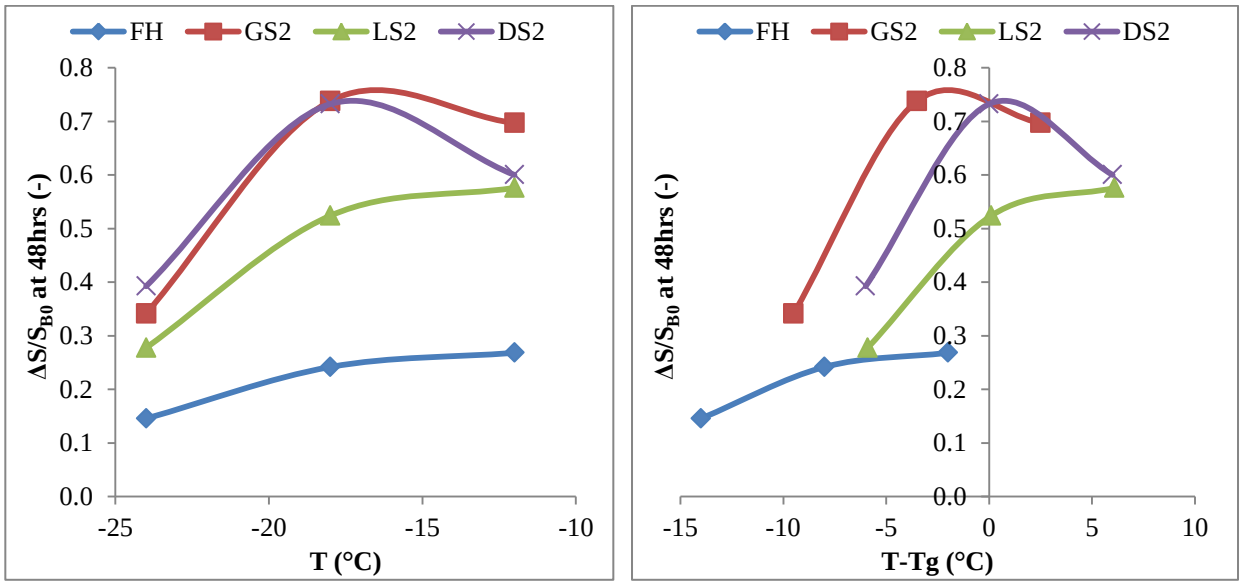

(a) without adjustment **(b) with adjustment**

Figure 42 (a) Measured mastic hardening index after 48 hrs without adjustment, and (b) mastic hardening index after 48 hrs adjusted for binder content and shifted to Tg

From Figure 42 It is observed that for all filler types, the mastics showed higher hardening indexes than that of the pure binder sample. The difference further increased once the hardening indexes were adjusted for the binder volume fraction. Furthermore, it is observed that

if the hardening index curves are plotted on an axis of temperature difference with mastic T_g, all binders and mastic hardening index curves seem to peak near their respective glass transition temperatures. This observation is in agreement with previous discussion of the relationship between binder physical hardening and Tg, and subsequently the developed model. Based on these results the binder physical hardening model was fitted to the mastic hardening curves, as shown in Table 7 for both adjusted and unadjusted data. Figure 43 shows the unadjusted hardening index after 48 hrs of conditioning. The unadjusted goodness of fit is shown in terms of predicted versus measured hardening indices in Figure 44.The fit was relatively good, although occasionally some difficulty was encountered due to experimental repeatability. Analysis of model parameters in Table 7 shows that the addition of mastic decreased the *G* parameter by an average of 2.5 times and η by an average of 3.1 times. The biggest change in parameters was for granite, while the dolomite decreased model parameters the least. Comparison of overall hardening values for all fillers at all test times to that of the base showed that by average presence of 40 percent filler by volume of mastic increased hardening by 2.55 times, with a standard deviation of 0.55, approximately a 6.4% increase in hardening per increase of 1% of mineral aggregate volume fraction in mastic.

Table 7 Fitted model parameters for studied asphalt mastics

Model Parameter	Base (Flint Hills)	Base+GS2	Adjusted Base+GS2	Base+LS2	Adjusted Base+LS2	Base+DS2	Adjusted Base+DS2
G	3.45	4.7	1.29	4.84	1.57	3.3	1.34
η	52.5	72.7	21.67	123.3	42.67	17.5	7.07
T_0	-10.00	-14.50	-14.50	-18.10	-18.10	-18.00	-18.00
x	27.37	19.05	17.25	30.00	30.00	11.65	13.40

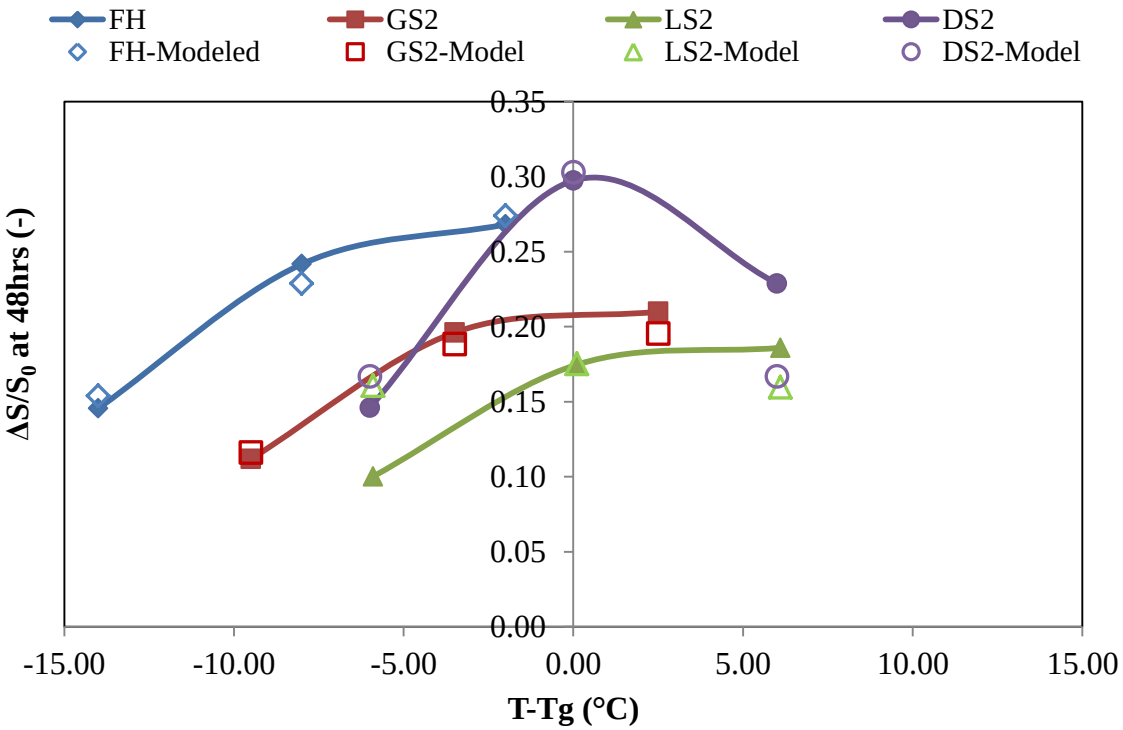

Figure 43 Comparison of mastic hardening with fitted model predictions

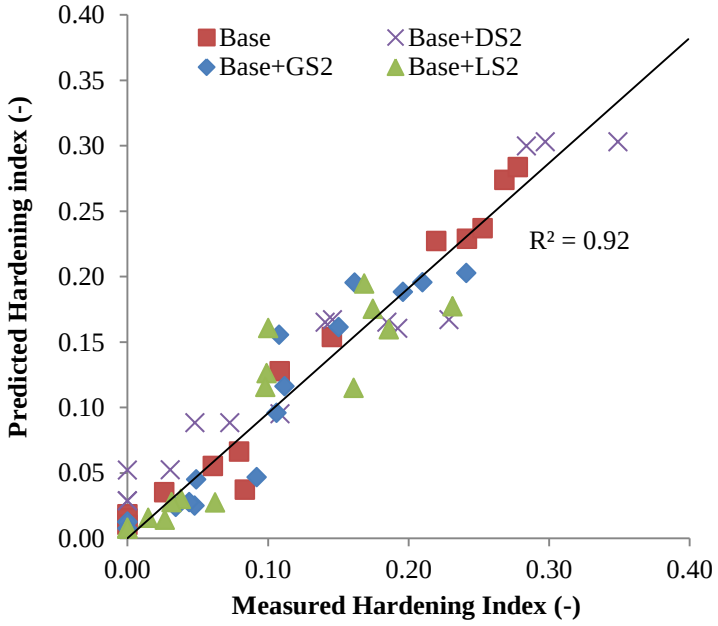

Figure 44 Goodness of fit for mastic hardening prediction

As previously mentioned, all mastics showed higher hardening than that of the asphalt binder without mineral filler. It is postulated that this may be due to the absorption of binder asphaltene on the significant surface area of the particles, thus leaving an asphalt matrix with a higher maltene volume fraction. The low service temperature glass transition temperature in asphalt is due to its maltene phase, as the asphaltene phase glass transition temperature is expected to be near high service temperatures. Thus it is believed that the maltene phase, consisting of aromatics and polar components, is the primary hardening fraction in asphalt. Consequently by increasing the maltene volume fraction in the asphalt it is expected that the rate of isothermal hardening would also increase. Details of the asphaltene absorption mechanism and the physico-chemical interaction of asphalt and mineral fillers are beyond the scope of the present study and have been discussed elsewhere [95].

5.4.2. Physical Hardening of Asphalt Mixtures

Assuming that the matrix softening is a function of aggregate specific area, as suggested by Clopotel et al [95], in it is reasonable to assume that the change of glass transition in the whole mixture could be estimated by extending the specific area of the mineral filler to that of the total mixture and adjusting the glass transition temperature accordingly.

The sieve analysis results for the overall aggregates in the mixture was used to determine the approximate ratio of total aggregate area to that of the passing #200 sieve filler, and subsequently adjust the change in T_g accordingly. The approximate surface area of the total aggregate gradation to the mineral filler, R_s, was calculated as shown in (13), assuming spherical particles:

$$R_s = \frac{\sum_{n=1}^{N}(P_n - P_{n-1}) \cdot \frac{4\pi(D_n/2)^2}{4/3\pi(D_n/2)^3}}{P_{\#200} \cdot \frac{4\pi(D_{\#200}/2)^2}{4/3\pi(D_{\#200}/2)^3}} = \frac{\sum_{n=1}^{N}\frac{(P_n - P_{n-1})}{D_n}}{\frac{P_{\#200}}{D_{\#200}}} \quad (13)$$

In which:

- n is the sieve number and N is the total number of sieves,
- P_n is the percent by weight of aggregate passing sieve n, and
- D_n is opening diameter of sieve n,

Using the above equation for a mixture made with granite aggregates of the gradation shown in Table 8, the R_s value was calculated to be 3.97. Using data from Clopotel et al. [95] the change of T_g with addition of volume fractions corresponding to the mixture P_{200} (24.2% of binder by volume) was determined to be approximately -3.5°C. Thus for an R_s of 3.97 the decrease in base binder Tg would be approximately 3.97×(-3.5°C), resulting in an estimated mixture T_g of -23.5°C. The actual measured T_g for the asphalt mixture in question was measured using the ATCA to be -21.9°C which seems to be reasonably close to the estimated value based on the granite mastic. Unfortunately complete mixtures using dolomite and limestone aggregates for comparison to the corresponding mastics were not available to further validate this estimation method.

Table 8 Aggregate gradation for mixture made with granite aggregates and Flint Hill base binder

Sieve Opening Size (mm)	Percent Passing (%)
25	100
19	99.7
12.5	78.6
9.5	64.5
4.75	41.1
2.36	27.4
1.18	18.7
0.6	12.9
0.3	7.8
0.15	4.9
0.075	3.2

Assuming that the free volume concept applies to physical hardening of asphalt, as shown extensively in the literature [59, 58, 8], the rate of hardening is proportional to the change in free volume of an amorphous material. As discussed previously, measuring the magnitude of free volume is extremely difficult; instead the change in free volume has been measured using extremely accurate mercury-based dilatometric systems. Attempts to measure free volume change in isothermal conditions using the ethanol dilatometric system used in the present study for asphalts was ultimately unsuccessful due to the signal ambient noise level being close to the order of expected free volume change.

Bahia [59] estimated asphalt binder free volume by measuring the difference in volume in the transition area to that of the extension of the liquid equilibrium volume. For the binders studied the average difference at the binders' T_g was approximately 1×10^{-4} cm^3/cm^3. Magnitudes of isothermal free volume change close to the glass transition for various amorphous materials

were gathered from literature as a point of reference and comparison. For a-PMMA the free volume isothermally decreased by 4 to 14×10^{-4} cm^3/cm^3 before stabilizing [50]. For poly-styrene these values were between 5 to 20×10^{-4} cm^3/cm^3 in [27], and between 7 to 21×10^{-4} cm^3/cm^3 in [29] when cooled to the isothermal temperature at 1°C/min, and around 20×10^{-4} cm^3/cm^3 when measured at polystyrene's glass transition temperature (95°C) [32]. For poly-vinyl-acetate (PVAc) the isothermal contraction at T_g was reported as being 15×10^{-4} cm^3/cm^3 [49]. For isotactic Polypropylene free volume reduction of 25×10^{-4} cm^3/cm^3 was reported [54]. For epoxy, volume relaxation during physical aging near the T_g was measured to be in 22×10^{-4} cm^3/cm^3 [45]. In all reported materials a range of 4 to 25×10^{-4} cm^3/cm^3 reduction in free volume is observed when material is kept isothermally near the glass transition. Furthermore, work by Hadac et al. [29] showed that for poly-styrene decreasing cooling rate down to the isothermal state from 1°C/min to 0.1 and 0.01°C/min reduced the ultimate volume relaxation magnitude by a factor of 0.6 and 0.3, respectively. Thus for the purpose of estimation, an average ultimate free volume change of 1×10^{-4} cm^3/cm^3 was selected for asphalt cooled at a rate of 1°C/min (60°C/hr) to its T_g and kept isothermally, which was reduced to 0.6×10^{-4} and 0.3×10^{-4} if cooled at a rates of 0.1°C/min (6°C/hr) and 0.01°C/min (0.6°C/hr), respectively.

Following the above discussion, it should be possible to convert the isothermal change in stiffness measured for the asphalt binder and mastic to linear isothermal contraction strain in the mixture, with consideration of the relatively small volume of binder in the entire asphalt mixture.

For the binders in the present study the average ultimate ratio of change in stiffness was about 30% close to the binder T_g. Assuming that the stiffness change is associated with the maximum isothermal volume change of 1×10^{-4} cm^3/cm^3, each percent of isothermal hardening would be associated with 0.033% volume change in the binder.

Using the increased hardening of 6.4% per for each 1.0% increase in mineral filler volume fraction calculated in the previous section, and the R_s filler to bulk mixture specific area ratio of approximately 4.0, for a filler with a specific weight of 2.4 kg/cm^3 and a 3.2% P200 (24.2% by volume of mastic), the binder physical hardening magnitude would increase by approximately 6 times. This would increase the previously derived value of 0.033% for volume change in the binder to 0.2% per percent hardening of binder, for the binder present in the mixture aggregate system.

Assuming isotropy in the asphalt binder and mixture, isothermal linear strain would be 1/3 the volumetric strain change of 0.2% per percent binder hardening. Thus linear isothermal strain in the binder phase of an asphalt mixture would be roughly 0.067% per each percent of binder isothermal hardening. Adjusting by volume fraction of binder in the total mixture (assuming 11% by volume binder, 4% air voids and 85% aggregate) this value would reduce to 0.0087% strain per each percent of binder isothermal hardening cooled at a rate of 1°C/min, and 0.0052% and 0.0026% for cooling rates of 0.1°C/min and 0.01°C/min. If no aggregate-asphalt interaction is assumed (no additional hardening due to the presence of mineral filler), these values would further decrease by a factor of 6 to 0.00145% at a cooling rate of 1°C/min, 0.00087% at 0.1°C/min, and 0.000435% strain per each percent of binder isothermal hardening at a cooling rate of 0.01°C/min. Intermediate rates are interpolated logarithmically. This conversion factor will hereby be referred to as the "Binder-Mixture Conversion Factor" or BMCF for short.

As previously discussed, one may describe creep in viscoelastic material as the gradual redistribution of the molecules or change in morphology, resulting in a decrease in the creep stiffness. The creep behavior can be envisioned as similar to the behavior observed in physical

hardening. Thus it is proposed that a modified version of the model shown in equation [4] be used for the prediction of the time dependent strain in asphalt mixtures caused by physical hardening at different temperatures and conditioning times. This model has the same general form of that of the asphalt binder (4), but the existence of an elastic aggregate component and the aggregate structural properties will affect the model constants. The resulting model would have the general form shown in equation (14).

$$\epsilon_{PH} = BMCF \cdot \frac{e^{\frac{-a(T-T_0)^2}{(2x)^2}}}{G_M}\left(1 - e^{-t_c\frac{G_M}{\eta_M}}\right) \quad (14)$$

In which:

- ϵ_{PH} is the time dependent strain (physical hardening),
- T_0 is the peak temperature for hardening rate, assumed to be the Tg (°C),
- T is the conditioning temperature (°C),
- t_c is the conditioning time (hrs),
- 2x is the length of the temperature range of the glass transition region (°C),
- G_M, and η_M are model constants, calibrated to fit asphalt mixture behavior,
- BMCF is the "Binder-Mixture Conversion Factor."

5.5. Chapter Summary

In this chapter a prediction model for the rate of physical hardening at different temperatures and conditioning times was proposed based on a creep viscoelastic model, and concepts derived from the study of a large number of modified and unmodified binders. Based on the results, the following important findings can be stated:

- The rate of physical hardening does not increase indefinitely as temperature decreases. Based on literature review and the experimental data collected, it is found that the rate of hardening peaks at a specific temperature, and approaches zero as the temperature increases or decreases toward the limits of the glass transition region. It is shown in this study that the peak temperature corresponds to the glass transition temperature of the binder as estimated from intersection of the liquid and glassy asymptotes representing equilibrium conditions.
- A creep model is developed and is shown to be able to reflect the change in physical hardening rate as a function of conditioning time and temperature. The model can be used to predict changes in BBR parameters (i.e. S(60) and m(60)) after various isothermal conditioning times.
- The model parameters, G and η, were shown to be unique material parameters that remain constant at all conditioning times and temperatures. Thus, by fitting the model to three stiffness values at a single temperature and having the T_g, one may predict the physical hardening at any other temperature or conditioning time.
- The model can be written in terms of S(60) measured after 1 hr conditioning and the binder T_g, using correlations from existing performance grading (PG) data.
- The proposed model can be very useful for specification purposes if isothermal conditioning needs to be taken into account. The use of this model can shorten lengthy tests usually needed for physical hardening characterization.

- The rate and magnitude of physical hardening in the binder was related to that observed in the asphalt mastics and used to develop a “Binder-Mixture Conversion Factor” to link measured binder isothermal hardening to isothermal contraction in asphalt mixtures.

6. Modeling Thermal Stress in Asphalt Mixtures Undergoing Glass Transition and Physical Hardening

6.1. Overview

In this chapter a model accounting for the glass transition and physical hardening during the thermal stress buildup in mixtures is proposed. The theoretical approach is derived using relaxation modulus master curves, the William-Landel-Ferry equation, Boltzmann superposition principle, and the modified creep model discussed in the previous chapter to account for physical hardening. The model is used to show that thermal stress relaxation and stress build-up induced by physical hardening can continuously affect thermal stress throughout the cooling process. Cooling rate also affected the amount of delayed stress buildup occurring after the temperature had stabilized at isothermal conditions, as a result of the physical hardening.

As described in previous chapters, using the ATCA device, many relaxation experiments were carried out at different cooling rates, isothermal temperatures and isothermal relaxation times. For all experiments thermal stress was observed to build up as the temperature decreased in the restrained beam. When the sample reached the isothermal stage, the sample continued to build up stress even after the core temperature had stabilized. Isothermal contraction was also observed simultaneously in the unrestrained beam. As the isothermal conditions continued, the stress gradually started to relax.

An important consequence of the observed behavior is that thermal stress builds up at a slower rate during cooling if the cooling rate is high enough to not allow for complete contraction during the cooling period. Although at first glance this seems counter intuitive, it must be pointed out that for sufficiently slow cooling rates in which full time and temperature

dependent contraction is taking place during cooling, the trend will be opposite, as the slower cooling rates allow for more thermal stress relaxation, and consequently a lower rate of stress build up during cooling.

The importance of the observed behavior is its implications for the validity of the current method for thermal stress calculations. Currently, the prevalent method for thermal stress measurements is to use a restrained beam geometry for which the rate of potential thermal strain is calculated using appropriate coefficients of thermal contraction; and coupling this input with the calculated change of the relaxation modulus, to ultimately estimate the resulting net stress in the specimen. The relaxation modulus in this method is a function of both loading time and temperature, thus accounting for stress relaxation in the viscoelastic material. On the other hand, thermal strain is assumed as only a function of temperature, thus the time dependency of the strain, especially when approaching the glass transition temperature is ignored. This assumption leads to a deviation from the true thermal stress build up as the temperature approaches the glass transition region. Such discrepancies have been noted by previous research when comparing experimental and calculated thermal stress, but have usually been attributed solely to the unreliability of relaxation modulus maser curves or the coefficients of thermal contraction in this temperature range.

In this chapter a method is introduced to address this deficiency by accounting for the time dependency of thermal strain in the glass transition region. The procedure is used to theoretically predict the aforementioned behaviors during the thermal history of an asphalt mixture. The results are used to demonstrate the importance of accounting for the glass transition temperature in the prediction of thermal stress in asphalt pavements.

6.2. Model Input and Assumptions

6.2.1. Constructing Relaxation Modulus Master Curve

Asphalt binders can be considered as thermo-rheologically simple material. For such materials, the change of rheological properties at a constant loading time due to temperature's change can be assumed to be equivalent to the change due to loading times' change at constant temperature. By shifting a range of material property curves (such as the relaxation modulus as a function of time) measured at different temperatures along the loading time, a "master curve" of the material property may be generated at a selected reference temperature.

The creep and relaxation behavior of viscoelastic materials are directly related to one another, such that a material that has a faster creep rate will also relax the built up stress quickly [62]. The relaxation modulus tests are rarely conducted for asphalt mixtures. Instead the creep compliance master curves or the dynamic modulus master curves are constructed based on the results of tests such as the indirect tensile creep test and the asphalt mixture dynamic modulus test, and numerically converted to relaxation modulus values [90]. Creep compliance and relaxation modulus are related by a convolution integral, which may be used to convert the creep compliance to relaxation modulus [62, 96].

In the present study the dynamic modulus master curves generated using WLF shift factors were fitted using a Generalized Maxwell Model master curve, for which a closed form solution for the conversion from complex to time-domain relaxation modulus exists [97], as shown in equations (1) and (2). The frequency was converted to time domain following procedure described by Christensen [98]. The relaxation modulus master curve was then

converted to a sigmoidal stretched exponential master curve form, so that it can be used in the thermal stress calculation framework, as will be described in following sections.

$$E^*(\omega) = E_e + \sum_{i=1}^{n} E_i \frac{\omega^2 \tau_i^2}{1+\omega^2 \tau_i^2} + i \sum_{i=1}^{n} E_i \frac{\omega \tau_i}{1+\omega^2 \tau_i^2} \quad (1)$$

$$E(t) = E_e + \sum_{i=1}^{n} E_i e^{-t/\tau_i} \quad (2)$$

Where

- E_e is the equilibrium modulus,
- E_i are spectral intensities, and
- τ_i are relaxation times.

6.2.2. Thermo-Volumetric Behavior and Glass Transition of Asphalt

Thermal stress calculations are based on the potential thermal strain of the mixture due to temperature differential. Thermal strain is measured directly for asphalt mixture beams using the ATCA device. In this study, the resulting strain is plotted as a function of temperature and fitted using a formulation proposed by Bahia et al. [9]. The relationship is shown in equation (3).

$$\epsilon_{th} = \frac{\Delta l}{l_0} = C + \alpha_g (T - T_g) + \ln\left\{\left[1 + e^{\frac{T-T_g}{R}}\right]^{R(\alpha_l - \alpha_g)}\right\} \quad (3)$$

In which:

- $\frac{\Delta l}{l_0}$ is the relative change of length, or thermal strain,
- C is an intercept with no physical meaning,
- α_l and α_g are the liquid and glassy coefficients of thermal contraction/expansion, and
- R is a parameter representing the curvature between the two linear asymptotes

The formulation fits two linear portions to the curves above and below the non-linear "glass transition" region, the slopes of which are defined as the liquid (α_l) and glassy (α_g) coefficients of thermal contraction/expansion. The temperature at the intersection of the two linear sections is defined as the glass transition temperature (T_g). The "R" parameter represents the "strength" of the transition, which is a measure of the difference of slopes before and after the transition as well as the length and curvature of the transition region. Equation (3) was used to predict thermal strain at any given temperature in the present study.

6.2.3. Physical Hardening in Asphalt Binders and Mixtures

The prediction model for the rate of physical hardening at different temperatures and conditioning times is based on a viscoelastic creep model, as developed in the previous chapter. The model shown in equation (4) is used to account for the physical hardening strain in the thermal stress buildup.

$$\epsilon_{PH} = \mathrm{BMCF}\frac{e^{\frac{-a(T-T_g)^2}{(2x)^2}}}{G}\left(1 - e^{-t_c\frac{G}{\eta}}\right) \quad (4)$$

In which:

- ϵ_{PH} is the time dependent strain (physical hardening),
- T_g is the glass transition temperature and peak temperature for hardening rate (°C),
- T is the conditioning temperature (°C),
- t_c is the conditioning time (hrs),
- 2x is the length of the temperature range of the glass transition region (°C),
- G, and η are model constants, and
- BMCF is the binder-mixture conversion factor.

6.2.4. Prediction of Thermal Stress Buildup and Relaxation

Thermal stress in a restrained beam of visco-elastic material is calculated using the following convolution integral [10, 6, 62]:

$$\sigma(t) = \int_0^t E(t-\xi)\frac{\partial \varepsilon(\xi)}{\partial \xi} d\xi \qquad (5)$$

In which:

- $\sigma(t)$ is stress as a function of time,
- E is the relaxation modulus,
- ε is strain,
- ξ is reduced time.

The true nature of this integral is better understood if it is broken down to a finite number of increments. The input thermal strain can be divided into small step increments for which the relaxation response can be easily computed and added in time to obtain the total thermal stress, according to Boltzmann's superposition principle. Thus stress is calculated at any point in time through summation of all stress increments at that time. This concept, known as the "Stieltjes integration" [93], is depicted in Figure 45.

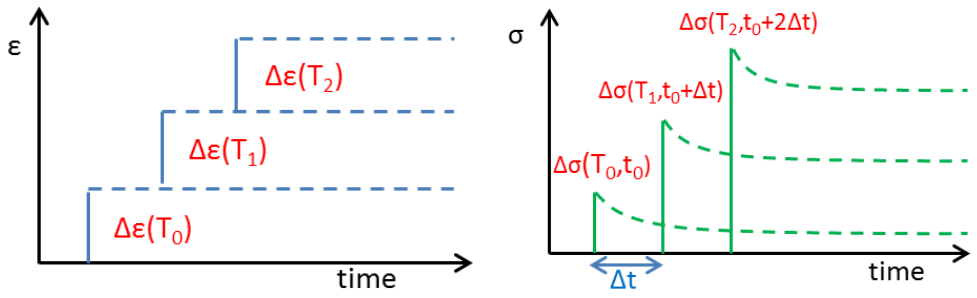

(a) **(b)**

Figure 45 Concept of incremental stress buildup and relaxation in viscoelastic material

Following this logic, if at any point the temperature is held constant, stress in subsequent steps will only be the sum of the relaxing stresses in previous steps, thus will continue to decrease over time, since no additional stress can build up once temperature is held constant, the total stress will begin to decrease immediately due to relaxation. This expectation, however, does not match what is observed in the ATCA experiments due to the physical hardening and continued shrinkage at constant temperature. In the proposed model, the addition of a time and temperature dependent strain term is shown to be able to describe stress buildup trends very similar to observations. The time and temperature dependent strain is calculated using equation (4). Thus the total thermal strain would be as shown in equation (6).

$$\epsilon_{Tot}(t,T) = \epsilon_{th}(T) + \epsilon_{PH}(t,T) \tag{6}$$

Thus equation (5) is modified for consideration of both contraction due to temperature reduction and time-dependent thermal strain, as shown in equations (7) and (8).

$$\sigma_{tot}(t) = \int_0^t E(t-\xi)\frac{\partial \varepsilon_{tot}(T,\xi)}{\partial \xi}\,d\xi \tag{7}$$

or

$$\sigma_{tot}(t) = \int_0^t E(t-\xi)\frac{\partial\left[\varepsilon_{th}(T) + \varepsilon_{ph}(T,t-\xi)\right]}{\partial \xi}\,d\xi \tag{8}$$

As equation (8) becomes exceedingly difficult to solve in comparison to the simpler form of equation (5), σ_{tot} is calculated through the use of Stieltjes integration method previously described over *n* time increments. In this methodology the strain term is applied to the aforementioned procedure by multiplying the strain term by the relaxed modulus at the

corresponding loading time, as shown in equations (9) to (12). The initially high rate of isothermal strain will result in a gradual isothermal stress buildup. The rate of buildup will gradually decrease as the modulus further relaxes, ultimately resulting in a gradual stress relaxation.

$$\Delta\sigma_{(T_n,t)} = \Delta\epsilon_{(T_n)} E_{(T_n,t_i+(n-i)\Delta t)} \tag{9}$$

$$\sigma(T_n,t) = \sum_{i=0}^{i=n} \Delta\sigma(T_i, t_i + (n-i).\Delta t) \tag{10}$$

$$\sigma_{ph(T_n,t)} = \sum_{i=0}^{i=n} \epsilon_{ph(T_n,t_i+(n-i)\Delta t)}\, E_{(T_n,t_i+(n-i)\Delta t)} \tag{11}$$

$$\sigma_{tot(T_n,t)} = \sigma_{(T_n,t)} + \sigma_{ph(T_n,t)} \tag{12}$$

6.3. Validation

Thermal stress buildup and relaxation tests were performed on selected asphalt mixtures to verify the accuracy of the proposed calculation scheme, and to show the influence of binder physical hardening on mixtures stress history. The tests were done at 0.1 and 1 °C/min cooling rates, during which the stress and strain in the beams were continuously monitored.

A full validation of the analysis setup was carried out for a well graded mixture of Flint Hill neat binder and granite aggregate. For this binder and its corresponding mixture a full set off dynamic modulus tests were performed at 3 temperatures (10, 25 and 40°C) and 4 frequencies (0.01, 0.1, 1, 10 Hz) each to form the mixture master curves.

The binder and mastic containing granite mineral filler using the Bending Beam Rheometer by isothermal conditioning at 3 temperatures (-12, -18, and -24°C) and up to 72 hrs to enable the fitting of the physical hardening model described in chapter 5. This model was then shifted using the derived Binder-Mixture Conversion Factor (BMCF) for use in the mixture calculation spreadsheet.

ATCA thermal strain and thermal stress tests were performed at both 6°C/hr and 60°C/hr (0.1 and 1°C/min) for model input and comparison. Dynamic modulus conversion to time domain relaxation modulus is shown in Figure 46 for the mixture with the neat binder and Figure 47 for the mixture with PMA binder. The dynamic modulus curves at each temperature were first shifted using the WLF equation to generate a Generalized Maxwell Model master curve, and converted to time-domain relaxation modulus using the existing closed form solution previously discussed. All master curve parameters as well as the WLF constants were inputted into the calculation spreadsheet.

Thermal strain measured by the ATCA, and the calculated relaxation modulus curves as a function of temperature for both cooling rates (60°C/hr and 6°C/hr) are shown in Figure 48 and Figure 49. The physical hardening model was calibrated using the neat binder and granite filler mastic experimental tests and shifted using the un-adjusted BMCF. As expected, it is observed that best agreement of predictions with the results is achieved if physical hardening terms used are based on the mastic glass transition temperature measurements, instead of the binder or mixture measurements.

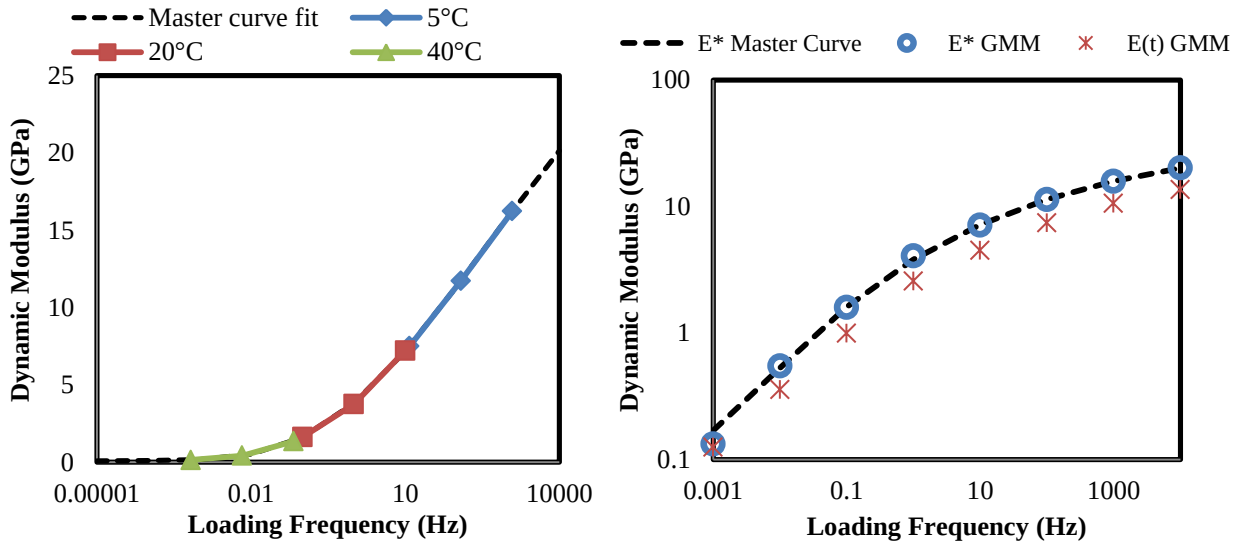

Figure 46 Conversion of dynamic modulus experimental data to relaxation modulus master curve in the time domain for the neat mixture (E(t) plotted in frequency domain using t = 1/ω)

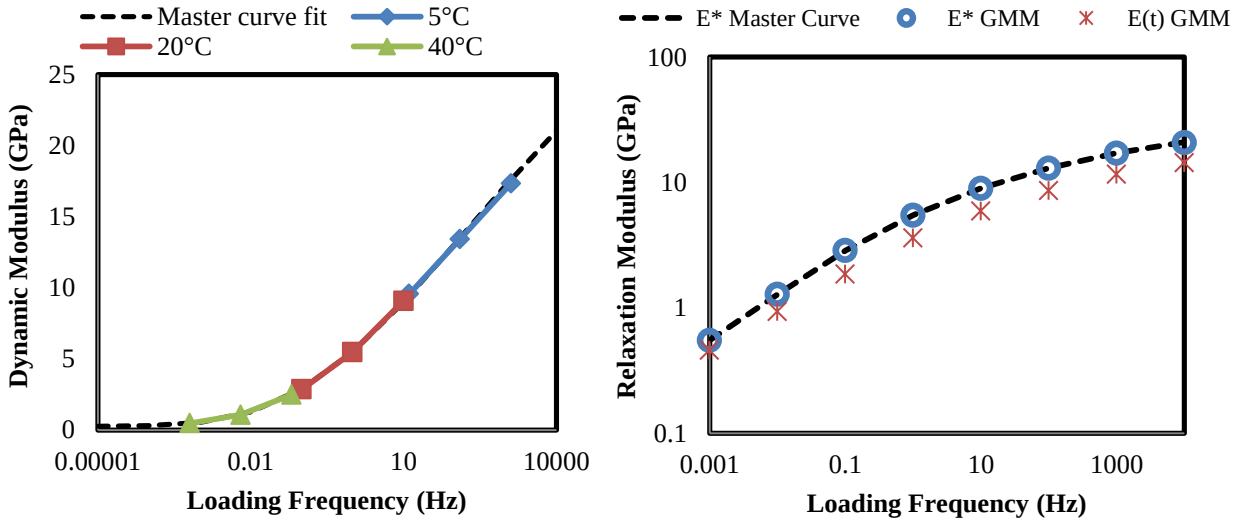

Figure 47 Conversion of dynamic modulus experimental data to relaxation modulus master curve in the time domain for PMA mixture (E(t) plotted in frequency domain using t = 1/ω)

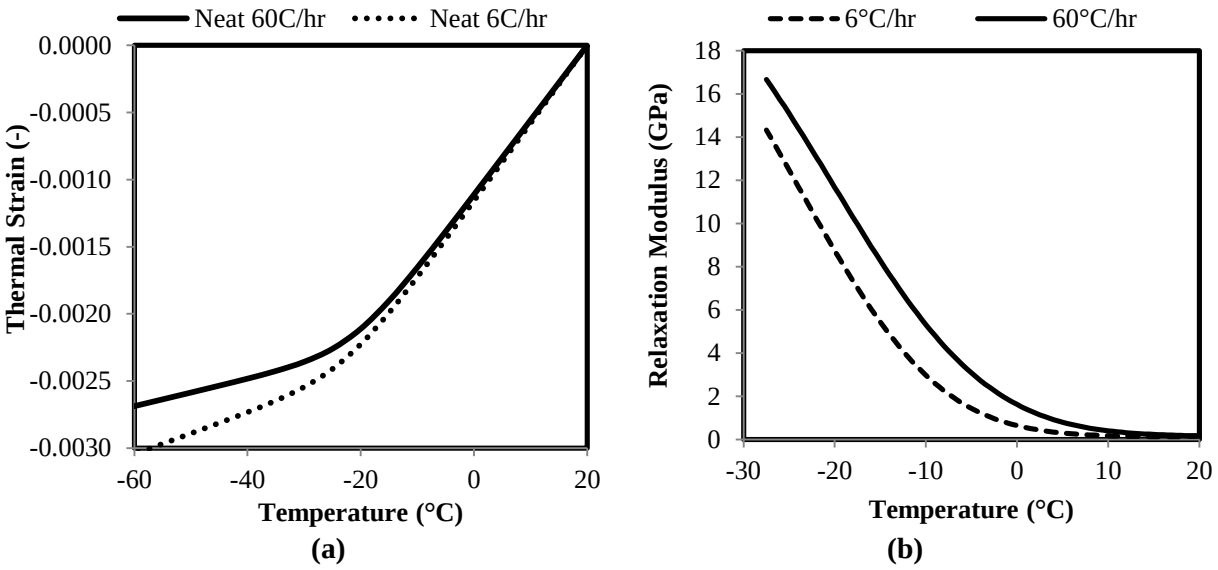

Figure 48 (a) Thermal strain curves, and (b) relaxation modulus curves for the Flint Hills mixture cooled at rates of 60°C/hr and 6°C/hr.

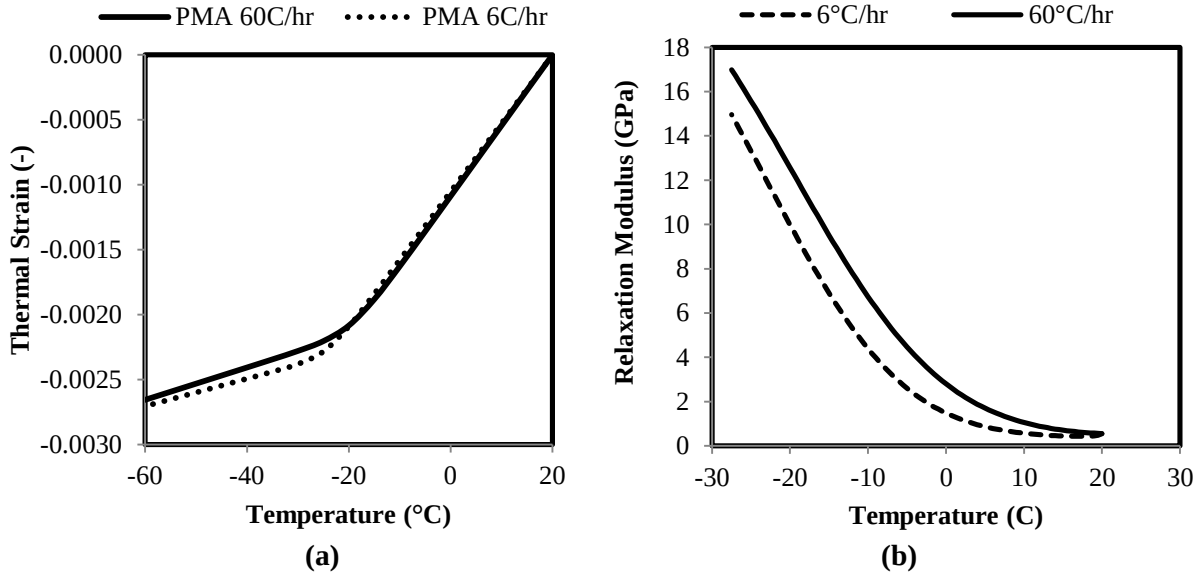

Figure 49 (a) Thermal strain curves, and (b) relaxation modulus curves for the PMA mixture cooled at rates of 60°C/hr and 6°C/hr.

Results of the calculations are compared with experimental results derived at both 60°C/hr and 6°C/hr cooling rates for both binders in Figure 50 through Figure 53. In each figure section (a) represents the comparison without considering physical hardening and section (b) represents the comparison with accounting for physical hardening. It can be seen that at both rates the standard linear visco-elastic thermal stress solution underpredicted the thermal stress

values, with higher differences observed at the slower cooling rate, which consequently allowed for more physical hardening to occur during cooling, as shown using the time-dependent physical aging strain correction at both cooling rates improved the linear viscoelastic prediction of the thermal stress, resulting in much closer agreement between the observed and measured thermal stress.

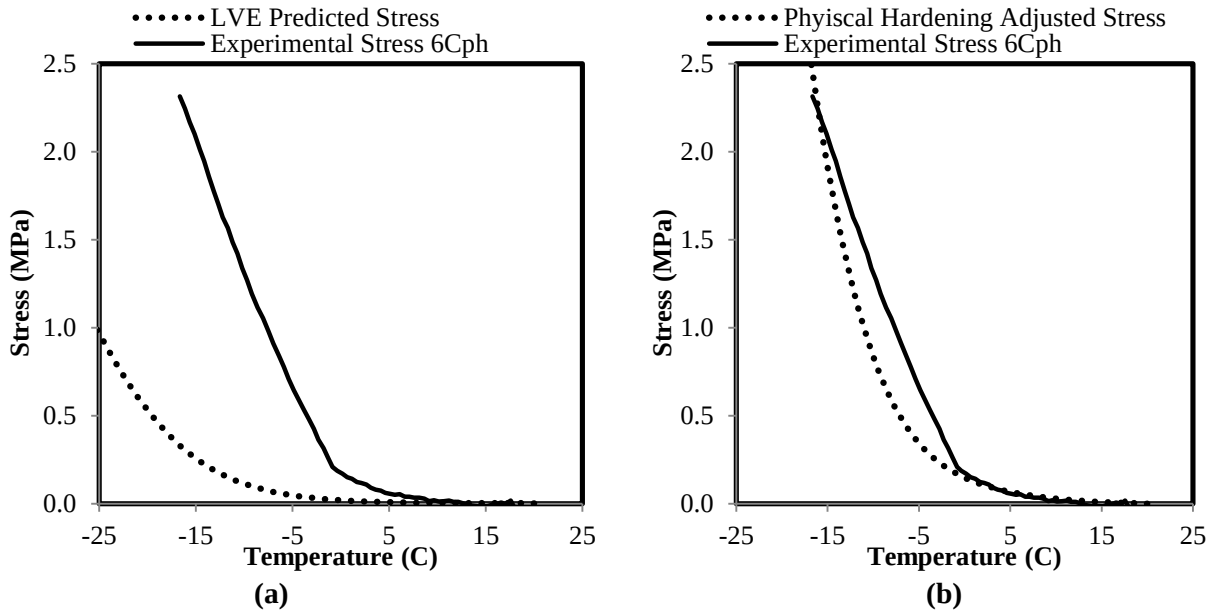

Figure 50 Measured thermal stress for neat asphalt mixture at 6°C/hr cooling rate as compared to (a) LVE predicted thermal stress, and (b) LVE thermal stress adjusted for physical hardening.

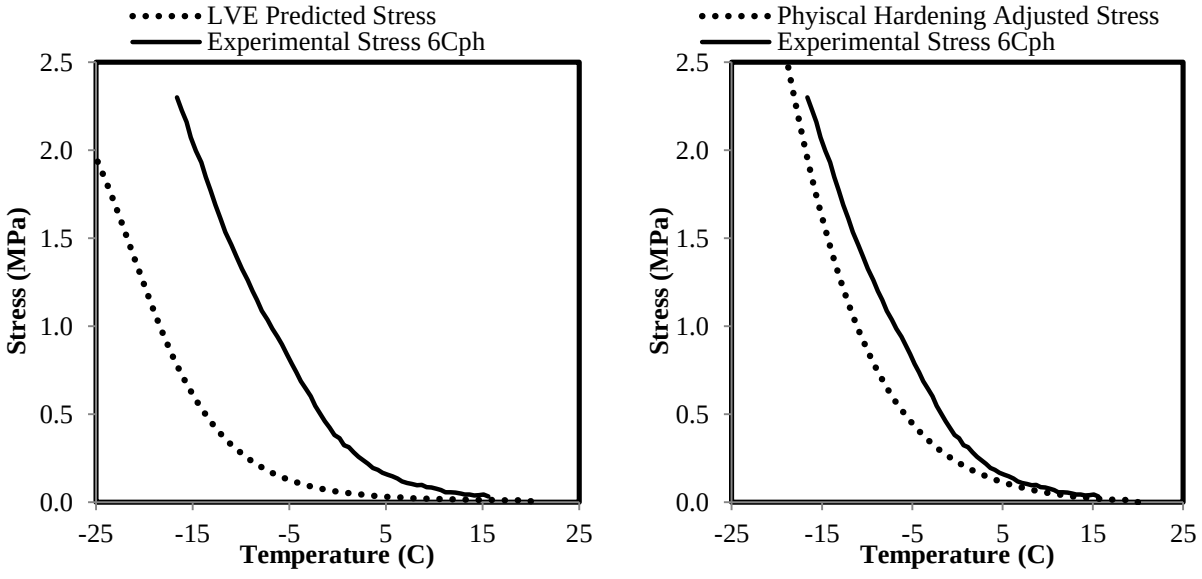

Figure 51 Measured thermal stress for PMA asphalt mixture at 6°C/hr cooling rate as compared to (a) LVE predicted thermal stress, and (b) LVE thermal stress adjusted for physical hardening.

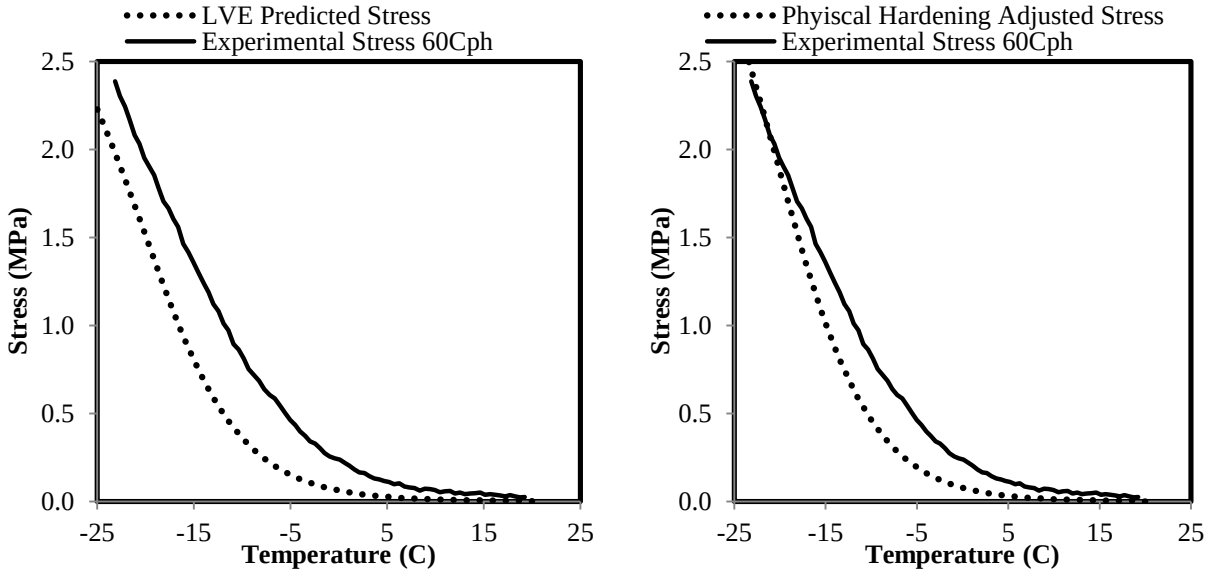

Figure 52 Measured thermal stress for neat asphalt mixture at 60°C/hr cooling rate as compared to (a) LVE predicted thermal stress, and (b) LVE thermal stress adjusted for physical hardening.

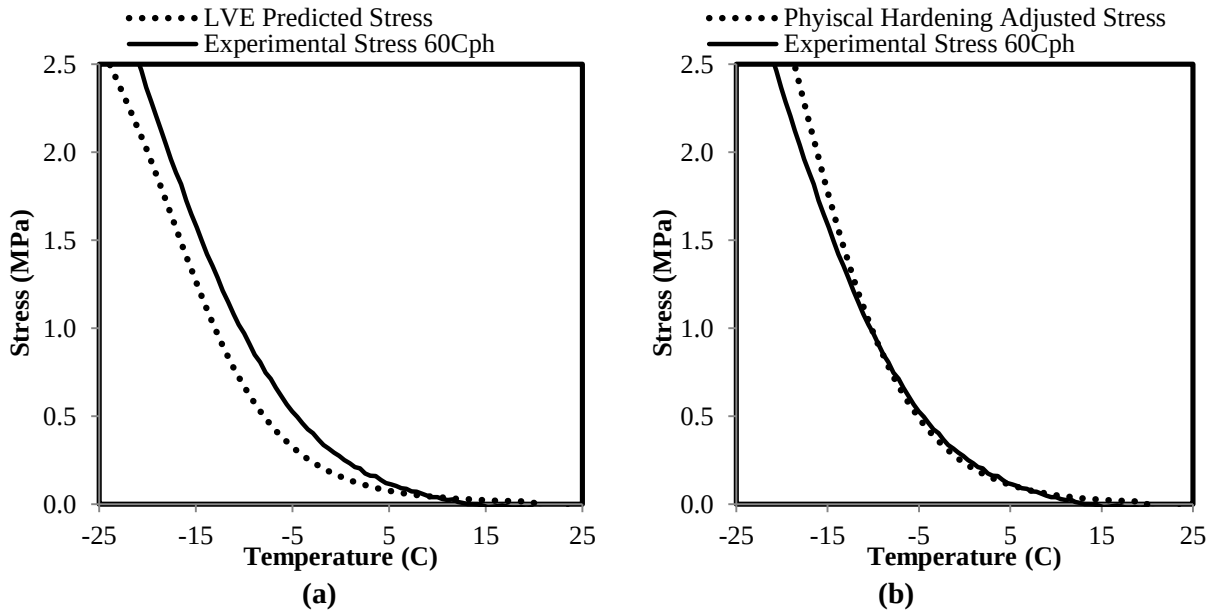

Figure 53 Measured thermal stress for PMA asphalt mixture at 60°C/hr cooling rate compared to (a) LVE predicted thermal stress, and (b) LVE thermal stress adjusted for physical hardening.

The results demonstrated in this section using a fully calibrated model in which all input was experimentally derived and all models were experimentally calibrated, validate the premise of the thermal stress correction procedure using time-dependent physical aging strain through the use of a mastic-calibrated physical hardening model. All predictions are not perfect; the corrected calculation scheme seems to offer a clear improvement in comparison to present methodology.

6.4. Chapter Summary

A model for the calculation of thermal stress buildup in mixtures was derived using relaxation modulus master curves, and a model describing the isothermal contraction of asphalt as a continuous function of conditioning time and temperature. The key idea behind this model is that the input thermal strain can be divided into small increments for which the physical hardening, the thermal hardening and relaxation response can be easily computed and added in time to

obtain the total thermal stress. The model was validated using an elaborate set of experimentally measured input properties for two mixtures at two different cooling rates.

7. Finite Element and Micromechanical Modeling of Thermal Stress and Strain in Asphalt Binders and Mixtures

7.1. Overview

Understanding the distribution of temperature and thermal gradients in the asphalt mixture, as well as evolution of critical stresses in as asphalt mixture during thermal cooling can be very important for determination of thermal cracking resistance of pavements.

To achieve this understanding two finite element modeling approaches were utilized, a continuum model of the ATCA restrained beam geometry including the plastic-steel epoxy putty and the steel end-plates for modeling of thermal gradients during cooling; and an experimentally calibrated multi-phase micromechanical model of asphalt mixture undergoing thermal loading and glass transition developed in a finite element platform using actual 2D images and binder properties.

Good agreement was achieved between thermal stress predictions from the micromechanical simulation and the experimentally measured thermal stress curves. Significant stress concentration was observed in the modeled asphalt mixtures in the vicinity of the aggregate interfaces due to the irregular angular aggregate geometry, and due to the known significant difference in stiffness between the asphalt and aggregate phase, causing a stiffening effect in the binder elements in the immediate vicinity of the fully bonded binder-aggregate interface. Analysis also showed that significant localized strains occur in the binder phase of a fully restrained asphalt mixture sample due to the gradual reorientation of aggregates in the contracting binder medium. To apply the knowledge gained from the simulations, results were used to determine average binder strain rates in pavements undergoing typical cooling rates, for

possible usage in low temperature binder characterization procedures, such as the Single Edge Notch Beam (SENB).

7.2. Temperature Gradient Model

To model the temperature distribution in the asphalt pavement sample used in the ATCA, finite element simulations were performed using ANSYS 12.1. The modelled was meshed using PLANE55 2-D thermal solid elements and was used for 2-D transient thermal analysis of the model. The boundaries were constrained using a decreasing temperature function on the model surface at 6 and 60°C/hr and the temperature evolution were monitored within the sample depth. The model was based on the ATCA sample geometry, consisting of a solid asphalt mixture beam capped at both ends with stainless steel end plate and wedges of plastic-steel putty linking the two materials, as shown in Figure 54. Densities, thermal conductivity, and specific heat values were inputted for all three constitutive materials in the model. Values are shown in Table 9.

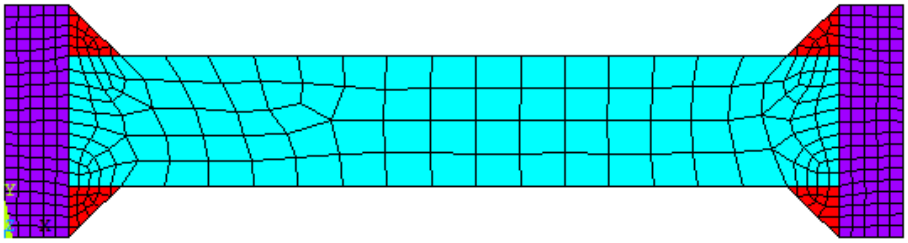

Figure 54 FE model structure, used for simulation of temperature gradients in ATCA asphalt sample (light blue: asphalt mixture; red: steel-epoxy putty; purple: stainless steel)

Table 9 Material thermal properties used in FE analysis [99, 100, 101, 102, 103, 104, 105, 106]

Property	Stainless Steel	Asphalt Mixture	Granite	Asphalt Binder	Plastic-Steel Putty
Thermal Conductivity (W/m-°C)	16.26	1.52	2.55	0.17	5.73
Specific Heat (J/kg-°C)	502.4	1220	790	1758.4	1110
Density (kg/m^3)	8027.2	2400	2600	1041	2330

Thermal conductivity values for asphalt mixtures have been measured in a number of studies, with results ranging from 0.744 to 2.880 W/m-°C with an average of 1.523 W/m-°C, as provided in a comprehensive summary in [107], as well as in [100]. Granite thermal conductivity in literature ranges from 2.1 to 3.12 W/ m-°C with an average of 2.55 W/m-°C [105, 106, 104]. Thermal conductivity of steel is a heavily temperature dependent, reducing as temperature decreases. Reported values range from 12 to 18 W/m-°C [108, 101, 106].

Asphalt mixture specific heat values ranged from 920 to 1852 J/kg-°C, with an average of 1220 J/kg-°C [100, 107]. For the liquid asphalt binder specific heat values ranged from 1758.4 to 2093.4 [99, 100]. Specific heat of granite has been reported consistently approximately 790 J/kg-°C in the literature [103, 102]. Specific heat of stainless steel is also consistently reported around 500 to 504, and average value of 502.4 is used here [109, 99, 101]. Thermal properties for the plastic-steel putty were derived from the manufacturer's specification sheet [110].

Figure 55 and Figure 56 show the temperature distribution for both 60 and 6°C/hr cooling rates, as the surface temperature reaches close to 16.7°C. It can clearly be seen that a larger temperature gradient exists in the sample cooled at a faster cooling rate, with an approximately 1°C differential exists between the core and surface temperatures of the asphalt sample. For the sample cooled at 6°C/hr, the maximum differential between the core and surface is much smaller, approximately 0.1°C. These trends are better shown in Figure 57 for a portion of the cooling curve. In both cases the largest differential was with the stainless steel end plates due to the massive density of these parts in comparison to the asphalt mixture which significantly outweighs its lower specific heat. Furthermore, due to the high conductivity of the plastic-steel putty, the presences of the wedges of glue on the sample extremities does not cause any appreciable effect on the sample's temperature profile.

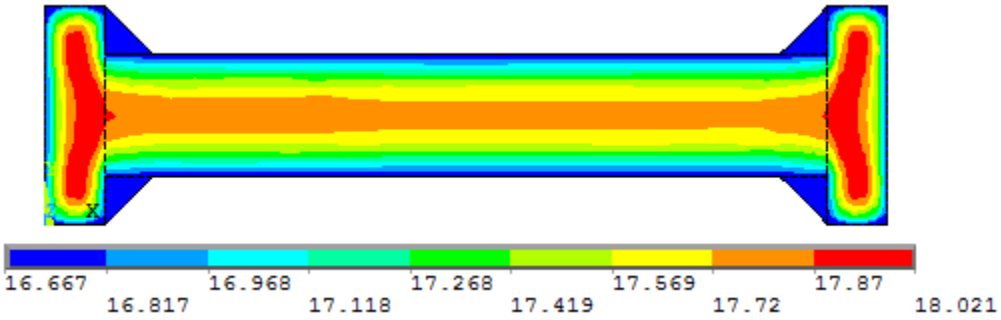

Figure 55 Temperature gradient in ATCA sample subjected to cooling on the boundaries at a rate of 60°C/hr.

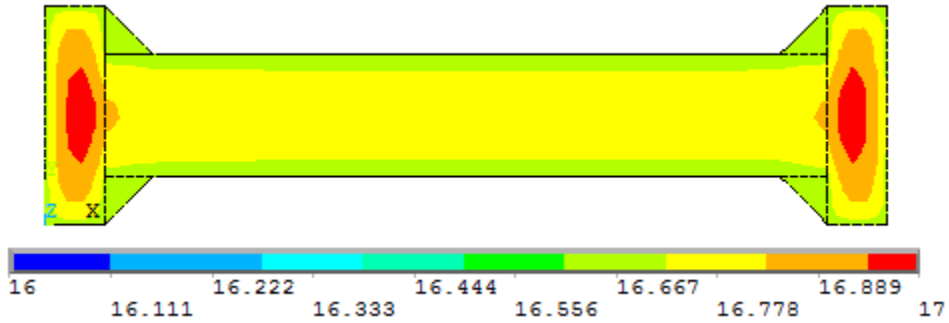

Figure 56 Temperature gradient in ATCA sample subjected to cooling on the boundaries at a rate of 6°C/hr.

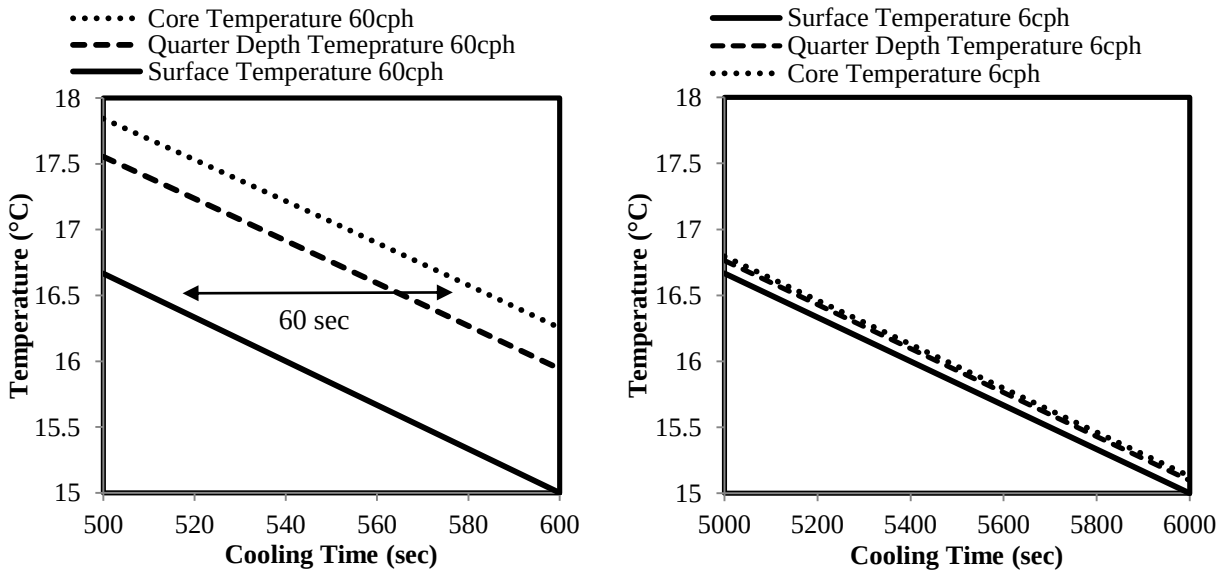

Figure 57 Temperature difference between asphalt surface and core during cooling at 6 and 60°C/hr.

The conclusion from this analysis is rather important, as it shows that even for the rapid cooling rate of 60°C/hr, the temperature differential is relatively small (1°C) and it takes the less than 60 sec for the core to reach the surface temperature. These results show that the delayed thermal strain discussed in previous chapters is not an artifact of temperature differential in the sample, as significant stress buildup in these samples continues for close to an hour after the chamber temperature becomes constant, significantly longer than needed for the asphalt to achieve full temperate consistency through the sample.

7.3. Micromechanical Analysis of Stress And Strain

Although the importance of strain values and strain rates in viscoelastic failure are well known for asphalt materials, strain tolerance have rarely been considered as failure criteria in low temperature cracking models. Asphalt thermal cracking studies have traditionally focused on limiting strength values as the temperature decreases in the pavement, thus predicting crack occurrence temperature based on the comparison between the predicted thermal tensile stress curve and the ultimate tensile strength on a temperature scale [79, 80, 81]. Stress calculation methodologies used have included elastic, pseudo-elastic, and viscoelastic analysis on a beam or a slab [10]. Alternatively, some researchers have used crack tip stress calculations for a pre-cracked pavement and subsequent comparison with estimated pavement fracture toughness through Linear Elastic Fracture Mechanics (LEFM), to predict cracking temperature and crack propagation in the pavement. In this method the pavement layer is discretized into a number of sub-layers or beams, for which the stress is calculated similar to the approach discussed above, based on temperature in each sub-layer, resulting in a stress gradient estimation for the whole layer [82]. In all aforementioned procedures the basis of thermal cracking prediction is solely

strength and limiting stress criteria, while the use of strain tolerance criteria [6] has gathered little attention due to the apparent restrainment of the pavement against large scale strain.

Finite element simulation of thermal stress buildup in asphalt mixtures is not a new topic, and a number of extensive studies have offered useful findings to apply the results of simulation to prediction of pavement cracking [111, 112, 113, 114]. The models used in these studies are all based on assumption that asphalt mixtures can be assumed as continuous isotropic and homogeneous single phase domains with a single constitutive relationship. Such simplification although convenient for macro-scale analysis of thermal stress, yields little insight into the internal stress and strain distribution in the asphalt mixture. Micromechanical analysis of thermal stresses and strains using multi-phase models able to account for stress and strain distributions in each phase is needed, as cracking can start at points of critical stress concentration within the structure and propagate into macro-cracks. The factors involved in identifying these stress concentration points and propagation paths cannot be precisely understood when average, bulk moduli of mixtures are used. This chapter aims to address this issue through the coupling of image analysis and FE modeling and take a deeper look at the internal stress and strain state in asphalt mixtures during thermal contraction, as will be discussed in later sections.

To achieve this objective, experimental procedures were used to measure required thermal and mechanical input values for the development of a multi-phase micromechanical model of a restrained asphalt mixture undergoing thermal loading. Finite element methodology was utilized through the use of the ABAQUS FEM package. The simulations developed were modeled based on the restrained beam geometry used in the TSRST, as performed using the Asphalt Thermal Cracking Analyzer (ATCA), to allow for experimental comparison and

validation. In the following sections the development of this model as well as the derivation of the input properties is discussed in detail, followed by a discussion of results and findings.

7.3.1. General Description of FEM Simulation

The Finite Element (FE) analysis software ABAQUS was used to model asphalt mixtures undergoing thermal contraction and glass transition. A 4-node, plane strain, quadratic, reduced integration element (i.e., CPE4R) was used to mesh the model. Colored images of asphalt mixtures obtained using a flatbed scanner were converted to binary images using the digital image processing software, iPas, as described in [115, 116]. The pixels in the binary image were mapped into CPE4R elements in the FE model using a MATLAB code. The asphalt binder response was modeled assuming linear viscoelastic behavior, while aggregates were considered elastic.

The upper and lower boundaries of the 2-dimensional model were constrained against vertical and horizontal translation as well as rotation in the XY plane. This level of constrain was sufficient to prevent rigid body motion in the model while preventing large scale strain in the axial direction. The model was subjected to a continuously decreasing temperature profile at the constant rate of 0.1°C/min from 20 to -40°C and the stress and strain response within the model were monitored. The zero-stress reference temperature was assumed to be 20°C. The transient "VISCO" procedure was used for stress and strain analysis of the model.

The material used in the experimental study consisted of mixtures using a granite aggregate source with a neat and a modified asphalt binders. The neat base binder, graded as a PG 64-22, was modified to a PG 70-22 using a plastomeric poly-ethylene based polymer, hereby referred to as PMA. Further details pertaining to sample preparation and modification procedure

is available elsewhere [117]. Details pertaining to the derivation of input properties and the calculations involved are described next.

7.3.2. Relaxation Modulus Master Curve Calculation

An important input in the FE model is the relaxation modulus of the viscoelastic asphalt binder phase. Viscoelastic mechanical properties are inputted either in the time or frequency domain. For the current analysis Bending Beam Rheometer (BBR) creep data were used to derive the required properties. BBR creep is performed under a constant load over 240 seconds, during which the mid-point deflection is measured and reported at 0.5 sec intervals. The BBR tests were performed at three temperatures, -6, -18 and -24°C.

For usage in the ABAQUS FEM package, viscoelastic modulus should be expressed in terms of relaxation modulus Prony series. The BBR creep data was used to construct a creep stiffness master curve in stretch exponential sigmoidal format, as shown in (1). Creep data from the three temperatures were shifted to 20°C, which is the zero-stress reference temperature, using the William-Landel-Ferry (WLF) time-temperature shift factor formulation shown in (2). A simultaneous squared error minimization technique was used to determine the WLF material constants, c_1 and c_2, and the master curve parameters simultaneously. The resulting WLF parameters and reference temperature were inputted in the Thermo-Rheological Simple properties tab (TRS) under the viscoelastic mechanical properties category in ABAQUS to enable shifting of the master curve as the temperature varied in the simulation.

A phenomenological model proposed by Christenson and Anderson [118] and later used by Bahia et al. [6] in a low temperature modeling procedure was used to generate the modulus master curve. The equation is shown below:

$$S(t) = S_g \left(1 + \left(\frac{a_T t}{t_c}\right)^k\right)^{-m_e/k} \quad (1)$$

$$\log_{10} a_T = -\frac{C_1(T_t - T_0)}{C_2 + (T_i - T_0)} \quad (2)$$

Where:

- S_g is the glassy modulus,
- t_0 is a location constant with time dimension,
- k is a fitted constant, and
- m_e is the slope of the creep stiffness-loading time slope on a log-log scale when $t \rightarrow \infty$.
- T_i is current temperature, and T_0 is the reference temperatures,
- a_T represents the time-temperature shift factor.
- C_1 and C_2 are the WLF constants.

In the next step the creep stiffness master curve was converted to relaxation modulus. Relaxation modulus and creep compliance are related through the viscoelastic hereditary integral. One may be rewritten in terms of the other by manipulating this relationship through Laplace Transformation [93]. Using the Hopkins and Hamming algorithm the solution to this transformation may be numerically estimated quite accurately [119]. The relaxation modulus values were then fitted with a 3-element Prony series, formulated as shown in (3). The Prony series parameters inputted to ABAQUS are normalized such that the sum of all element coefficients is less than one. The normalizing parameter, E_0, was inputted as the instantaneous elastic modulus. A constant Poisson ratio of 0.49 was used for the asphalt binder. For granite aggregates cited values of elastic modulus usually range from 2.0 to 30.0 GPa, with Poisson ratio values ranging from 0.1 to 0.3 [120, 121, 122, 123]; thus in the present study an elastic modulus

of 15.0 GPa and a Poisson ratio of 0.25 were used. Results of relaxation modulus as a function of loading time for the neat and modified binders are shown in Figure 58.

$$E(t) = E_0\left(1 - \sum_{k=1}^{N} \bar{e}_k^P (1 - e^{-t/\tau_k}\right) \quad (3)$$

where

- *E(t)* is the relaxation modulus as a function of loading time
- E_0 is the instantaneous modulus
- $\bar{e}_k^P$ is the relaxation modulus ratio
- τ_k is relaxation time

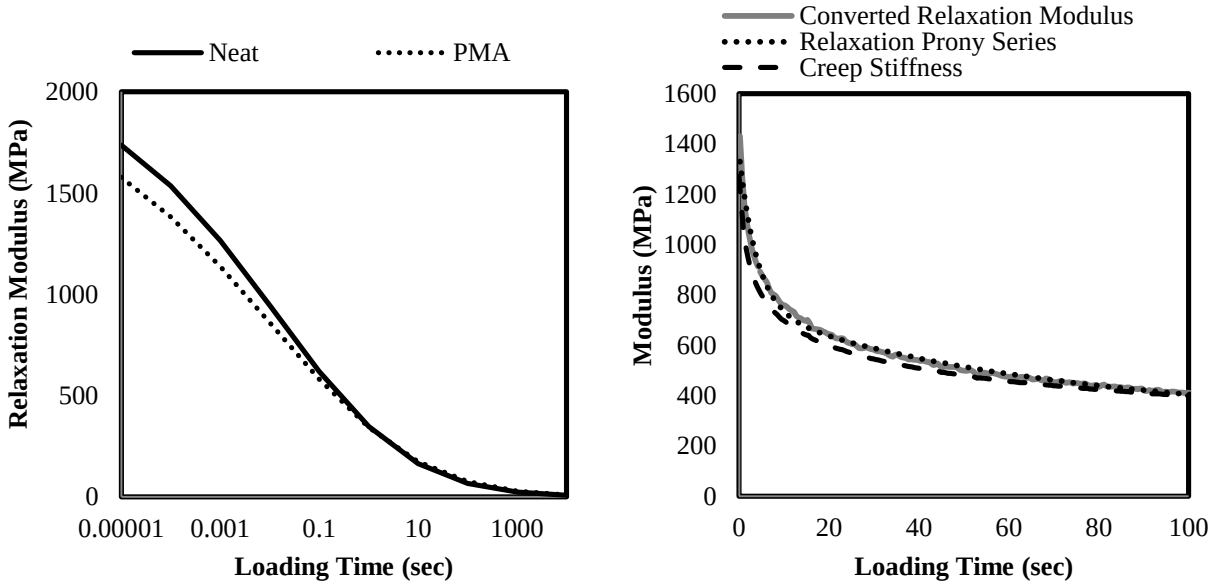

Figure 58 (a) Asphalt binder relaxation modulus master curves constructed from BBR data, and (b) Example of BBR creep stiffness for PMA at -18°C, converted to relaxation modulus, and fitted with relaxation modulus Prony series.

7.3.3. Simulating Thermal Shrinkage and Modeling the Coefficients of Contraction

It is well known that asphalt binders undergo a "Glass Transition" as temperature decreases toward lower service temperatures. As the binder temperature decreases toward the glass

transition region the "liquid" coefficient of contraction (α_l) gradually decreases until settling at a lower constant "glassy" coefficient (α_g). Comprehensive description of this phenomenon is provided elsewhere [57, 51]. Using the dilatometric system described earlier, the CTE values were measured for each binder at decreasing temperatures. Accurately capturing the glass transition behavior of asphalt binders and incorporating this effect into the simulation was deemed important for accurate prediction of thermal strain, and consequently thermal stress buildup in the binder phase of the mixture.

Cited CTE values for granite range from 7.9 to 9.0×10^{-6} m/m°C [124, 125, 126], thus a constant temperature-independent CTE of 8.5×10^{-6} m/m°C was used for the granite aggregate phase, which was easily defined in the model assuming a zero-stress reference temperature of 20°C. On the other hand, the FE platform was not readily equipped to handle the continuous analysis of thermal strain using temperature-dependant CTE of the binders. ABAQUS by default calculates thermal strain at any temperature in comparison to the reference temperatures, and not the temperature at previous increments. Consequently, a step-wise transient analysis of a cooling problem with temperature-dependent decreasing CTE values will incorrectly yield a local minima in the thermal strain-temperature curve, with thermal strain gradually decreasing as the CTE decreases. This is because the accumulated strain in each step is calculated with regards to a fixed reference temperature rather than the temperature at the end of the previous step. To correct for this deficiency, the experimentally measured CTE values were adjusted using the formulation derived in equation (4), such that when used in the ABAQUS analysis scheme the resulting thermal strain is equal to that of a step-wise analysis in which accumulated thermal strain is calculated against the temperature at the end of the previous step. The adjusted CTE values for the binder phase were entered in tabular form at 5°C intervals from 20 to -40°C. Accumulated

thermal strain calculation results using the ABAQUS calculation scheme, with- and without the derived adjustment, are compared to experimental values in Figure 59. Figure 59(a) also compares the experimentally derived CTE values for the neat and PMA binders, showing that the sharp and rapid transition in the neat binder is broadened and extended when binder was modified to produce the PMA. Furthermore, at most temperature ranges, the neat CTE is higher than that of the PMA, which can potentially lead to larger stress buildup due to higher thermal strain in the neat binder.

$$\alpha_{cr}(T_i) = \alpha(T_i)\left[\frac{\sum_{i=0}^{n}\alpha(T_{i+1})\cdot(T_{i+1}-T_i)}{\sum_{i=0}^{n}\alpha(T_{i+1})\cdot(T_{i+1}-T_0)}\right] \quad (4)$$

In which:

- T_i is current temperature, and T_0 is the reference temperatures,
- $\alpha(T_i)$ represents the CTE as a function of current temperature.
- $\alpha_{cr}(T_i)$ represents the adjusted CTE for input to ABAQUS.

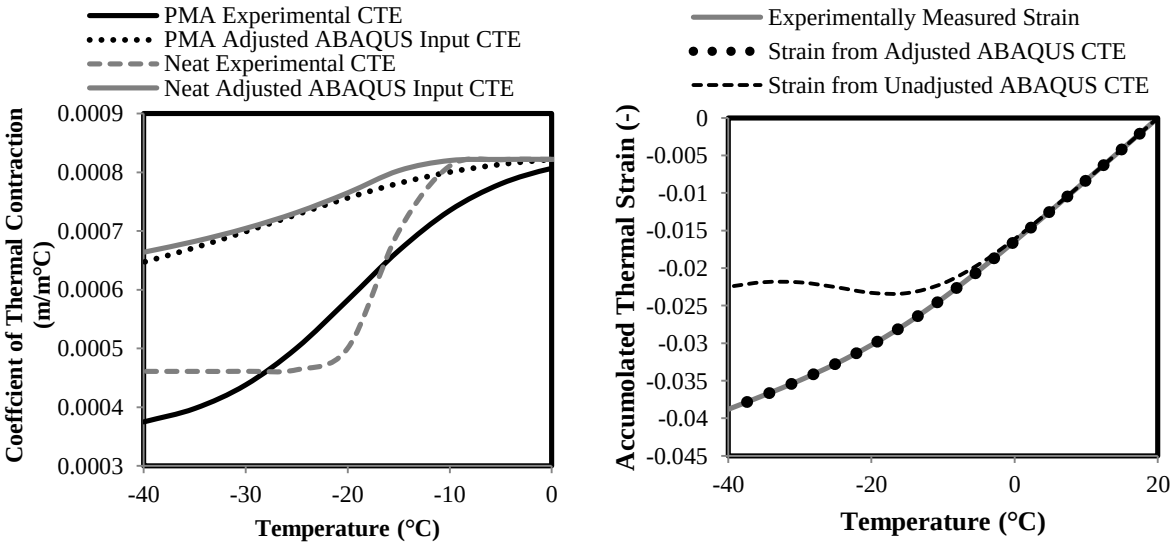

Figure 59 Comparison of (a) measured and adjusted CTE, and (b) measured and calculated thermal strain with and without adjustment

7.3.4. Discussion of Results

Researchers in earlier studies have used many different cooling rates to test and model field conditions. Bouldin et al. [10] used 3°C/hr to match studied field sections, while suggesting that resulting cracking temperature may be "bumped" up or down for faster and slower rates. Model calculations by Bahia et al. [6] for rates lower than 10°C/hr showed that reducing cooling rate corresponded to a shift in thermal stress buildup toward lower temperatures. SHRP researchers reported that although typical field cooling rates seldom exceed 2.7°C/hr, most TSRST tests are done at rates of 10°C/hr or higher to reduce testing time [15]. Although tests ran during the SHRP study showed a decrease in fracture temperature as the cooling rate varied between 1 to 5°C/hr, it was concluded that although cooling rates higher than 5°C/hr do not necessarily match typical field conditions, they are sufficient to assess relative performance of specimens.

In the present study using the ATCA tests cooling tests were performed on restrained beams at 0.1°C/min (6°C/hr). FE model simulation were also performed at the same rate, inputting the derived material properties described earlier for the binder and aggregate phase of the neat and PMA models. Results are compared in Figure 60. It can be seen that generally good agreement resulted from the micromechanical FE simulation and the experimentally measured thermal stress curves.

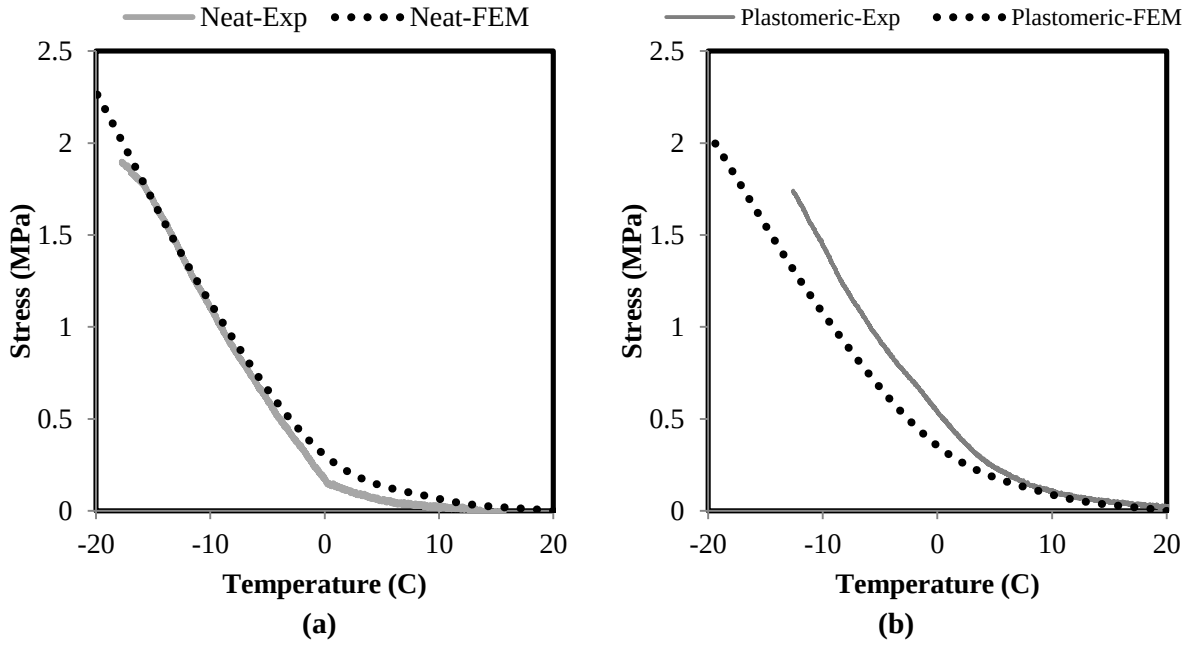

Figure 60 Experimentally measured thermal stress buildup compared to micromechanical model prediction

The discrepancy between measured and simulated results observed in Figure 60(b) can be attributed to inherent model simplifications as filler particle were not captured in the imaging procedure, thus any possible effects were not considered. Furthermore, the inability of the FE model to account for delayed thermal strain, also referred to as physical hardening, may also contribute to the under-prediction of stresses for the case of the PMA mixture. This phenomenon is discussed in greater detail in earlier work by the author and coworkers [127, 51]. It is believed that if cooling rates are slower than a specific material dependent critical rate, much of the time dependent delayed thermal strain due to physical hardening will occur at experimental times, as sufficient time is available during cooling. At such rates relaxation will be the primary time-dependent phenomenon occurring, leading to lower stress buildup as the cooling rate decreases. In the present work the cooling rate was selected as to minimize the potential effect of physical hardening (time-dependent (delayed) thermal strain), as to avoid further complexities in the model.

Stress and Strain Distribution in Binder Phase during Cooling

Although the aggregate phase in the asphalt mixture is the major phase both in terms of volume fraction and relative stiffness to the minor phase, asphalt binder still transfers a significant portion of the induced thermal stress in the mixture. Although resultant stress reaction on the sample boundaries is tensile due to the restrainment against shrinkage, stress state in the binder phase can be a complex combination of tensile, compressive and shear stresses, due to the multi-directional nature of the internal interaction of aggregate particles with increasing proximity in the continuously contracting medium. Thus for binder stress analysis, the use of the Von Mises "effective stress" parameter was deemed most appropriate. Figure 61(a) shows the average stress built-up in the binder phase in comparison to the mixture's tensile reaction stress. Figure 61(b) shows the calculated ratio of average bulk tensile stress in the mixture to the average binder stress. It can be seen that at higher temperatures where the stiffness ratio between the aggregate and binder is very high, the stress ratio is highest, but gradually decreases and finally becomes relatively constant as binder stiffness increases significantly with temperature, before becoming relatively constant below the glass transition temperature. The stress ratio became constant at close to 23 for the relatively softer PMA and at 14 for the stiffer neat binder. These results are logical as they show that in the mixture with the softer binder (PMA), a smaller portion of the stress was carried by the binder phase.

Some previous research on thermal stress in asphalt pavements have made the assumption that all tensile stress in the pavement is carried by the binder phase [10]. This belief is probably based on the assumption that the aggregate structure is unable to form effective interlock under tensile loading, thus aggregates are floating in a stress-bearing binder medium. As a result, the difference in measured and predicted thermal stresses in the asphalt mixture has

been mostly explained by the difference in strain rate throughout the binder phase due to changes in film thickness and geometry. This has led to the development of stress correction factors referred to as "pavement constants" [10, 128]. Pavement constants used in literature are usually between 18 and 24 [10, 128]. It is interesting to see from the results in Figure 4 that these constants, which have been purely empirically selected in the literature, are in the same order of the mixture to binder stress ratios derived in the present study.

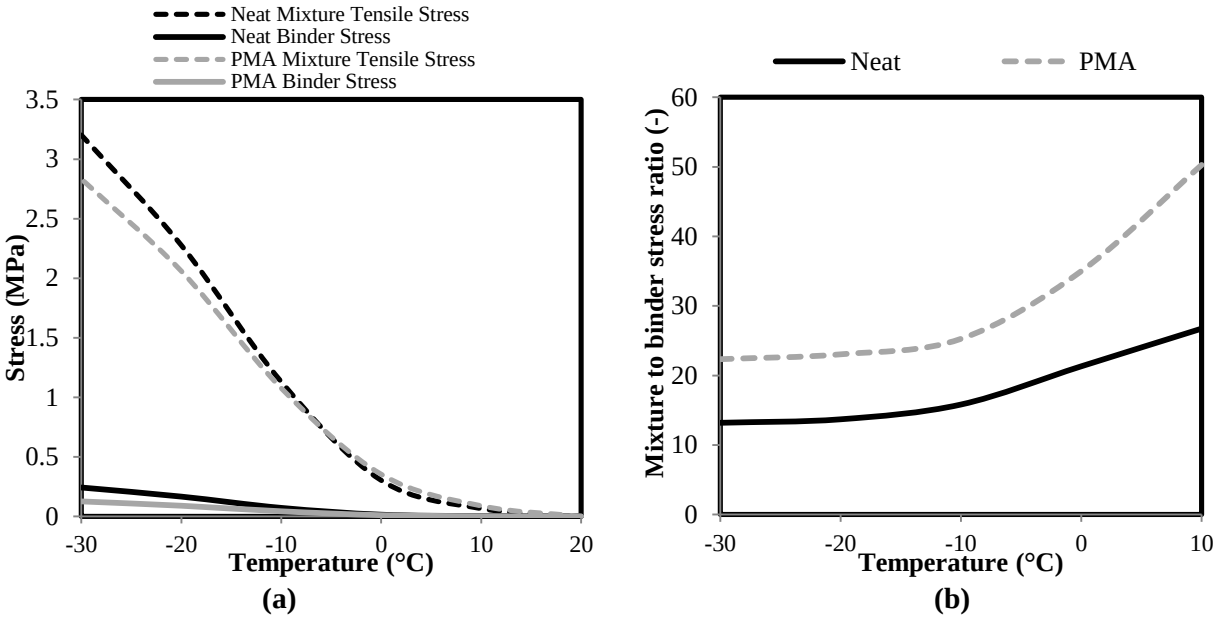

Figure 61 Comparison of (a) thermal stress buildup in binder phase and the whole mixture, and (b) mixture to binder stress ratio for PMA and neat binders.

It should also be noted that the micromechanical modeling results in this study raise some important questions about the assumption of all tensile stress being totally concentrated in the binder phase. It is clearly seen that most of the stress is in fact concentrated in the aggregate phase. This is very logical since the binder phase is most susceptible to thermal strain and it is heavily restrained locally at the aggregate- interface throughout the mixture, as the aggregate CTE is much smaller than that of the binder.

The restraining of binder contraction at the binder-aggregate interface due to the difference in thermal contraction of the two phases, leads to the formation of large stresses in the interface to satisfy the strain compatibility at the surface of aggregates. Furthermore, differences in specific heat of the aggregate and binder phase may lead to a discontinuity in temperature in the asphalt binder and aggregate phases, further exacerbating differences in thermal strain across the aggregate-binder interface. In such conditions, the aggregate phase will buildup larger thermal stresses than that of the binder phase, due to the significant difference in aggregate and binder stiffness. As the modulus of the binder phase increases due to temperature decrease, the stiffness differential between the two phases decreases which makes the stress in the binder phase grow closer to that of the aggregate. This is clearly shown in Figure 61(b) which depicts the ratio of stresses in the mixture to the binder phase. The trends for both binders show that the ratio of mixture to binder stresses decreases with decreasing temperatures.

Stress and strain distributions calculated from the Finite Element Method in the restrained beam model are shown in Figure 62. In a composite of asphalt binder and aggregate, a number of factors could lead to the formation of localized, non-uniform stress distribution in the sample. The simplest cause of stress non-uniformity is stress concentration due to the irregularity of aggregate geometry in the asphalt matrix. Secondly, the significant difference in stiffness between the asphalt and aggregate phase, coupled with the assumption of complete bonding at the interface of the two phases leads to an inherent stiffening effect in the binder elements in the immediate vicinity of the aggregate interface, thus concentrating a larger stress field in these elements. Furthermore, stress concentrations are also observed at the aggregate proximity contact points (Figure 62(a)). The aforementioned factors lead to the formation of non-uniform, continuously evolving stress fields at the local aggregate scale in the asphalt mixture as the

sample is cooled. Significant localized strains occur in the binder phase of a fully restrained asphalt sample due to the gradual reorientation of aggregates in the contracting binder medium. The buildup of high values of stress and strain at the aggregate-binder interface can lead to aggregate debonding if the pavement is cooled to sufficiently low temperatures.

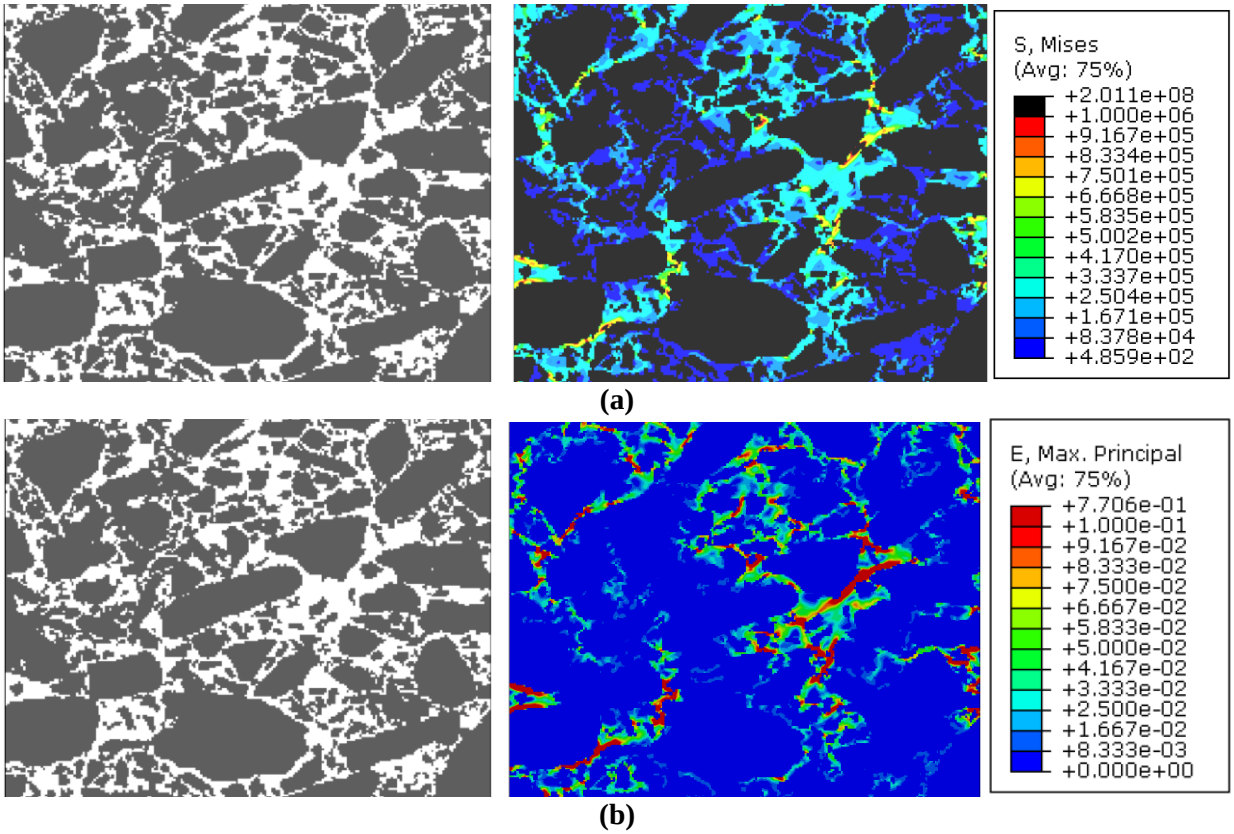

Figure 62 (a) principal strain distribution, and (b) Von Mises stress distribution (Pa) in modeled restrained asphalt mixture (PMA) undergoing thermal loading.

Figure 63 and 64 are prepared to depict the continuous evolution of the internal binder stress and strain distribution, respectively, as the samples are continuously cooled, for both the neat and PMA mixtures. The first noteworthy observation in Figure 63 is that at 10°C almost all binder elements had zero stress. As the temperature decreases the stress distribution curves begin to flatten out and the peak (highest frequency) stress level begins to move from zero to higher stress levels as more binder elements build-up stress. Comparing Figure 63(a) and (b), one

immediately notices that the stress distribution curves for the PMA binder are much narrower and closer to zero than that of neat binder. This is a clear indication of the significant role of binder visco-elastic properties for a given aggregate skeleton.

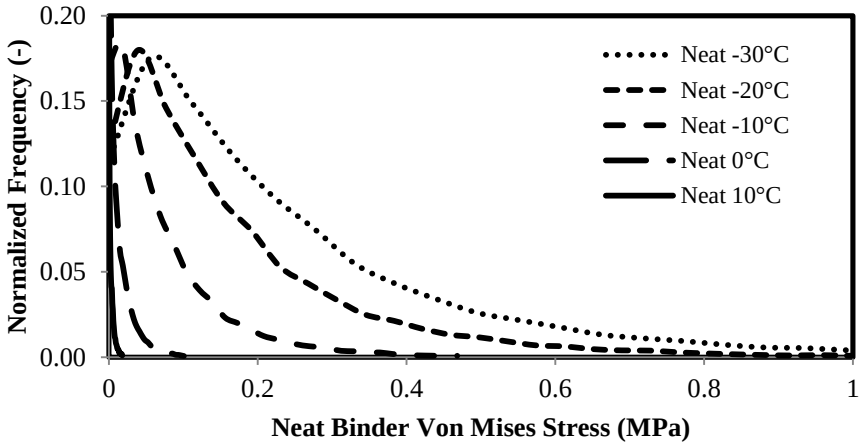

(a)

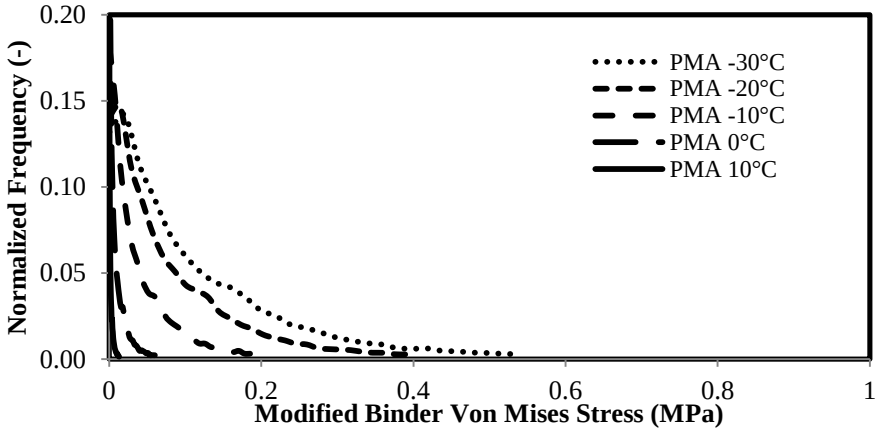

(b)

Figure 63 Nodal stress histograms for neat (a) and PMA (b) binder phases in the mixture

Figure 64 shows the binder maximum tensile strain histograms for the neat and PMA binders as temperature was continuously decreased. It can be seen that the PMA and neat strain histograms are relatively similar, with the PMA histogram being slightly flatter than that of the neat asphalt. Comparing these trends to the stress distributions in Figure 63, one may observe that the relatively similar strain distributions in the two binders correspond to significantly different

stress distributions for the two binders, as would be expected due to the modulus difference of the neat and PMA binders.

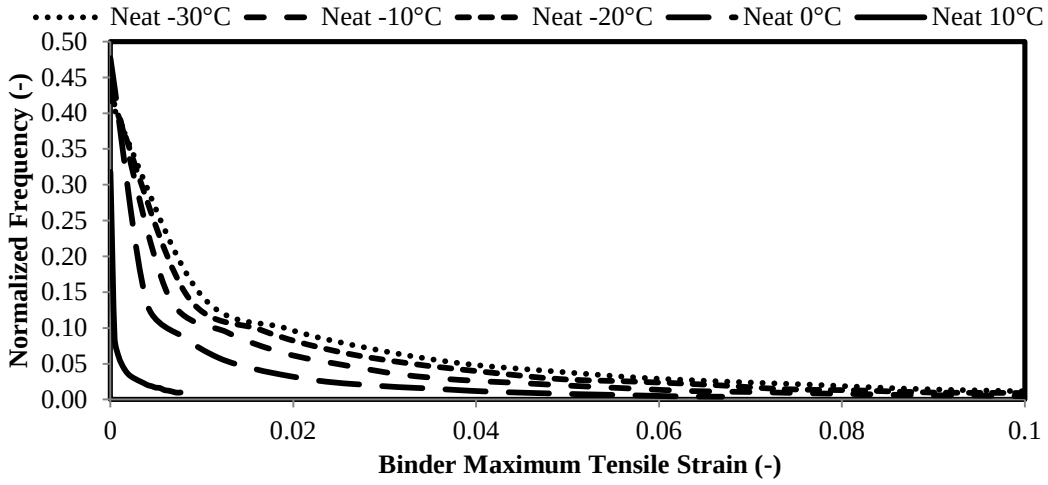

(a)

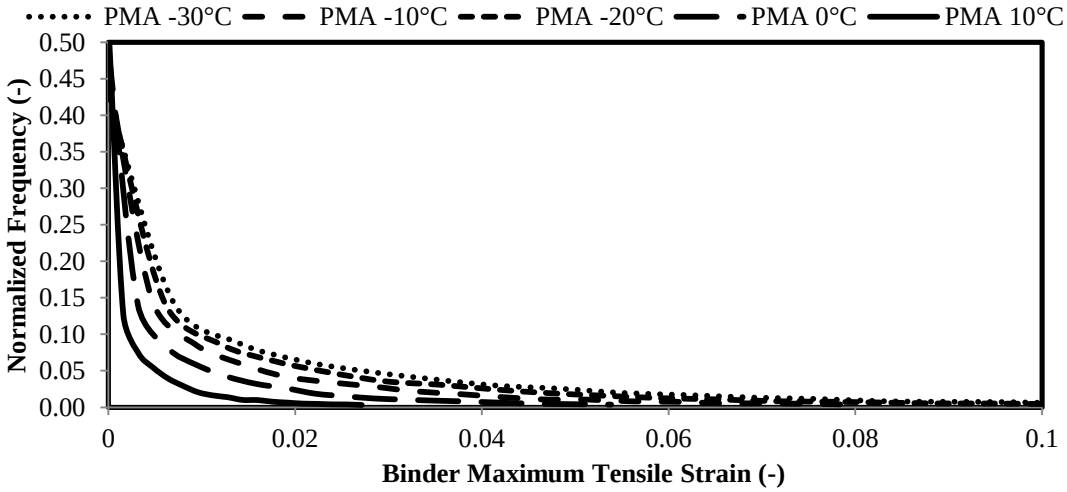

(b)

Figure 64 Nodal strain histograms for neat (a) and PMA (b) binder phases in the mixture

7.3.5. Binder and Mixture Strain Rates during Cooling

An important consequence of the occurrence of such strains in the asphalt-aggregate interface is the potential importance of considering ultimate failure strain criteria in addition to the prevalent tensile strength criteria used commonly for thermal cracking ranking and characterization. Such

observations are in agreement with recent reports that a clear relationship between crack severity in monitored field sections and strain tolerance measured for binders at low temperatures using the Single Edged Notched Beam (SENB) [129].

An important factor when characterizing asphalt binders using fracture tests such as the SENB is the target binder strain rate. Using data collected in the present study, tensile strain buildup was plotted against cooling time, as shown in Figure 65(a) and (b). Both the average binder strain and the maximum tensile strain occurring at each temperature are considered, as seen in Figure 65(a) and (b). A relatively linear relationship is observed for both the average and maximum strain trends, although the maximum strain buildup rate begin to decrease as the binder temperature approached the glass transition (T_g) range.

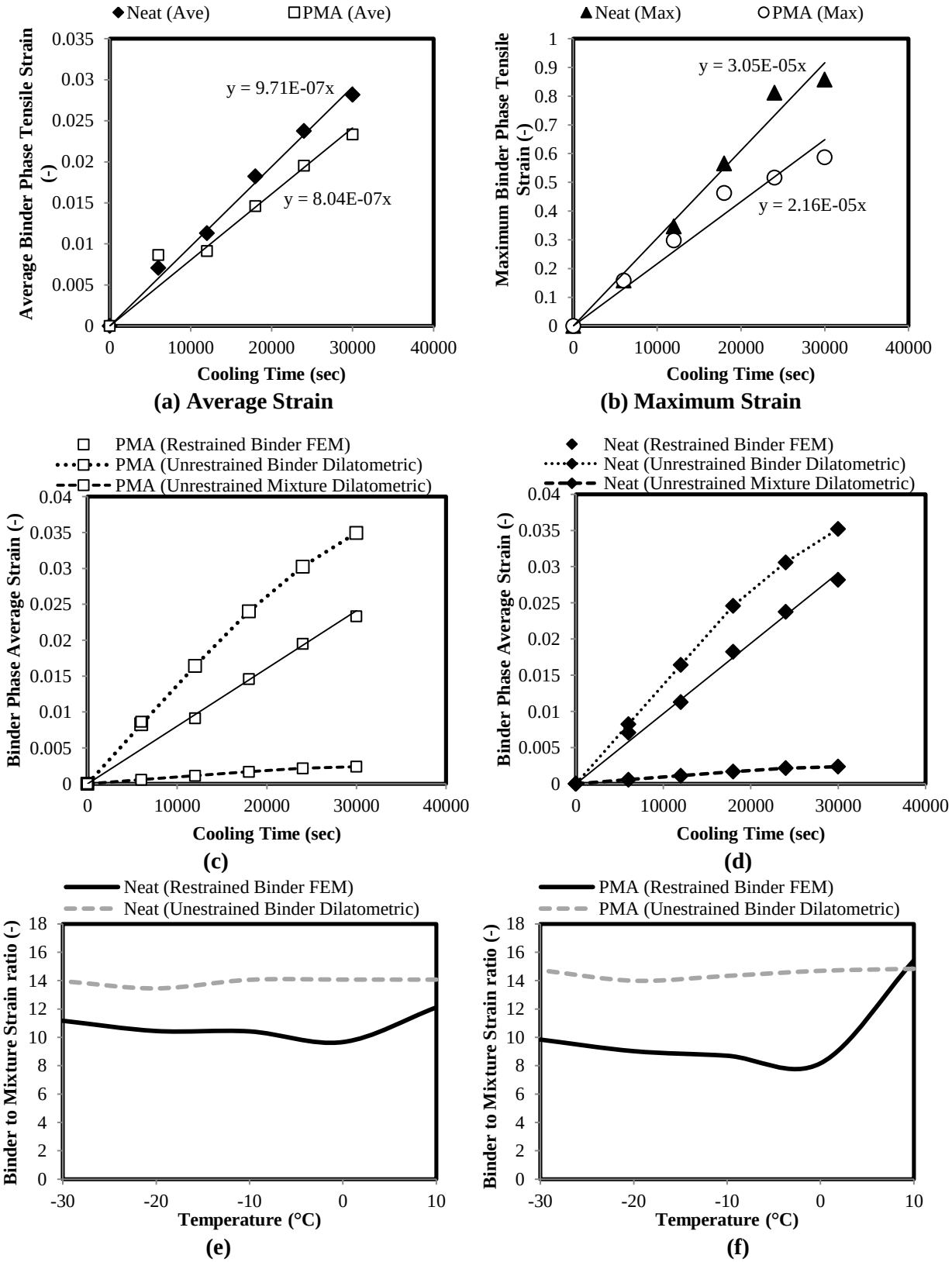

Figure 65 (a) Average binder tensile strain buildup, and (b) maximum binder tensile strain buildup during cooling for binder studied

Figure 65(c) and (d) compare the average binder strain in the modeled restrained asphalt mixtures with thermal strain measured in the unrestrained mixture beam of the ATCA and the binder dilatometric system. Restrained binder strain rates varied from average values of 0.00009%/sec, up to a maximum of 0.003%/sec at a cooling rate of 6°C/hr. In comparison, strain rates for the freely contracting binders and mixtures were in the order of 0.00012%/sec and 0.000008%/sec, respectively. It is observed that the binder strain in the restrained mixture, being restrained on the aggregate interfaces, is lower than the freely contracting asphalt binder, while being much higher than the bulk mixture thermal strain. Furthermore, the ratio of unrestrained dilatometric measurements of binder and mixture strain, as shown in Figure 65(e) and (f), is relatively similar for neat and PMA, and constant with temperature. On the other hand, the ratio for PMA restrained binder strain is slightly lower than that of the neat binder, indicating higher restrainment of the softer PMA binder by the aggregates. Unlike thermal stress and relaxation modulus, it is expected that thermal strain rate values to be adjustable for minor changes in cooling rates.

An important implication of the analysis is that unlike the bulk thermal strain in the mixture, thermal strain in the binder is not fully restrained (Figure 65(c) and (d)). Thus asphalt mixture thermal stress predictions based on scaling binder thermal stress continuum analysis results using “pavement constants” is not appropriate. Bulk mixture thermal strain must be used for accurate continuum calculations.

7.4. Chapter Summary

In this chapter a multi-phase micromechanical model for asphalt mixture undergoing thermal shrinkage and glass transition was developed in a finite element platform. The results where

compared to experimental data measured using the ATCA device which allow measuring strain and stress build up during cooling. The following major findings can be stated:

- The findings of this analysis show that even for the rapid cooling rate of 60°C/hr, the temperature differential is relatively small (1°C) and it takes less than 60 sec for the core of sample to reach the surface temperature. These results prove that the delayed thermal strain discussed in previous chapters is not an artifact of temperature differential in the sample. In fact it is observed that significant stress buildup in these samples continues for close to an hour after the chamber temperature becomes constant, which is significantly longer than needed for the asphalt to achieve full temperate consistency through the sample.
- Good agreement is observed between thermal stress predictions from the experimentally calibrated micromechanical Finite Element simulation and the experimentally measured thermal stress curves in the present study. This indicates that the procedure followed for simulation using 2D imaging is promising. Significant stress concentration occurs in the binder phase in asphalt mixtures in the vicinity of aggregate interfaces due to sharp aggregate angularity, the difference in coefficient of contractions, and the significant difference in stiffness between the asphalt and aggregate phase. It is believed that such stresses could lead to binder debonding from aggregate if the temperature drops sufficiently and strains exceeds tolerance of binder phase.
- The formation of non-uniform, continuously evolving localized strains in the binder phase surrounding the aggregates leads to gradual reorientation of the aggregates, leading to potentially high binder strains on the constrained binder-aggregate interface. These

changes could happen while the overall sample dimensions in the restrained directions remain unchanged.

- The mixture to binder thermal stress ratio becomes relatively constant at values close to 23 (mixture to binder ratio) for the relatively softer PMA and at 14 for the stiffer neat binder. “Pavement constants” reported in the literature are in the same order of the mixture to binder stress ratios derived in the present study.
- A relatively linear relationship was observed between binder strain buildup and cooling time, although the maximum strain buildup rate seems to have begun to decrease as the binder temperature approached the T_g. Strain rates varied between neat and PMA binders, with average strain rate values ranging between 0.00009%/sec to 0.003%/sec at a 6°C/hr cooling rate.
- Unlike the bulk thermal strain in the mixture, thermal strain in the binder is not fully restrained. Thus asphalt mixture thermal stress predictions based on scaling binder thermal stress continuum analysis results using “pavement constants” is not appropriate. Bulk mixture thermal strain must be used for accurate continuum calculations.

8. Definition of Factors of Importance and Criteria for Low Temperature Performance

8.1. Overview

In this chapter the model developed was used to conduct a matrix of analytical runs to determine the relative importance of each of the contributing parameters in thermal stress buildup through an analysis of variance. The results are used to develop possible asphalt mixture low temperature failure criteria based on using the ATCA, binder fracture, physical hardening and thermo-volumetric results. Results from a number of low temperature performance tests for both asphalt binders and mixtures are discussed in terms of applicability for development of limiting material criteria for prevention of thermal cracking in asphalt pavements.

8.2. Sensitivity Analysis

Sensitivity analysis of thermo-volumetric properties was performed for 8 parameters during cooling and heating. The parameters include T_g, α_l and α_g in cooling and the width of the glass transition region. The width is considered as a potentially important parameter, partially described by the parameter "R". These parameters were defined in chapter 5.

Parameter values for a typical mixture are used as a baseline. The parameters were then systematically varied by ±20% to capture the sensitivity of the stress buildup in mixture to the changes in these parameters. The 20% variation was selected as the maximum percentage of change allowable to keep all parameters in a realistic and practical range. Table 10 and Table 11 show the analysis matrix and the values used in this study.

Table 10 Analysis matrix used for the sensitivity analysis

	Run 1	Run 2	Run 3	Run 4	Run 5	Run 6	Run 7	Run 8	Run 9
T_g	1	1.2	0.8	1	1	1	1	1	1
R	1	1	1	1.2	0.8	1	1	1	1
α_l	1	1	1	1	1	1.2	0.8	1	1
α_g	1	1	1	1	1	1	1	1.2	0.8

Figure 66(a-d) show results of thermal stress calculations for a mixture sample cooled at 1°C/min from 10 to -22°C and then held isothermally for 180 minutes before being heated back up to 10°C at the same rate. The stress calculations were made with and without taking time-dependent strain into account (solid and dotted lines respectively).

A qualitative analysis of Figure 67 shows that changing α_l has the most effect on the thermal stress buildup during cooling, when not accounting for physical hardening, while changing the glass transition temperature and the related parameters (α_l and R) did not show significant effects. On the other hand, the stress sensitivity to T_g and R increased significantly when accounting for the physical hardening. These variations are shown in Figure 67 by plotting the thermal stress buildup for every condition, normalized to the initial unchanged state of the parameters.

Table 11 Parameter values used for the sensitivity analysis

	Run 1	Run 2	Run 3	Run 4	Run 5	Run 6	Run 7	Run 8	Run 9
T_g	-17	-20	-13	-17	-17	-17	-17	-17	-17
R	6	6	6	7	5	6	6	6	6
α_l	5E-5	5E-5	5E-5	5E-5	5E-5	6E-5	4E-5	5E-5	5E-5
α_g	1E-5	1E-5	1E-5	1E-5	1E-5	1E-5	1E-5	1.3E-5	9E-6

A noteworthy trend in Figure 67 can be seen when comparing the T_g+ and T_g- conditions to the base condition. If no time dependent strain (physical hardening) is considered in the stress calculations, a higher T_g would simply lead to a net decrease in the CTE value since α_l will reduce to the lower value of α_g at higher temperatures, thus less over all shrinkage and subsequent less stress buildup will be calculated for any given temperature below the T_g. As mentioned earlier, for the calculation of physical hardening it is assumed that the rate of time dependent strain increases as the temperature approaches the T_g, from both sides. Thus if physical hardening is considered in the stress calculations, increasing the T_g would also mean that time dependent strain accumulate at a higher rate at higher temperatures, potentially resulting in a higher stress buildup in the sample, as seen in Figure 67.

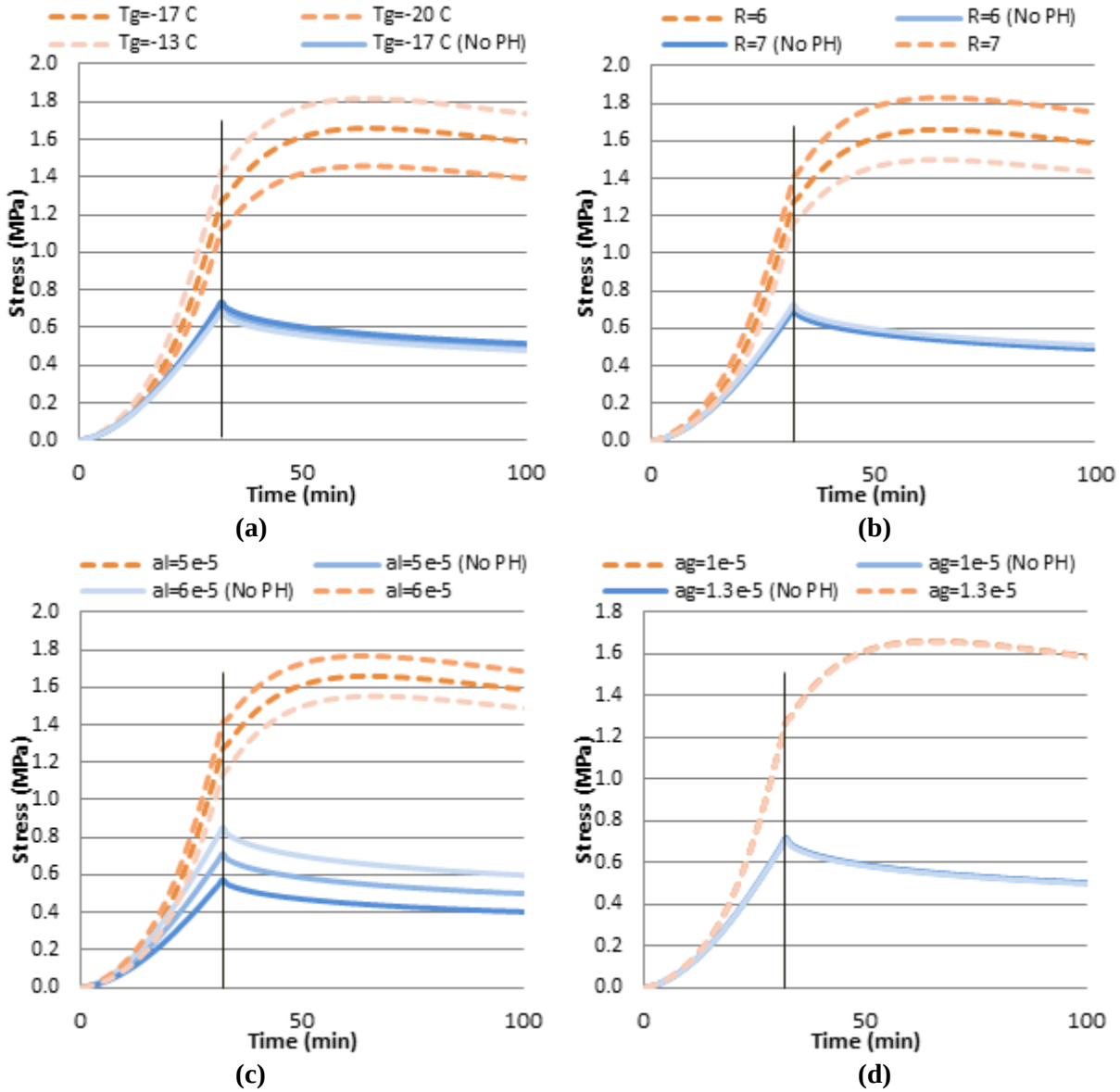

Figure 66 Sensitivity analysis of calculated mixture stress buildup with and without accounting for physical hardening, by changing (a) T_g, (b) R, (c) α_l, and (d) α_g.

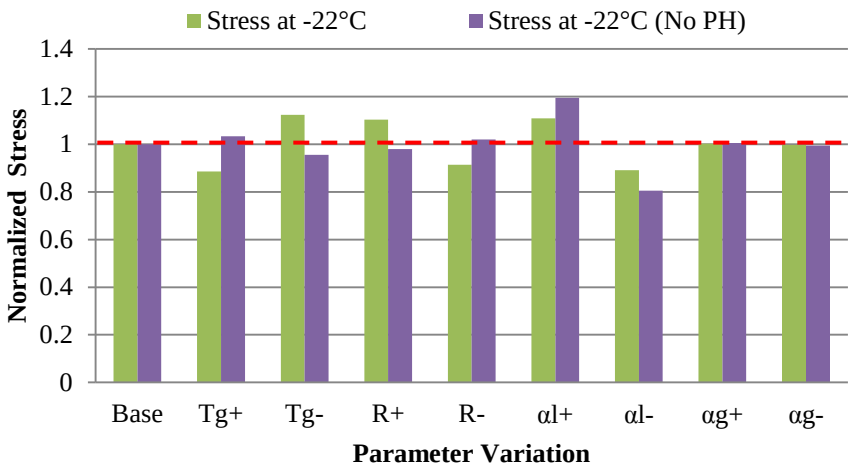

Figure 67 Variation of thermal stress at -20°C, by changing dependent parameters by ±20% (X± shown in the chart indicates that parameter X has been changed by ±20%)

The glassy coefficient of expansion/contraction ($\alpha_{g.}$) does not appear to result in much sensitivity as shown in the current plots. This observation however does not indicate that α_g values are not important. The importance of $\alpha_{g.}$ is highlighted in Figure 68(a, b), in which the thermal stress is calculated using three methods: (a) using full strain-temperature curve considering glass transition, (b) using a constant CTE equal to α_l, and (c) using a constant CTE equal to the average of α_l and α_g for all temperatures. It can be seen that the simplifying assumptions made for the CTE lead to up to more than 25% difference in the total accumulated thermal stress at -30°C. On the other hand, the small amount of sensitivity to the typical range changes in α_g observed in Figure 66(d) would indicate that using a typical average value for α_g may be sufficient for thermal stress calculation, and measurement of an exact α_g may not be necessary.

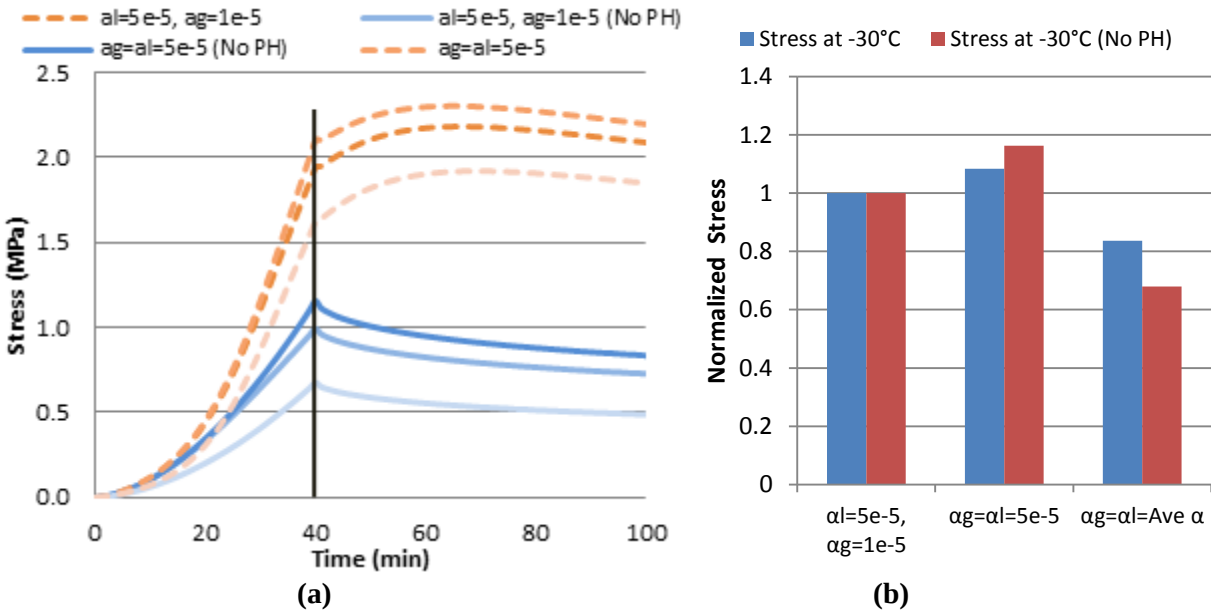

(a) (b)

Figure 68 Comparison of effect of different assumptions for CTE on (a) Thermal stress curves, and (b) stress at -30°C normalized to stress at when both α_l and α_g are considered

8.3. Defining Thermal Cracking Failure Envelopes

As previously discussed in Chapter 2, in contrast to the current state of relative theoretical robustness in constitutive relationships of viscoelastic materials, the study and prediction of failure in viscoelastic materials is still as much dependent on empiricism as to sound mechanistic concepts. Most early studies of failure in asphalt mixtures focused on the use of the "Smith Failure Envelope" [86], showing that such an envelope in many instances works sufficiently well for asphalt mixtures [88, 130].

Researchers studying viscoelastic fracture have shown that there is a close dependency between failure stress and strain rate, such that the stress decreases monotonically as the strain rate is decreased. On the other hand, researchers have observed the existence of a "definite maximum strain at failure" for viscoelastic material tested to failure at different strain rates [131, 86, 87, 85]. The strain at failure increases as the strain rate decreases continuously to a certain

strain rate, after which any decrease in strain rate will cause the strain at failure to decrease [131].

In the present study it was initially hypothesized that a failure criterion for low temperature fracture of asphalt material could be defined using a log-linear fit through two failure stress-strain data-points of sufficiently different conditions (i.e. varying temperatures or strain rates).

The concept was first explored by constructing a failure envelope using asphalt binder low temperature fracture data from the Single Edged Notched Beam (SENB) device under development at UW-Madison [132] for samples tested at varying conditioning temperatures and rates but at a constant conditioning time of 1 hr. The data points were gathered by testing asphalt binders to fracture at -12, -18, and -24°C, at three constant deflection rates. Figure 69 shows how increasing the deflection rate at the same temperature (i.e. -12°C) decreases the failure deflection, while the failure stress seems to increase up to a point, after which the failure stress does not significantly increase as loading rate increases. The same trends with loading rates and temperature can be seen in Figure 70, in which the asphalt binder low temperature failure envelope as constructed from SENB data is shown.

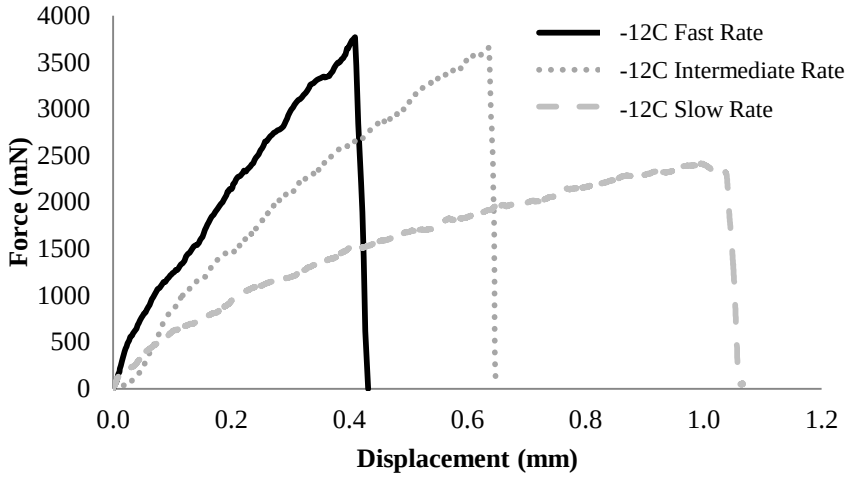

Figure 69 Effect of deflection rate on asphalt binder failure load and deflection; tested using the SENB at -12°C

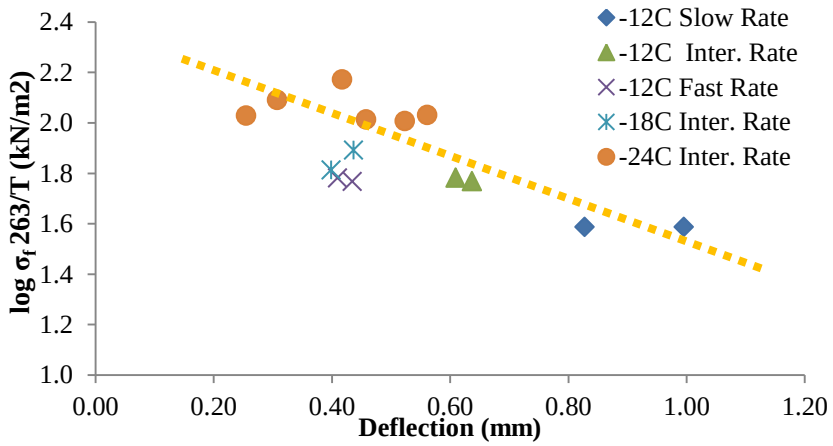

Figure 70 Asphalt binder failure envelope from SENB failure data at different low temperatures and deflection rates

Following the apparent success in generating a failure envelope using the SENB for asphalt binders at low temperatures, it was decided to attempt constructing a similar envelope for asphalt mixture thermal stress and strain during cooling using the ATCA. In this case the approximate low temperature failure envelope was postulated to be definable using two points acquired through testing a mixture in the ATCA at two extreme cooling rates, thus imposing different strain rates, resulting in the failure envelope schematically shown in Figure 71.

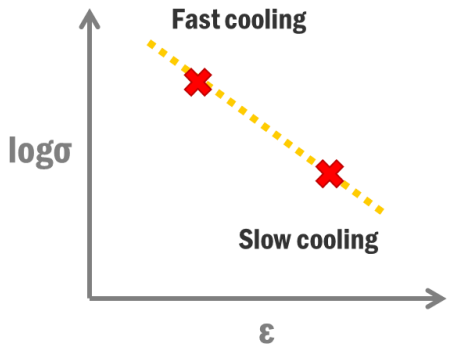

Figure 71 Schematic representation of ATCA failure envelope

To validate the procedure two asphalt mixtures using different binder types (a neat binder and one modified using a poly-ethylene type plastomeric modification) were tested at two different cooling rates. The results, as shown in Figure 72, indicate that the postulated behavior shown in Figure 71 did not occur in reality. This contradictory behavior is actually in agreement with previously observed thermal stress behavior in which the sample that was cooled at a lower rate built up more stress as it cooled down (Figure 24). The explanation for this behavior is the ability of the binder cooled at a slower rate to accumulate more time-dependent (delayed) strain as it cools, thus building up a higher amount of stress. It must be noted that at slow enough rates where most of the rapid physical hardening is expected to take place during cooling, not much change in the rate of thermal strain is expected if rates are further decreased, and thus the main effect is believed to be related to relaxation in such conditions. Testing at such slow cooling rates was not experimentally possible in the present study.

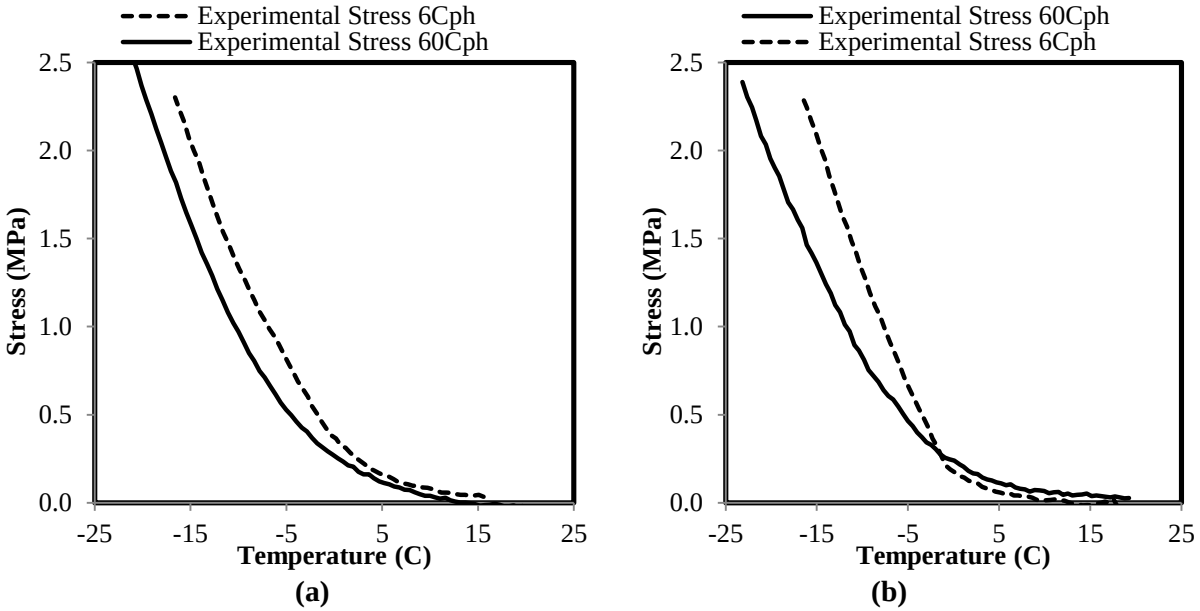

Figure 72 Comparison of thermal failure stress and strain at 6 and 60°C/hr for (a) neat, and (b) PMA mixtures.

For the case of the SENB binder testing conducted at consistent conditioning times from sample to sample, failure stress and strain shifted with reducing strain rate or increasing temperatures; but for restrained mixture cooling problems the trend is much more complex due to the combined effect of added time-dependent strain at lower cooling rates, as displayed in Figure 72. It is believed that the behavior of asphalt mixtures under thermal strain and time-dependent strain would be very similar up to the point of ultimate failure, thus depending on the susceptibility of the asphalt to physical hardening, decreasing the cooling rate may result in faster, slower or similar rates of thermal stress build-up, consequently limiting the success in using of thermal stress and strain at failure for building low temperature cracking failure envelopes. Thus efforts to construct failure envelopes from ATCA results were abandoned in the present study. Instead, it would seem that the most practical method for determining the failure stress and strain of the asphalt mixture would be either through performing ATCA testing at cooling rates similar to those expected in the field, or development of failure envelopes based on

asphalt mixture fracture tests conducted at a number of constant temperatures with consistent conditioning times, such as the Semi-circular Bend (SCB), Disc Compact Tension (DCT) or the Indirect Tensile Strength test (IDT) [90]. Another possible option would be through the use of binder fracture stress and strain from the SENB test in a micromechanical failure analysis of asphalt mixtures. Such analysis is expected to be complex and time-consuming, and outside the scope of the present study.

8.4. Limiting Criteria for Prevention of Thermal Cracking

Throughout this study a wide range of low temperature properties, parameters and test procedures were discussed in varying capacities and were used to explain behaviour with regards to thermal stress, thermal strain, contraction rates, and low temperature fracture and failure properties of asphalt binders and mixtures. In order to make some practical sense of these measurements they need to be coupled with field evaluation results. The field data are taken from the Transportation Pooled Fund Low Temperature Cracking Investigation conducted by the joint efforts of researchers at the University of Wisconsin Madison, University of Minnesota, University of Illinois at Urbana-Champaign, and University of Iowa [90]. Many of the experimental results used in the present study were conducted as part of this national effort to better understand low temperature cracking.

Field performance data from a number of field sections in a Minnesota county road are used as basis of comparison to the wide range of binder experimental results measured in this study, including SENB binder fracture, Tg and CTE measurements and physical hardening assessment. The results are used to identify critical ranges and values of measured low temperature properties that seem to have contributed to low temperature performance of field

section, and subsequently defining possible limiting material property criteria that could minimize thermal cracking potential based on the available data.

The field section consisted of four 500 meter sections located in Minnesota (MN) county road 112. Each section was paved with a binder from different asphalt crude source. Binder samples from each section were available for the present study, results of which are discussed in the following sections. The total length of transverse thermal cracks detected in the latest field survey is shown in Table 12, and were used for the subsequent analysis.

Table 12 MN county road 112 thermal cracking performance results

Binder	Transverse Cracking (m)
"VAL"	60.3
"CIT"	32.1
"MTN"	33.7
"CAN"	3.4

8.4.1. Binder Physical Hardening

One of the noteworthy differences between the binders used in the MN county roads was their susceptibility to physical hardening, as measured using the BBR at different conditioning times. All four binders were tested at their respective glass transition temperatures for 46 hrs and their hardening index was calculated for this period. The physical hardening model previously discussed was fitted to the model and used to derive the G and η parameters for comparison. Figure 73 shows the hardening index curves and along with their respective fitted model curves.

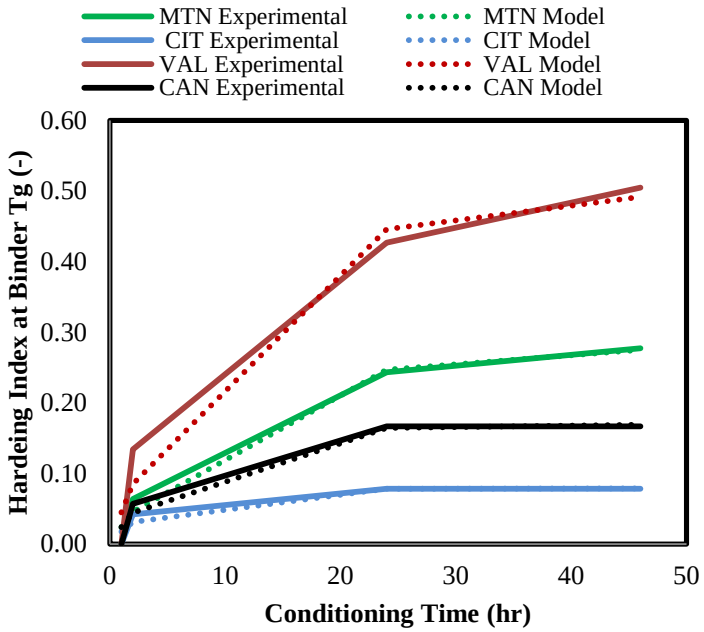

Figure 73 Binder hardening index at various conditioning times for binders used in the MN county road sections, fitted with physical hardening model at their respective Tg.

Figure 74 compares various physical hardening measures with the observed field cracking. A clear distinction between physical hardening potential of the highly cracked VAL section and the other binders is observed, especially for model parameter "η" and hardening index after 24hrs of conditioning. For the physical hardening model parameters, the lower the values, the higher the resultant physical hardening rate is. Thus approximate visually defined minimum limit lines are plotted on the graphs for "G" (3.0) and "η" (30.0) based on section performance. Furthermore, the binder with hardening index above 0.3 at its T_g showed excessive cracking in the field. As expected, it is also seen that 2 hrs of conditioning was not sufficiently long to differentiate binder physical hardening potential in any meaningful fashion.

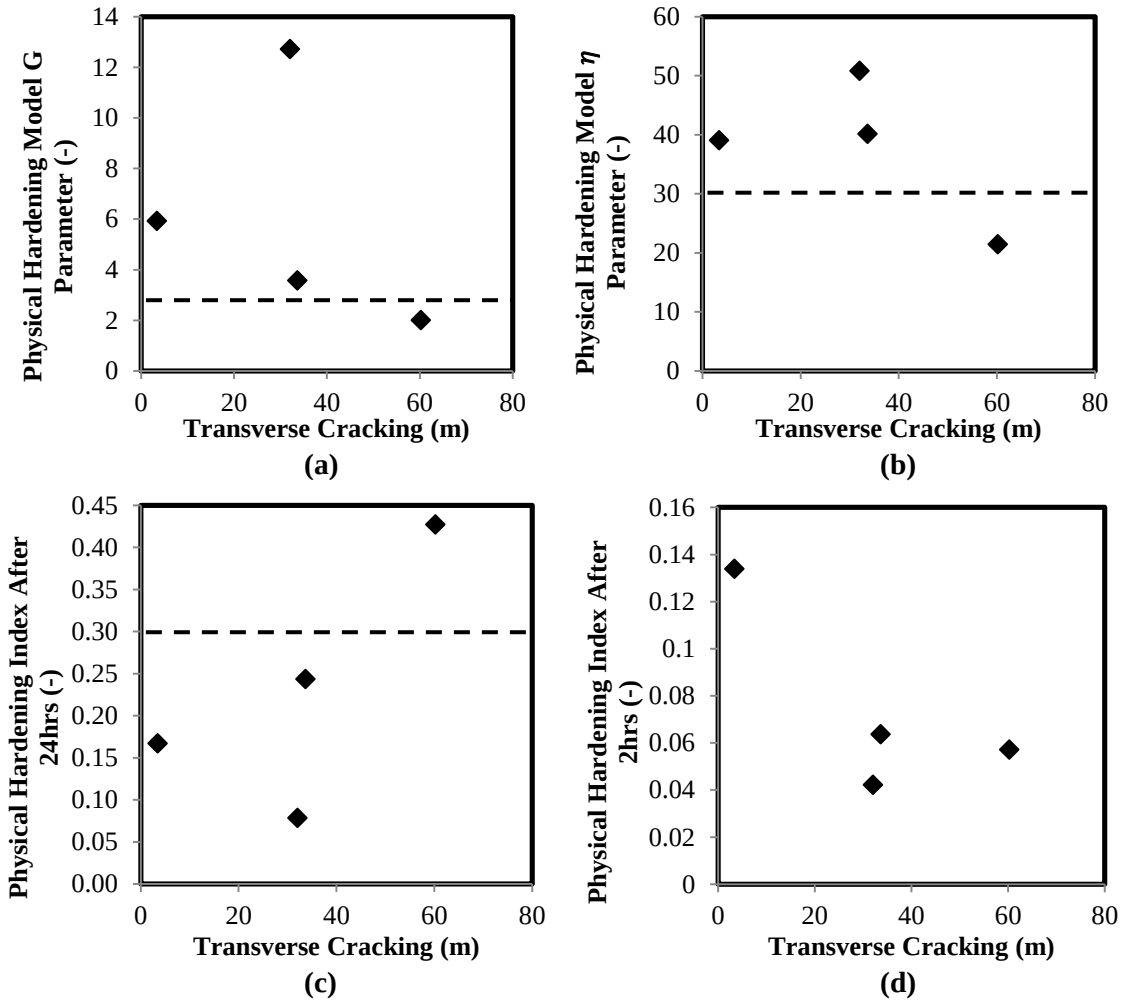

Figure 74 Comparison of binder physical hardening potential at T_g to corresponding thermal cracking in field: (a) physical hardening model parameter "G", (b) physical hardening model parameter "η", (c) hardening index after 24hrs, and (d) hardening index after 2 hrs of conditioning.

8.4.2. Binder Fracture Properties

To further validate the relevance of the fracture properties, the field performance from four sections in Minnesota, USA, were also compared to BBR-SENB results obtained at -12°C. The results, shown in Table 13, indicate that the BBR-SENB G_f parameter was able to distinguish the worse performing binder properly, among binders of the same PG, but could not detect the superior performance demonstrated by the section using PG 58-23 Elvaloy modified binder. In order to better investigate this discrepancy, the load-deflection curves of the binders showing very similar G_f, but very different field performance were compared.

In **Figure 75** it can be seen that although the area under both curves are very similar, the Elvaloy modified binder shows a softer response but deflects much more than the PG 58-28 from source "MTN". This result seems to indicate that the strain tolerance of the binder, as measured by the deflection at break, may in fact play a critical role for field performance, and that judging binder performance by fracture energy alone may yield misleading results. The deflection at facture and failure energy at -12 and -24°C are shown in Table 13. A deflection at fracture higher than 1.5 mm seemed to results in superb low temperature cracking performance. It can be seen that a combined criterion based on both u_f and G_f as measured by the BBR-SENB will be necessary to assess binders in terms of susceptibility to thermal cracking in the field. This is further explored in this section.

Table 13 Comparison between MN CR 112 thermal cracking performance and BBR-SENB results (ranking)

Binder	G_f (J/m^2) at -12°C	U_f (mm) at -12°C	G_f (J/m^2) at -24°C	U_f (mm) at -12°C	Transverse Cracking (m)
"VAL"	15.62	1.04	12.86	0.283	60.3
"CIT"	27.88	1.29	8.91	0.178	32.1
"MTN"	22.48	0.82	9.93	0.219	33.7
"CAN"	25.12	1.87	13.14	0.286	3.4

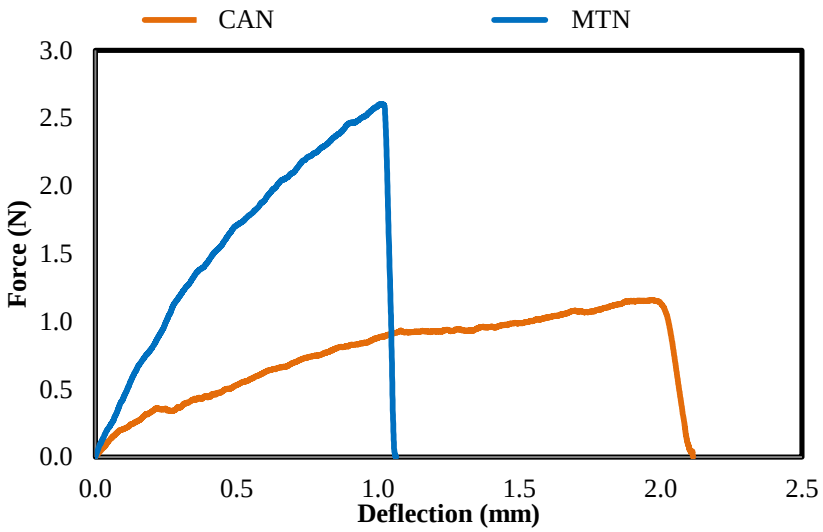

Figure 75 Comparison of BBR-SENB load-deflection curves for two MN CR112 binders with similar G_f but very different field performance

The ability of Fracture energy and Fracture deflection to capture the brittle-ductile transition behavior of binders (assumed to be due to material undergoing glass transition) is presented in Figure 76 in which fracture energy (G_f) and failure deflection (U_f) were plotted versus the relative distance of the testing temperature to the respective binder's glass transition temperature.

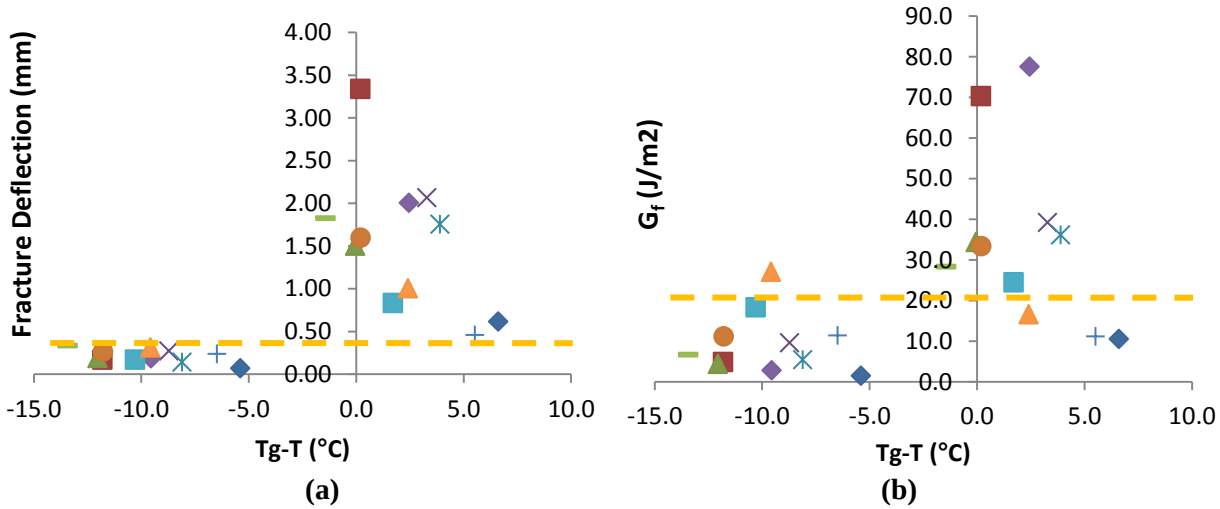

Figure 76 Brittle-ductile transition behavior using BBR-SENB parameters (a) Fracture deflection, (b) Fracture energy, (c) Fracture toughness.

The results shown in Figure 76(a) indicate that binders tested at temperatures below their T_g show fracture deformation/deflection consistently at or below 0.35 mm, which could be considered as the limit for the brittle to ductile transition. The ductile to brittle cut-off value is harder to discern when using fracture energy (G_f), which is influenced by both fracture load as well as the fracture deflection. Although most of the binders tested in the brittle temperatures fractured at energies at or below 20.0 J/m^2, a few binders in the ductile zone also fractured at energies below this value.

Using limit values derived from ductile-brittle analysis for G_f and U_f, as well as the U_f threshold of 1.5 mm for superb performance derived earlier, Figure 77 was plotted for the binders used in the MN county sections.

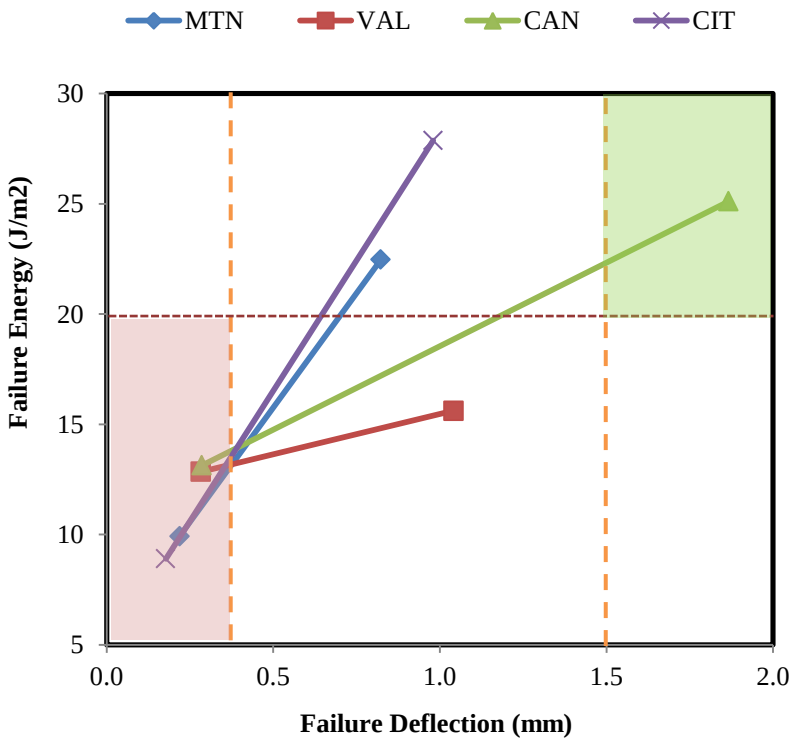

Figure 77 SENB binder performance criteria for MN county sections (for each set values at the left were measured at -24°C and values at the right at -12°C)

It can be seen in Figure 77 that at the lowest temperature used in testing(-24°C) all binders became brittle, with performance approaching similar values and binders performing poorly, failing both U_f and G_f ductile-brittle threshold values of 0.35 mm and 20 J/m^2. At -12°C "CAN" satisfied both the G_f and U_f ductile-brittle thresholds, while also satisfying the "good performance" U_f threshold value of 1.5 mm. This section showed minimal cracking in the field. The "CIT", and "MTN" sections satisfied the G_f and U_f brittle-ductile thresholds but did not satisfy the "good performance" U_f threshold. These sections showed intermediate levels of cracking in the field. Finally "VAL" failed both the G_f and U_f ductile-brittle thresholds at -24°C, as well as failing the G_f ductile-brittle threshold and the "good performance" U_f threshold at -12°C, as a consequence showing severe thermal cracking in the field. Overall the results seem to indicate that the suggested BBR-SENB criteria for U_f and G_f are capable of determining the expected performance of the binder in the field, by comparing results from testing near expected low temperature performance temperatures to the plotted threshold values in Figure 77.

A side study on the effect of isothermal conditioning on fracture properties of binders confirmed the assumption stated above, showing that the effect of physical hardening on failure stress and strain was similar to the effect of decreasing the failure temperature. Figure 78 shows the typical trend resulting from conditioning for 72 hours.

Figure 79 depicts results of testing selected binders from Table 1 after 0.5 and 72 hr of conditioning at their glass transition temperature (T_g). The results are shown in term of normalized values (ratio of value after 72 hours of conditioning divided by the value after 0.5 hour) indicate significant changes in the overall response to load and also in the fracture properties.

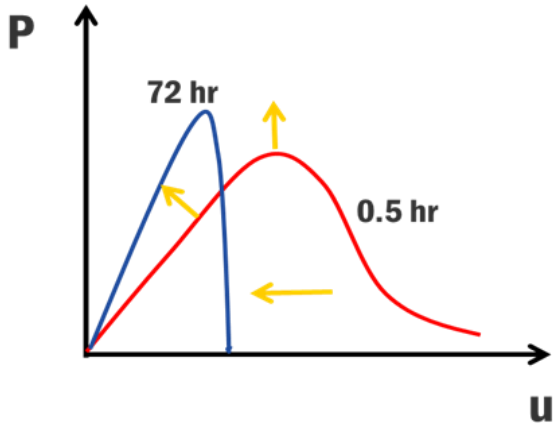

Figure 78 Typical changes in load (P) - deformation (U) curve before and after isothermal conditioning at Tg.

In Figure 79 it can be seen that the slope of the load-deflection (P-u) curve increased significantly after conditioning. The fracture toughness (a product of failure stress) also increased for all binders tested after conditioning, however, a varying trend was observed for fracture energy. Fracture energy increased or was constant for the two unmodified binders (i.e., MnROAD Cell 20 and New York, NY), while decreasing for the three modified binders. This reduction is explained by the relative loss of strain tolerance with conditioning time. In other words, the increase in load at fracture is offset by reduction in deformation at break for the modified binders. The observed trend is more clearly shown for the deflection parameter (U_f) in Figure 79(d), in which the normalized value of deflection are all below one when normalized relative to their respective values measured after 0.5 hr of isothermal conditioning.

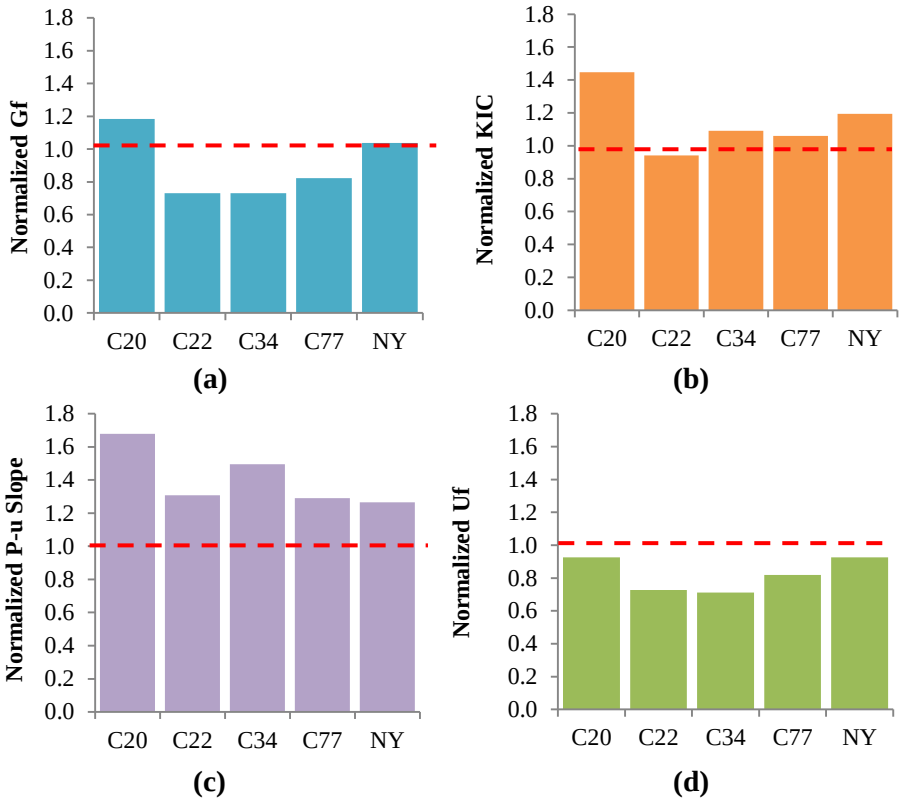

Figure 79 SENB parameters after 72 hrs normalized to results after 0.5 hr of conditioning, (a) G_f, (b) K_{IC}, (c) slope of P-u curve, and (d) deflection at fracture (U_f).

8.4.3. Binder Glass Transition and Contraction Properties

The asphalt binder glass transition temperature and liquid and glassy coefficients of contraction were measured using the dilatometric system previously described. Results are plotted against cracking observed in the field in Figure 80. While no meaningful relationship between the glass transition temperature as well as the glassy CTE and field cracking was observed, the liquid CTE for the section with excessive cracking was well above that of the other binders.

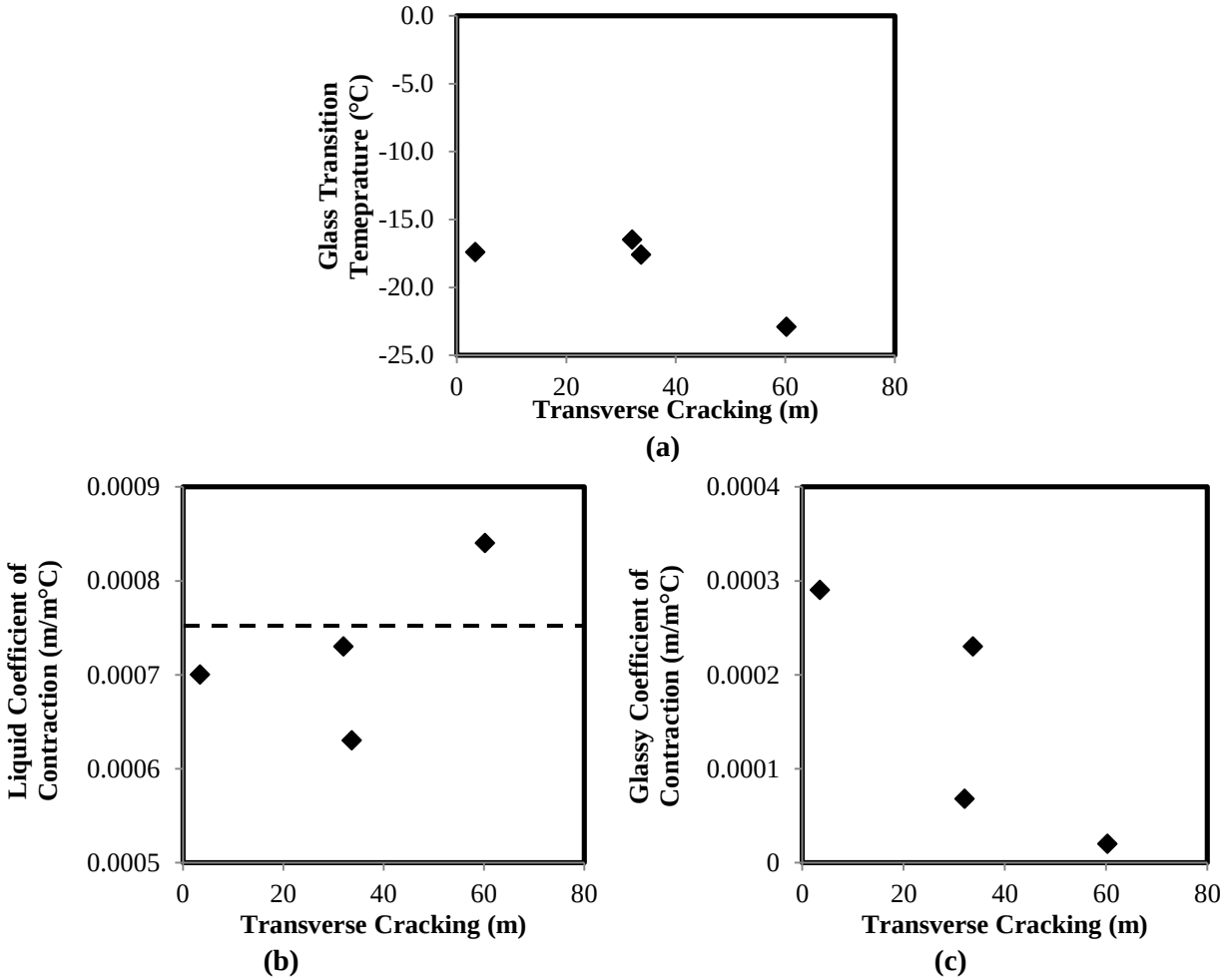

Figure 80 Comparison of binder glass transition and contraction properties to cracking potential: (a) glass transition temperature, (b) liquid CTE, α_l, (c) glassy CTE α_g.

These observations are consistent with the analysis of variance results shown earlier in the chapter. A maximum liquid CTE limit of 7.5×10^{-4} m/m°C was visually derived based on the available data. A high liquid CTE leads to larger thermal strain during cooling, thus leading to the formation of higher thermal stresses in the pavement.

8.4.4. Combined Comparison of Criteria

Using criteria limits and threshold values for binder properties derived in the previous sections, an overall comparison of criteria pass/fail status was compared to observed field performance, as shown in Table 14.

Table 14 Comparison of relevant binder low temperature criteria to field performance

		Physical Hardening			Thermo-Volumetric	Binder Fracture	
Section	**Cracking**	**G**	**η**	**HI at 24hr**	**α_l (1/°C)**	**U_f at -12°C**	**G_f at -12°C**
MTN	MID	P	P	P	P	F	P
VAL	SEVERE	F	F	F	F	F	F
CAN	LOW	P	P	P	P	P	P
CIT	MID	P	P	P	P	F	P

It can be seen that the VAL section that showed the severest cracking failed all criteria, while binder used in CAN section that passed all criteria had the best field performance with minimal cracking. The materials used in the MTN and CIT sections that showed medium levels of cracking, passed the physical hardening and thermo-volumetric property criteria, but did not satisfy the U_f limit for superb tolerance against cracking. The results are promising, as they demonstrate the relevance of the studied binder properties to low temperature cracking performance in the field.

8.5. Chapter Summary

The thermal stress buildup during cooling was investigated using the calculation model previously described, capable of accounting for time dependent strain (physical hardening). By varying the thermal volumetric properties a sensitivity analysis on these parameters was performed. Attempts were made to establish binder and mixture failure criteria using the low temperature experimental properties. The following notable findings can be stated:

- The liquid phase CTE, α_l and the glass transition temperature, T_g, showed the most influence on the rate and trend of thermal stress buildup; the later becoming more prominent when accounting for the time dependency of strains in the glass transition region. Comparison to field thermal cracking observations confirmed this finding, yielding an approximate maximum liquid CTE limit of 7.5×10^{-4} m/m°C.

- Predicted dependency of thermal stress on α_g was low, which was also shown when comparing to field thermal cracking performance. The limited sensitivity of thermal stress to changes in magnitude of α_g indicates the possibility of using a typical value for α_g in place of experimental measurement.

- Assumption of a constant CTE at low temperatures can lead to significant error in calculation of thermal stress. Overall, it is concluded that accurate calculation of thermal stress during cooling is not possible without reliable measures of the α_l, T_g and the transition width.

- It is believed that the behavior of asphalt mixtures under thermal strain and time-dependent strain would be very different up to the point of ultimate failure. The differences depend on the susceptibility of the asphalt to physical aging. Decreasing the cooling rate may result in faster, slower or similar rates of thermal stress build-up, consequently limiting the use of thermal stress and strain at failure for building low temperature cracking failure envelopes.

- Using limit values derived from ductile-brittle analysis for G_f (20 J/m^2) and U_f (0.35 mm), as well as the U_f threshold of 1.5 mm can be sued as performance criteria. A proposed chart was plotted for the BBR-SENB results.

- A clear distinction between physical hardening potential of the highly cracked sections and the other binders was observed, especially when considering physical hardening model parameter "η" and hardening index after 24hrs of conditioning. Minimum limit lines were defined for "G" (3.0) and "η" (30.0) based on section performance. Furthermore, the binder with hardening index above 0.3 at its T_g showed excessive cracking in the field.

- The field section that showed the severest cracking failed all criteria, while the best performing section passed all criteria. The material that showed medium levels of cracking passed most of the criteria while failing one of the SENB criteria. The results demonstrate the relevance of the binder properties studied to low temperature cracking performance in the field.

9. Summary of Findings and Conclusions

9.1. Summary of Findings

In this study, the Asphalt Thermal Cracking Analyzer (ATCA) was used to show how asphalt mixtures undergo isothermal contraction, and the consequences of this behavior for the performance and buildup of thermal stress. A prediction model for the rate of physical hardening at different temperatures and conditioning times was proposed based on a creep viscoelastic model and concepts derived from the study of a large number of modified and unmodified binders. The model was used to predict changes in BBR parameters (i.e. S(60) and m(60)) after various isothermal conditioning times. The model was then extended to mastics and a conversion factor was derived to shift results for applicability in asphalt mixture thermal strain calculation.

The physical hardening model of binders was coupled with relaxation modulus master curves and glass transition measurements to propose a model for the calculation of thermal stress buildup in mixtures as a continuous function of conditioning time and temperature. The key idea behind this model is that the input thermal strain can be divided into small increments for which the relaxation response can be easily computed and added in time to obtain the total thermal stress. The model was validated using an elaborate set of experimentally derive input properties for two mixtures at two different cooling rates.

An experimentally calibrated multi-phase micromechanical model for asphalt mixture undergoing thermal shrinkage and glass transition was developed in a finite element platform. The results where compared to experimental data measured using a special TSRST device which allow measuring strain and stress build up during cooling.

The following main findings are derived from the analysis of results:

- The rate of physical hardening does not increase indefinitely as temperature decreases. Based on literature review and the experimental data collected, it is found that the rate of hardening peaks at a specific temperature, and approaches zero as the temperature increases or decrease toward the limits of the glass transition region. The peak temperature was shown to correspond to the glass transition temperature of the binder.

- The liquid phase CTE, α_l and the glass transition temperature, T_g, showed the most influence on the rate and trend of thermal stress buildup; the later (T_g) becoming more prominent when accounting for the time dependency of strains in the glass transition region. Comparison to field thermal cracking observations confirmed this finding.

- Dependency of thermal stress on α_g was found to be relatively low, as also shown when comparing to field thermal cracking performance. The limited sensitivity of thermal stress to changes in magnitude of α_g indicates the possibility of using a typical value for α_g in place of experimental measurements.

- It is believed that the behavior of asphalt mixtures under thermal strain and time-dependent strain would be different depending on the susceptibility of the asphalt to physical hardening. Decreasing the cooling rate may result in faster, slower or similar rates of thermal stress build-up, consequently limiting the use of thermal stress and strain at failure for building low temperature cracking failure envelopes.

- A clear distinction between physical hardening potential of the highly cracked sections and the other binders was observed, especially when considering physical hardening model parameter "η" and hardening index after 24hrs of conditioning.

- The field section that showed the severest cracking failed all criteria, while the best performing section passed all criteria. The material that showed medium levels of cracking passed most of the criteria while failing one of the SENB criteria. The results demonstrate the relevance of the studied binder properties to low temperature cracking performance in the field.
- Using limit values derived from ductile-brittle analysis for G_f and U_f, as well as an additional U_f threshold for good performance a performance criteria chart is proposed based on comparison with field performance results.

9.2. Conclusions

The results of this study indicate that physical hardening of binders has important effects on the thermal stress and thermal strain accumulation in mixtures during cooling cycles. Failure to consider this time dependent behavior, which varies among binders, could lead to failure in predicting performance. The existing modulus and strain used in predicting thermal cracking of asphalt pavements need revisions to integrate a function for the time dependent changes. A model is proposed in this thesis that requires measuring glass transition and creep stiffness of binders.

10. References

1] H. Bahia, H. Tabatabaee and R. Velasquez, "Asphalt Thermal Cracking Analyzer," in *7th International Conference on Cracking in Pavements*, Netherlands, 2012.

2] J. Ojo, D. Fratta, H. Bahia and C. Daranga, "Thermo-volumetric Properties of Asphalt Binders and Mixtures," in *Pavement Cracking Mechanisms, Modeling, Detection, Testing, and Case Histories*, London, 2008.

3] D. Anderson, D. Christenson, H. Bahia, R. Dongre, M. Sharma, C. Antle and J. Button, "Binder Characterization and Evaluation Vol. 3: Physical Characterization," Strategic Highway Research Program, National Research Council, Washington D.C..

4] J. Planche, P. Claudy, J. Letoffe and D. Martin, "Using Thermal Analysis Methods to Better Understand Asphalt Rheology," *Thermochimica Acta,* vol. 324, pp. 223-227, 1998.

5] D. Anderson and M. Marasteanu, "Physical Hardening of Asphalt Binders Relative to Their Glass Transition Temperatures," *Transportation Research Record: Journal of the Transportation Research Board,* vol. 1661, pp. 27-34, 1999.

6] H. Bahia, M. Zeng and K. Nam, "Consideration of Strain at Failure and Strength in Prediction of Pavement Thermal Cracking," *Journal of the Association of Asphalt Pavement Technologists,* vol. 69, pp. 497-540, 2000.

7] P. Kriz, J. Stastna and L. Zanzotto, "Temperature Dependence and Thermo-reversibility of Physical Hardening of Asphalt Binders," in *4th Eurasphalt & Eurobitume Congress*, Copenhagen, Denmark, 2008.

8] H. Bahia and R. Velasquez, "Understanding the Mechanism of Low Temperature Physical Hardening of Asphalt Binders," in *55th Annual Meeting of the Canadian Technical Asphalt Association*, 2010.

9] H. Bahia, "Low-Temperature Isothermal Physical Hardening of Asphalt Cements," 1991.

10] M. Bouldin, R. Dongre,, G. Rowe, M. Sharrock and D. Anderson, "Predicting Thermal Cracking of Pavements from Binder Properties-Theoretical Basis and Field Validation," *Journal of the Association of Asphalt Pavement Technologists,* vol. 69, p. 455, 2000.

11] D. Jung and T. Vinson, "SHRP-A-400: Low-Temperature Cracking: Test Selection," Strategic Highway Research Program, National Research Council, Washington D.C., 1994.

12] H. Bahia and D. Anderson, "The Development of the Bending Beam Rheometer: Basics and Critical Evaluation of the Rheometer," *Physical Properties of Asphalt Cement Binders: ASTM STP 1241,* 1995.

13] C. Monismith, G. Secor and K. Secor, "Temperature Induced Stresses and Deformations in Asphalt Concrete," *Journal of the Association of Asphalt Pavement Technologists,* vol. 34, pp. 245-285, 1965.

W. Arand, in *4th International Symposium on Mechanical Tests for Bituminous
14] Mixes Characterization, Design and Quality Control, RILEM*, Budapest, Hungary, 1990.

T. Vinson, H. Kanerva and H. Zeng, "SHRP-A-401," Strategic Highway Research
15] Program, Washington D.C., 1994.

P. Romero, J. Youtcheff and K. Stuart, "Low-Temperature Physical Hardening of
16] Hot-Mix Asphalt," *Transportation Research Record: Journal of the Transportation Research Board,* vol. 1661, pp. 22-26, 1999.

P. Sebaaly, A. Lake and J. Epps, *Journal of Transportation Engineering,* pp. 578-
17] 586, 2002.

G. Chehab and R. Kim, *Journal of Materials in Civil Engineering,* pp. 382-392,
18] 2005.

C. Sauzéat, H. Di Benedetto, P. Chaverot and G. Gauthier, in *Advanced
19] Characterization of Pavement and Soil Engineering Materials*, Athens, Greece, 2007.

R. Velasquez, N. Gibson, T. Clyne, M. Turos and M. Marasteanu, in *6th RILEM
20] International Conference on Cracking in Pavements*, Chicago, Illinois, 2008.

M. Marasteanu, R. Velasquez, A. Cannone Falchetto and A. Zofka, "Development
21] of a Simple Test to Determine the Low Temperature Creep Compliance of Asphalt Mixtures," Minneapolis, 2009.

L. Struik, "Physical Aging in Amorphous Glassy Polymers," *Annals of the New
22] York Acadamy of Science,* vol. 239, no. 9, pp. 78-86, 1976.

I. Hodge, "Physical Aging in Polymer Glasses," *Science,* vol. 267, pp. 1945-1947,
23] 1995.

I. Hodge, "Enthalpy relaxation and recovery in amorphous materials," *Journal of
24] Non-Crystalline Solids,* vol. 169, pp. 211-266, 1994.

L. STRUIK, Physical Hardening in Amorphous Polymers and Other Materials,
25] Elsevier, 1978.

J. Ferry, Viscoelastic Properties of Polymers, 3 ed., New York, NY: Wiley, 1980.
26]

K. Adachi and T. Kotaka, "Volume and Enthalpy Relaxation in Polystyrene,"
27] *Polymer Journal,* vol. 14, no. 12, pp. 959-970, 1982.

L. Guadagno, C. Fontanella, V. Vittoria and P. Longo, "Physical Aging of
28] Syndiotactic Polypropylene," *Journal of Polymer Science: Part B: Polymer Physics,* vol. 37, p. 173–180, 1999.

J. Hadač, P. Slobodian, P. Říha, P. Saha, R. Rychwalski, I. Emri and A. Kubát,
29] "Effect of cooling rate on enthalpy and volume relaxation of polystyrene," *Journal of Non-crystalline Solids,* vol. 353, no. 28, p. 2681–2691, 2007.

Y. Kobayashi, W. Zheng, E. Meyer, J. McGervey, A. Jamieson and R. Simhall,
30] "Free Volume and Physical Aging of Poly(viny1 acetate) Studied by Positron Annihilation," *Macromolecules,* vol. 22, no. 5, 1989.

E. Oleinik, "Glassy Polymers as Matrices for Advanced Compsites," *Polymer
31] Journal,* vol. 19, no. 1, pp. 105-117, 1987.

S. Simon, J. Sobieski and D. Plazek, "Volume and enthalpy recovery of

32] polystyrene," *Polymer,* vol. 42, p. 2555–2567, 2001.

J. Cowie, S. Harris and I. McEwen, "Physical Ageing in Poly(vinyl Acetate) 1.
33] Enthalpy Relaxation," *Journal of Polymer Science Part B: Polymer Physics,* vol. 35, no. 7, p. 1013–1166, 1997.

W. Kauzmann, "The Nature of the Glassy State and the Behavior of Liquids at Low
34] Temepratures," *Chemical Reviews,* vol. 43, pp. 219-256, 1948.

Z. Cernošek, J. Holubová and E. Cernoškováa, "Kauzmann Temperature and the
35] Glass Transition," *Journal of Optoelectronics and Advanced Materials,* vol. 7, no. 6, pp. 2941 - 2944, 2005.

G. Adam and J. Gibbs, "On the Temperature Dependence of Cooperative
36] Relaxation Properties in GlassForming Liquids," *Journal of Physical Chemistry,* vol. 43, pp. 139-146, 1965.

J. Bartos, J. Moiler and J. Wendorff, "Physical ageing of isotropic and anisotropic
37] polycarbonate," *Polymer,* vol. 31, pp. 1678-1685, 1990.

L. Struik, "The mechanical enhancement of physical aging," *Polymer,* vol. 21, pp.
38] 962-967, 1980.

H.-N. Lee and M. Ediger, "Interaction between physical aging, deformation, and
39] segmental mobility in poly-methyl methacrylate glasses," *Journal of Chemical Physics,* vol. 133, 2010.

L. Struik, "The Mechanical Behavior and Physical Ageing of Semicrystalline
40] Polymers: 2.," *Polymer,* vol. 28, pp. 1534-1542, 1987.

J. Hay, "The physical ageing of amorphous and crystalline polymers," *Pure and
41] Applied Chemistry,* vol. 67, no. 11, pp. 1855-1858, 1995.

M. Tant and G. Wilkes, "Physical Aging Studies of Semicrystalline Poly (e thylene
42] Tereph thalate)," *Journal of Applied Polymer Science,* vol. 26, pp. 2813-2825, 1981.

A. Yavari, M. Tonegaru, N. Lupu, A. Inoue, E. Matsubara, G. Vaughan, A. Kvick
43] and W. Botta, "Quenched-in Free Volume Vf, Deformation-induced Free Volume, the Glass Transition Tg and Thermal Expansion in Glassy ZrNbCuNiAl Measured by Time-resolved Diffraction in Transmission," in *Materials Research Society Symposium*, 2004.

A. Aref-Azar, F. Biddlestone, J. Hay and R. Haward, "The effect of physical ageing
44] on the properties of poly(ethylene terephthalate)," *Polymer,* vol. 24, pp. 1245-1251, 1983.

G. Odegard and A. Bandyopadhyay, "Physical Aging of Epoxy Polymers and Their
45] Composites," *Journal of Polymer Science Part B: Polymer Physics,* vol. 49, no. 24, p. 1695-1716, 2011.

J. Arnold, "The Effects of Physical Aging on the Brittle Fracture Behavior of
46] Polymers," *Polymer engineering and Science,* vol. 35, no. 2, pp. 165-169, 1995.

D. Matsumoto, "Time-Temperature Superposition and Physical Aging in
47] Amorphous Polymers," *Polymer Engineering and Science,* vol. 28, no. 20, pp. 1313-1317, 1988.

J. Sullivan, "Creep and Physical Aging of Composites," *Composites Science and
48] Technology,* vol. 39, pp. 207-232, 1990.

M. Delin, R. Rychwalski, J. Kubat and C. Klason, "Physical Aging Time Scales

49] and Rates for Poly(Vinyl Acetate) Stimulated Mechanically in the Tg-Region," *Polymer Engineering and Science,* vol. 36, no. 24, pp. 2955-2967, 1996.

50] P. Slobodian, P. Pavel Riha, A. Lengalova and J. Hadac, "Enthalpy and volume relaxation of PMMA, PC, and a-Se: evaluation of aging bulk moduli," *Journal of Non-Crystalline Solids,* vol. 344, p. 148–157, 2004.

51] H. Tabatabaee, V. R. and H. Bahia, "Predicting Low Temperature Physical Hardening in Asphalt Binders," *Submitted for publication in the Journal of Construction and Building Materials,* 2012.

52] J. Royal and J. Torkelson, "Physical Aging Effects on Molecular-Scale Polymer Relaxations Monitored with Mobility-Sensitive Fluorescent Molecules," *Macromolecules,* vol. 26, pp. 5331-5335, 1993.

53] J. Hooker and J. Torkelson, "Coupling of Probe Reorientation Dynamics and Rotor Motions to Polymer Relaxation As Sensed by Second Harmonic Generation and Fluorescence," *Macromolecules,* vol. 28, pp. 7683-7692, 1995.

54] M. Agarwal and J. Schultz, "The Physical Aging of lsotactic Polypropylene," *Polymer Engineering and Science,* vol. 27, no. 12, 1981.

55] R. N. Traxler, "The Physical Chemistry of Asphaltic Bitumen," *Chemical Reviews 19,* vol. 2, pp. 119-143, 1936.

56] R. Traxler and C. Coombs, "The Colloidal Nature of Asphalt as Shown by its Flow Properties," *Journal of Physical Chemistry,* vol. 40, p. 1133–1147, 1936.

57] H. Bahia and D. Anderson, "Glass Transition Behavior and Physical Hardening of Asphalt Binders," *Journal of the Association of Asphalt Paving Technologists,* vol. 62, pp. 93-129, 1993.

58] H. Bahia and D. Anderson, "Physical Hardening of Asphalt Binders and Relation to Compositional Parameters," in *204th American Chemical Society (ACS) national meeting, Division of Fuel Chemistry,* 1992.

59] H. Bahia and D. Anderson, "Low-Temperature Physical Hardening of Asphalt Cements," in *International Symposium for Chemistry of Bitumen,* Rome, 1991.

60] A. Brown, J. Sparks and F. Smith, "Steric hardening of asphalts," in *Association of Asphalt Paving Technologists,* 1957.

61] "Standard Specification for Performance-Graded Asphalt Binder," AASHTO Provisional Standards, Washington D.C., 2002.

62] M. Marasteanu, "Role of Bending Beam Rheometer Parameters in Thermal Stress Calculations," *Transportation Research Record: Journal of the Transportation Research Board,* vol. 1875, pp. 9-13, 2004.

63] S. Hesp and S. Subramani, "Another Look at the Bending Beam Rheometer for Specification Grading of Asphalt Cements," in *6th MAIREPAV Conference,* Torino, Italy, 2009.

64] A. Basu, M. Marasteanu and S. Hesp, "Time-Temperature Superposition and Physical Hardening Effects in Low-Temperature Asphalt Binder Grading," *Transportation Research Record: Journal of the Transportation Research Board,* vol. 1829, pp. 1-7, 2003.

A. Shenoy, "Stress Relaxation can Perturb and Prevent Physical Hardening in a

65] Constrained Binder at Low Temperatures," *Road Materials and Pavement Design,* vol. 3, no. 1, pp. 87-94, 2002.

66] A. Cannone Falchetto, T. Mugurel, M. Ki Hoon, M. Marasteanu and R. Dongre, "Physical Hardening: from Binders to Mixtures," in *90th Annual Meeting of the Transportation Research Board*, Washington D.C., 2011.

67] M. Evans and S. Hesp, "Physical Hardening Effects on Stress Relaxation in Asphalt Cements and Implications for Pavement performance," in *90th Annual Meeting of the Transportation Research Board*, Washington D.C., 2011.

68] A. Cannone Falchetto, M. Marasteanu and H. Di Benedetto, "Analogical Based Approach to Forward and Inverse Problems for Asphalt Materials Characterization at Low Temperatures," in *Association of Asphalt Pavement Technologists*, 2011.

69] X. Lu and U. Isacsson, "Laboratory Study on the Low Temperature Physical Hardening of Conventional and Polymer Modified Bitumens," *Construction and Building Materials,* vol. 14, pp. 79-88, 2000.

70] K. Murali and K. Rajagopal, "On the mechanical behavior of asphalt," *Mechanics of Materials,* vol. 37, no. 11, pp. 1085-1100, 2005.

71] "Standard method of test for determining the flexural creep stiffness of asphalt binder using the Bending Beam Rheometer (BBR)," American Association of State Highway and Transportation Officials (AASHTO), 2005.

72] P. Claudy, J. Planche, G. King and J. Letoffe, "Characterization of Asphalt Cements by Thermomicroscopy and Differential Scanning Calorimetry: Correlation to Classic Physical Properties," in *Proceedings of the 204th American Chemical Society National Meeting,* 1993.

73] A. Doolittle, "Studies in Newtonian Flow II: The Dependence of Viscosity of Liquids on Free-Space," *Journal of Applied Physics,* vol. 22, no. 12, p. 1471, 1951.

74] A. Doolittle and D. Doolittle, "Studies in Newtonian Flow V: Further Verification of the Free Space Viscosity Equation," *Journal of Applied Physics,* vol. 28, no. 8, p. 901, 1957.

75] M. Williams, R. Landel and J. Ferry, "The Temperature Dependence of Relaxation Mechanisms in Amorphous Polymers and Other Glass-forming Liquids," *Journal of the American Chemical Society,* vol. 77, pp. 3701-3706, 1955.

76] J. Brandrup, E. Immergut and E. Grulke, Polymer Handbook, 4th ed., New York: Wiley-Interscience, 2003.

77] Q. Z. N. I. Daly WH, "Differential Scanning Calorimetry Study of Asphalt Crystallinity," *Transportation Research Record: Journal of the Transportation Research Board,* vol. 1535, pp. 54-60., 1996.

78] J.-F. Masson, G. Polomark and P. Collins, "Time-Dependent Microstructure of Bitumen And its Fractions by Modulated Differential Scanning Calorimetry," *Energy & Fuels,* vol. 16, no. 2, pp. 470-476, 2002.

79] J. Hills and D. Brien, "The Fracture of Bitumens and Asphalt Mixes by Temperature Induced Stresses," in *Association of Asphalt Paving Technologists*, 1966.

80] J. Christison, D. Murray and K. Anderson, "Stress Prediction and Low Temperature Fracture Susceptibility of Asphaltic Concrete Pavements," in *Association of Asphalt*

Paving Technologists, 1972.

81] F. Finn, C. Saraf, R. Kulkarni, K. Nair, W. Smith and A. Abdullah, "User's Manual for the Computer Program Cold," Transportation Research Board, Washington, D.C., 1977.

82] D. Hiltunen and R. Roque, "A Mechanics-Based Prediction Model for Thermal Cracking of Asphaltic Concrete Pavements," in *Association of Asphalt Paving Technologists*, 1994.

83] D. Kirkner and W. Shen, "Numerical Simulation of Thermal Cracking of Asphalt Pavements," in *Transportation Research Board Annual Meeting*, Washington, D.C., 1999.

84] C. Roland, Viscoelastic Behavior of rubbery Materials, New York: Oxford Press Inc., 2011.

85] A. Zak, "Multiaxial Failure of viscoelastic Materials," United States Air Force, 1964.

86] T. Smith, "Stress-strain-time-temperature Relationships in Polymers," in *Symposium on Stress-strain-time-temperature Relationships in Materials*, 1962.

87] R. Dong, "Description of Tensile Failure of Viscoelastic Materials Under Multiaxial Loading," *Polymer Engineering and Science*, vol. 10, no. 2, 1970.

88] D. Bynum Jr. and R. Traxler, "Failure Envelopes for Asphaltic Concrete," *Materiaux Et Constructions*, vol. 6, no. 36, 1973.

89] M. Mayama, M. Yoshino and K. Hasegawa, "An Evaluation of Heavy Duty Binders in the Laboratory," in *Polymer Modified Asphalt Binders*, K. Wardlaw and S. Shuler, Eds., Philadelphia, American Society for Testing and Materials, 1992.

90] M. Marasteanu, A. Zofka, M. Turos, X. Li, R. Velasquez, W. Buttler, G. Paulino, A. Braham, E. Dave, J. Ojo, H. Bahia, C. Williams, J. Bausano, A. Gallistel and J. McGraw, "Investigation Of Low Temperature Cracking In Asphalt," Minnesota Department of Transportation, 2007.

91] H. Tabatabaee, R. Velasquez and H. Bahia, in *91st Annual Meeting of Transportation Research Board*, Washington D.C., 2012.

92] H. Bahia, H. Tabatabaee and V. R., in *Submitted to the 5th Eurasphalt & Eurobitume Congress*, Istanbul, Turkey, 2012.

93] R. Lakes, Viscoelastic Materials, New York: Cambridge University Press, 2009.

94] S. Mangiafico, "Low Temperature Physical Hardening of Binders: Prediction model and Investigation on Effects of Thermal History," 2010.

95] C. Clopotel, R. Velasquez and H. Bahia, "Measuring Physico-Chemical Interaction in Mastics Using Glass Transition," *Journal of the Association of Asphalt Pavement Technologists*, 2012.

96] H. Bahia, M. Zeng and K. Nam, "Consideration of Strain at Failure and Strength in Prediction of Pavement Thermal Cracking," *Journal of the Association of Asphalt Pavement Technologists*, vol. 69, pp. 497-540, 2000.

97] S. Katicha, G. Flintsch, A. Loulizi and L. Wang, "Conversion of Testing Frequency to Loading Time Applied to the Mechanistic–Empirical Pavement Design Guide,"

Transportation Research Record: Journal of the Transportation Research Record, vol. 2087, pp. 99-108, 2008.

98] R. Christensen, Theory of Viscoelasticity An Introduction, 2nd Edition ed., New York: Academic Press, 1982.

99] "Specific Heat—Specific Gravity," Armstrong International, 2012.

100] J. May, T. Wilkey, M. Swanson, J. Daub, G. Farrow, J. Clayton, D. Clum, M. Moon, B. Eley and F. Eley, "Heating and Storing Asphalt at HMA Plants," Heatec Inc., 2003.

101] "Thermal Properties of Metals, Conductivity, Thermal Expansion, Specific Heat," Engineers Edge, LLC, 2012. [Online]. Available: http://www.engineersedge.com/properties_of_metals.htm. [Accessed 1 8 2012].

102] N. Atkins, "Specific Heats of Various Substances," Lyndon State Collage, 2006. [Online]. Available: http://apollo.lsc.vsc.edu/classes/met130/notes/chapter2/spec_heats.html.

103] "Specific heats and molar heat capacities for various substances at 20 C," Georgia State University, 2012. [Online]. Available: http://hyperphysics.phy-astr.gsu.edu/hbase/tables/sphtt.html. [Accessed 1 8 2012].

104] G. Elert, "Conduction," 2012. [Online]. Available: http://physics.info/conduction/. [Accessed 1 8 2012].

105] W. Cho, S. Kwon and J. Choi, "The thermal conductivity for granite with various water contents," *Engineering Geology,* vol. 107, no. 3-4, pp. 167-171, 2009.

106] "Conductivity table for various materials," Monachos, 2002. [Online]. Available: http://www.monachos.gr/en/resources/Thermo/conductivity.asp. [Accessed 1 8 2012].

107] J. Luca and D. Mrawira, "New Measurement of Thermal Properties of Superpave Asphalt Concrete," *ASCE Journal of Materials in Civil Engineering,* vol. 17, no. 1, pp. 72-79, 2005.

108] R. Morrell, "Thermal conductivities," 2011. [Online]. Available: http://www.kayelaby.npl.co.uk/general_physics/2_3/2_3_7.html. [Accessed 1 8 2012].

109] M. Richardson, "Specific heat capacities," 2011. [Online]. Available: http://www.kayelaby.npl.co.uk/general_physics/2_3/2_3_6.html. [Accessed 1 8 2012].

110] Devcon, "Plastic Steel Putty (A)," ITW Devcon, Denver, 2012.

111] G. Qian, J. Zheng and Q. Wang, "Calculating Thermal Stresses of Asphalt Pavement in Environmental Conditions," in *Symposium on Pavement Mechanics and Materials,* 2007.

112] X. Wensheng, T. Wei and L. Hui, "Analysis of Thermal Stress Response in Asphalt Overlay," in *ICCTP: Critical Issues in Transportation Systems Planning, Development, and Management,* 2009.

113] M. Minhoto, J. Pais, P. Pereira and L. Picado-Santos, "Predicting Asphalt Pavement Temperature with a Three-Dimensional Finite Element Method," *Transportation Research Record: Journal of the Transportation Research Board,* vol. 1919, pp. 96-110,

2005.

114] M. Zhang, G. Chen, L. Hou and L. Zhang, "The Analyses and Calculation for Thermal Stresses of SBR Modified Asphalt Pavement," *Advanced Materials Research,* Vols. 243-249, pp. 4112-4118, 2011.

115] T. L. B. H. Roohi N., "Internal Structure Characterization of Asphalt Mixtures for Rutting Performance Using Imaging Analysis," *Journal of Road Materials and Pavement Design,* vol. 13, pp. 21-37, 2012.

116] K. M. B. H. Coenen A., "Aggregate Structure Characterization of Asphalt Mixtures Using 2-Dimensional Image Analysis," *International Journal of Road Materials and Pavement Design,* 2011.

117] P. Teymourpour, R. Velasquez and H. Bahia, "The Role of Binder Modification and Aggregate Structure on the High and Low Temperature Performance of Asphalt Mixtures," *Submitted to Transportation Research Record, Journal of the Transportation Research Board,* vol. TBD, 2013.

118] D. Christensen and D. Anderson, "Interpretation of Dynamic Mechanical Test Data for Paving Grade Asphalt Cements," *Journal of the Association of Asphalt Paving Technologists,* vol. 61, pp. 68-116, 1992.

119] I. Hopkins and R. Hamming, "On Creep and Relaxation. Journal," *Journal of Applied Physics,* vol. 28, pp. 906-909, 1957.

120] S. Kose, M. Guler, H. Bahia and E. Masad, "Distribution of Strains Within Hot-Mix Asphalt Binders," *Transportation Research Record: Journal of the Transportation Research Board,* vol. 1728, pp. 21-27, 2000.

121] R. Abu Al-Rub, T. You, E. Masad and D. Little, "Mesomechanical modeling of the thermo-viscoelastic, thermo-viscoplastic, and thermo-viscodamage response of asphalt concrete," *International Journal of Engineering Science,* vol. 28, 2011.

122] T. Zhu, "Some Useful Numbers on the Engineering Properties of Materials (Geologic and Otherwise)," 2010. [Online]. Available: http://www.stanford.edu/~tyzhu/Documents/Some%20Useful%20Numbers.pdf. [Accessed 23 July 2012].

123] A. Graham, "Table of Modulus of Elasticity," Durham University, 1997. [Online]. Available: http://www.dur.ac.uk/~des0www4/cal/dams/geol/mod.htm. [Accessed 7 July 2012].

124] "Rock: Thermal Expansion," 2012. [Online]. Available: http://www.britannica.com/EBchecked/topic/505970/rock/80194/Thermal-expansion. [Accessed 23 July 2012].

125] "Coefficients of Linear Thermal Expansion," [Online]. Available: http://www.engineeringtoolbox.com/linear-expansion-coefficients-d_95.html. [Accessed 23 July 2012].

126] "Coeffcient of thermal Expansion per Degree Centigrade," [Online]. Available: http://www.supercivilcd.com/THERMAL.htm. [Accessed 23 July 2012].

127] H. Tabatabaee, R. Velasquez and H. Bahia, "Modeling Thermal Stress and strain in Asphalt Mixtures undergoing Glass Transition and Physical Hardening," *Transportation Research Record,* 2012.

"Standard Practice for Determining Low-Temperature Performance Grade (PG) of
128] Asphalt Binders," American Society of Testing Materials, 2002.

R. Velasquez, H. Tabatabaee, S. Puchalski and H. Bahia, "The Role of Asphalt
129] Binder Fracture Properties in Thermal Cracking Performance of Mixtures and Pavements," in *Canadian Technical Asphalt Association (CTAA)*, 2012.

R. Velasquez, H. Tabatabaee and H. Bahia, "Low Temperature Cracking
130] Characterization of Asphalt Binders by Means of the Single-Edge Notch Bending (SENB) Test," *Journal of the Association of Asphalt Pavement Technologists*, 2011.

T. Hoare and S. Hesp, "Low-Temperature Fracture Testing of Asphalt Binders:
131] Regular and Modified Systems," *Transportation Research Record: Journal of the Transportation Research Board*, vol. 1728, 2000.

K. Nam and H. Bahia, "Effect of Binder and Mixture Variables on Glass Transition
132] Behavior of Asphalt Mixtures," *Journal of the Association of Asphalt Paving Technologists*, vol. 73, p. 89, 2004.

C. Monismith, G. Secor and K. Secor, "Temperature Induced Stresses and
133] Deformations in Asphalt Concrete," in *Proccedings of the Association of Asphalt Pavement Technologists Annual Meeting*.

C. Roland, Viscoelastic Behavior of rubbery Materials, New York: Oxford Press
134] Inc., 2011.